University of Southern Queensland

Faculty of Health, Engineering and Sciences

Assessing Radio Frequency Attenuation through Cotton Crop Canopies in Satellite-Based Agricultural Communication Networks

A dissertation submitted by

Nicholas Manns

in fulfilment of the requirements of

ENP4111 Professional Engineer Research Project

towards the degree of

Bachelor of Engineering (Honours) (Electrical/Electronics)

Submitted October, 2024

Abstract

This research report focuses on the impact of cotton vegetation on signal attenuation, particularly within a post-harvest field near Dalby, Queensland. With the advent of Low Earth Orbit (LEO) satellites set to replace existing wireless communication systems such as LoRa, it is crucial to understand the effects varying forms of vegetation have on signal attenuation to ensure the reliable and efficient operation of such devices.

The investigation utilised LoRa transceivers operating at 915MHz, with transmission data being collected under varying Line of Sight (LoS) and Non-Line of Sight (NLoS) conditions. The obtained results indicate that even residual cotton stubble significantly impacts signal attenuation, with notable discrepancies between the measured data and the predictions made using existing empirical models including ITU Vegetation, ITU MA and Weissberger models. These discrepancies highlighted the need for a new empirical model to be created, better reflecting the conditions found in a cotton-field environment. This new empirical model was proposed, using key field measurements alongside the ITU's existing vegetation model. The proposed model successfully predicted the attenuation across different vegetation densities, with a RMSE of 6.4dB for a 30% foliage depth and 5.2dB for 50% foliage depth.

The model also was also found to be suitable for use in slant path applications, achieving a RMSE of 9.94dB. These findings have a direct correlation with use with the Myriota network, with the simulated satellite experiment demonstrating the accuracy of the proposed empirical model with varying transmission angles.

Future work should focus on data collection during earlier stages of the cotton growing season, to further validate the model and explore other factors such as plant moisture content, environmental factors and transmission parameters, all which could further impact attenuation.

University of Southern Queensland

School of Engineering

ENP4111 Research Project

Limitations of Use

The Council of the University of Southern Queensland, its School of Engineering, and the staff of the University of Southern Queensland, do not accept any responsibility for the truth, accuracy or completeness of material contained within or associated with this dissertation.

Persons using all or any part of this material do so at their own risk, and not at the risk of the Council of the University of Southern Queensland, its School of Engineering or the staff of the University of Southern Queensland.

This dissertation reports an educational exercise and has no purpose or validity beyond this exercise. The sole purpose of the course pair entitled “Research Project” is to contribute to the overall education within the student’s chosen degree program. This document, the associated hardware, software, drawings, and other material set out in the associated appendices should not be used for any other purpose: if they are so used, it is entirely at the risk of the user.

University of Southern Queensland

Faculty of Health, Engineering and Sciences

ENG4111/ENG4112 Research Project

Certification of Dissertation

I certify that the ideas, designs and experimental work, results, analyses and conclusions set out in this dissertation are entirely my own effort, except where otherwise indicated and acknowledged.

I further certify that the work is original and has not been previously submitted for assessment in any other course or institution, except where specifically stated.

Nicholas Manns

001092436

Acknowledgements

Firstly, I would like to thank my friends and family for their unwavering support, not only during this research project, but throughout my entire university journey. Your words of encouragement and belief in me have been a constant source of strength, helping me persevere through the past eight years.

Thank you to my supervisor Paul Wen whose guidance and insightful feedback have been crucial throughout this research project.

Lastly, I would like to extend my sincere thanks to my colleagues at Santos. I have been extremely fortunate enough to have worked alongside some of the brightest minds in the industry. Your willingness to impart knowledge and provide motivation has been instrumental in not only my career, but my academic journey. Without your assistance and motivation, I truly do not know if I would have ever gotten through it all.

Table of Contents

Contents

List of Figures

List of Tables

Glossary of Terms

BW - Bandwidth

dB - Decibel

Hz – Hertz

IEEE - Institute of Electrical and Electronics Engineers

IoT – Internet of Things

ITU – International Telecommunications Union

LEO – Low Earth Orbit

LoRa – Long Range

LoS – Line of Sight

NLoS – Non-Line of Sight

Rx - Receiver

RF – Radio Frequency

RSSI – Received Signal Strength Indicator

SF – Spreading Factor

SNR – Signal to Noise Ratio

TSR – Transmission Success Rate

Tx - Transmitter

WSN – Wireless Sensor Networks

1. Introduction

In today's rapidly evolving agricultural sector, farmers are confronted with an array of complex challenges related to water usage, resource allocation, and asset management, affecting agricultural communities worldwide. According to the United Nations, soil erosion alone costs the industry upwards of $400 billion, underscoring the critical need for enhanced erosion control measures and more sustainable farming techniques (Borelli, 2017). With agriculture accounting for approximately 70% of total global freshwater consumption, it is extremely alarming that an estimated 60% of this water wasted due to outdated and inefficient irrigation methods (Nuccitelli, 2022).

The emergence of wireless innovations like LoRaWAN has empowered agronomists to deploy in-field sensors, revolutionizing data gathering for irrigation optimization. This has led to enhanced crop yields, minimized water consumption, and improved soil health. However, the deployment of these technologies is often marred by connectivity challenges, undermining the confidence of farmers in the reliability of these systems. In this context, Low-Earth-Orbit (LEO) satellites emerge as a promising remedy to address these connectivity hurdles. LEO satellites are positioned at an altitude between 160 to 2,000 kilometres above the Earth’s surface. Being so close means, these satellites can only “see” a small area of the earth surface, so their coverage is much like say, a ribbon tied around the earth (Seneviratne, 2023). To provide anything like global coverage, with minimal latency would therefore require “constellations” of LEO satellites with orbits crisscrossing the earth. Fortunately, in an agricultural setting, high latency is not necessarily a major deterrent for data collection means (within reason).

Enter, Myriota. Global leaders in low-cost, low-power, secure direct-to-orbit satellite connectivity for the Internet of Things, this exciting communications company provides an alternative networking means particularly suited to an agricultural setting (Myriota, 2023). Leveraging advanced IoT devices and sensors integrated with Myriota's cutting-edge connectivity solutions, farmers can now access vital crop information from any location. This technology facilitates a range of applications, from monitoring livestock and soil moisture levels to assessing crop health and environmental conditions, empowering farmers to refine their practices for maximum efficiency.

Myriota's reliable connectivity empowers both farmers and other agricultural professionals to save water, reduce resource wastage, and transition to more environmentally friendly farming methods. The combination of reliable and secure connectivity, along with innovative IoT sensor technology is set to revolutionise the agricultural sector, paving the way for a more sustainable future for farmers globally.

Objectives and Aims:

The main aim of the work is to evaluate the impact of cotton crop canopies on radio-frequency (RF) signal attenuation and the subsequent implications for the reliability of satellite-based communications used in agriculture.

Specific Objectives:

- Understand fundamental principles of RF propagation in cotton crop canopies.
- Analyse physical characteristics (moisture content, crop height etc) and their individual effect on RF attenuation.
- Identify potential mitigation techniques to enhance communication reliability.
- Create a model that predicts RF attenuation levels based on both crop and environmental characteristics.
- Provide practical recommendations based on the findings of the project.

Expected Outcomes:

- Obtain a comprehensive data set, detailing RF attenuation under varying crop and environmental conditions.
- A predictive model that can estimate RF attenuation based on crop and environmental conditions.
- Strategies to mitigate effects on RF attenuation (device placement, signal frequency and signal processing techniques)
- Provide a framework for further research work that can be applied to other cropping applications.

2. Literature Review

2.1 Introduction

This literature review is structured into several key chapters, each aimed at thoroughly exploring distinct facets of radio-frequency propagation. The review begins by exploring the foundational concepts of radio frequency (RF) signal transmission, establishing a comprehensive understanding of the essential principles vital for effective transmission. The subsequent section delves into the methodologies employed in measuring and modelling RF attenuation. This part of the review sheds light on the various analytical and empirical approaches used in the field, offering insight into the various techniques and tools available. From there, an examination of prior studies focused on radio wave propagation through vegetated areas. This analysis serves to highlight existing knowledge while ensuring the novelty of this specific research project by identifying any overlapping concepts.
The focus then narrows to the specific phenomenon of RF attenuation within cotton crops, exploring the myriad environmental factors that significantly influence signal degradation. This section is complemented by an overview of current technological applications that employ RF communications within an agricultural context, providing a practical backdrop to the theoretical discussions.
The review then looks at how Wireless Sensor Networks are currently being utilised in the agricultural industry, and how understanding and improving signal attenuation rates could improve their reliability and effectiveness.
The final chapter summarises the findings from the literature, identifying gaps and areas that have yet to be explored. This critical evaluation sets the stage for the introduction of a unique and novel concept, which will serve as the focal point for the remainder of the research project.

2.2 Foundational Concepts

2.2.1 History

The first recorded use of utilising electrical signals to transmit information over a distance can be traced back to 1844, when the very first telegraph message was transmitted over cable. However, it would be nearly fifty years before American engineer G. M Marconi and Russian physicist A.S. Popov would succeed in their quest to transmit a signal between two spatially separated points using only radio waves, heralding the dawn of wireless communications (Saakian, 2020).
The concept of a radio wave, as defined by the Institute of Electrical and Electronics Engineers (IEEE) as “an electromagnetic wave within the frequency portion of the electromagnetic spectrum”. This spectrum encompasses a vast array of frequencies, from a several hertz up to 3THz. The spectrum is divided into several frequency bands, based on decimal division.

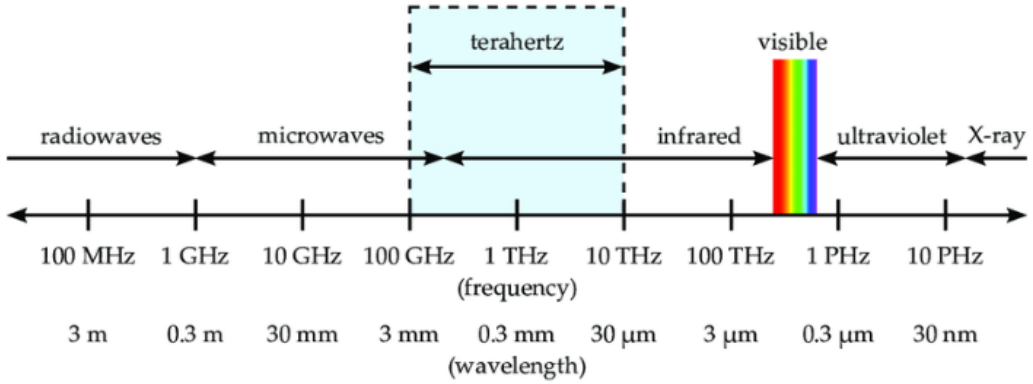

Figure 1. The electromagnetic spectrum and decimal banding (Patzold, 2017)

Table 1. Frequency Band Designations

Band	Designation	Frequency Range
Extremely Low Frequency	ELF	<3kHz
Very Low Frequency	VLF	3 – 30kHz
Low Frequency	LF	30 – 300kHz
Medium Frequency	MF	300kHz – 3Mhz
High Frequency	HF	3 – 30MHz
Very High Frequency	VHF	30 – 300MHz
Ultra-High Frequency	UHF	300MHz – 3GHz
Super-High Frequency	SHF	3 – 30GHz
Extra-High Frequency	EHF	30 – 300Ghz

Marconi and Popov's work was largely built on the theoretical concepts theorised by Scottish mathematician J. C. Maxwell. Maxwell had theorised the displacement currents in dielectrics and vacuums, generalising the concept of current continuity in Ampere's law. His fundamental equations surrounding electromagnetism (later known as Maxwell's equations) were later revised to achieve complete and symmetric form by the introduction of magnetic currents. This subsequently made possible the understanding of the nature of electromagnetic waves capable of propagating free space. This was verified through experimentation work carried out by Henry Hertz, where he successfully demonstrated a "propagation" of a spark from a transmitting Leyden jar to the terminals of a remote receiving antenna (Saakian, 2020).

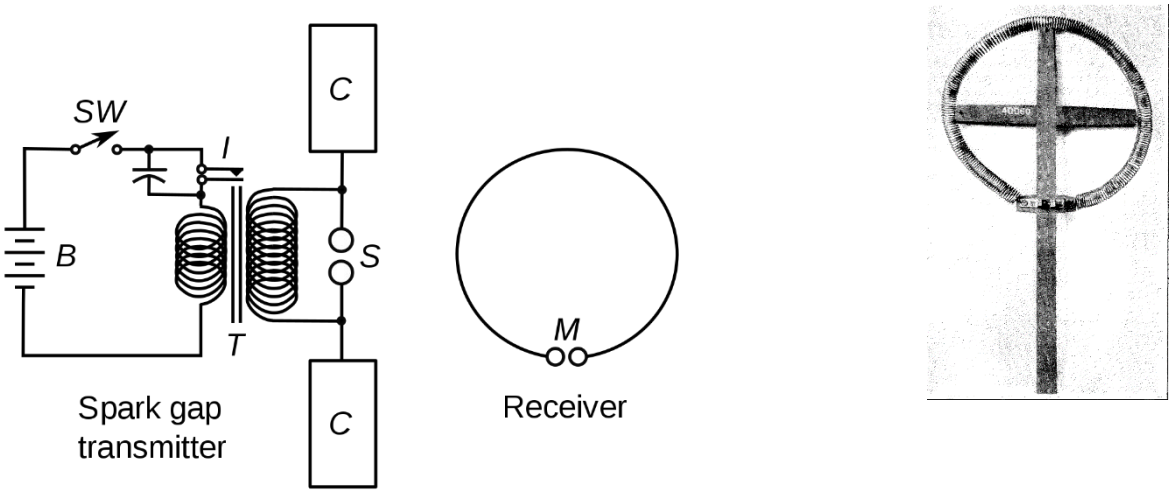

Figure 2. Hertz's 1987 apparatus for generating and detecting radio waves (Appleyard, 1927)

After Marconi and Popov's groundbreaking work, the field of wireless communications experienced significant development. A major breakthrough came in December 1901, when a wireless signal was successfully transmitted across the Atlantic Ocean, connecting the United Kingdom and Canada. This achievement demonstrated the potential of long-range wireless communication and laid the groundwork for rapid technological progress in the years that followed.
The subsequent decades, which included two world wars, significantly advanced the field of wireless communications, leading to the implementation of more sophisticated and secure methods of transmitting wireless signals. During this period, it was generally considered that lower radio wave frequencies offered more favourable propagation conditions than their higher frequency counterparts. Nevertheless, an increasing demand to transmit larger amounts of data within a single transmission necessitated the use of higher carrier frequencies. These higher frequency bands, whilst capable of carrying more data, were also more susceptible to attenuation under certain atmospheric conditions, as well as other propagation phenomena such as refraction, reflection, and scattering of the radio waves.

2.2.2 Propagation Basics

Understanding the mechanisms by which radio waves propagate is crucial for designing efficient and reliable communication systems.

Radio waves tend to propagate between a transmitting source and a receiving an antenna in two distinct manners;

1. Guided Propagation: The transmission of signals using a physically connected, guiding system such as a coaxial cable, optical fibre or wire-line. These systems confine the waves within the guiding system, minimising loss and interference.
2. Free Propagation: The transmission of signals over free space (Earth's atmosphere, underwater etc). In this application, radio waves travel from the transmitter to the receiver, without being confined within a physical medium.

(Richards, 2008)

For the purposes of this research project, discussion will be limited to free propagation. This is driven by the project's aim to understand the characteristics of radio wave transmission in open environments, as used in Myriota technology.
Within the free propagation domain, there are four predominate propagation mechanisms by which radio waves move between two antennas over free space.

Direct Wave: In this situation, the radio wave propagates from a transmitting source to the receiving antenna over 'an obstructed ray path'. Examples include Earth to space (uplink), space to Earth (downlink) or space to space parts of a satellite communication system. This mechanism is also applicable to Line-of-Sight (LOS) systems used on Earth.

Reflected Wave: The radio wave travels from a transmitting source to the receiving antenna via a reflection from a boundary of two media, where the boundary is of a size that is much than that of a wavelength and is relatively close to the flat surface.

Scattered or Secondary Wave: These arise during the propagation process when radio waves encounter scatterings, typically observed as the wave reflects off a rough or irregular surface. These scatterings are observable when the dimensions of scatters (or random globules) are the same size or smaller than the wavelength itself. Each globule then presents as a secondary radiator of the random origin. This phenomenon continues, with the creation of subsequent globules, each derived from its predecessor, forming a scattering of microwaves at a variety of angles.

Diffracted Wave: This term refers to a radio wave that has been altered by an obstacle or some other inhomogeneity in the medium by means other than a reflection or refraction. For diffraction to occur significantly, the obstruction must have dimensions that are comparable or greater than the wavelength itself. If the obstruction is smaller than the wavelength, the wave will typically just bend or 'diffract' around it, continuing with its propagation largely unaffected.

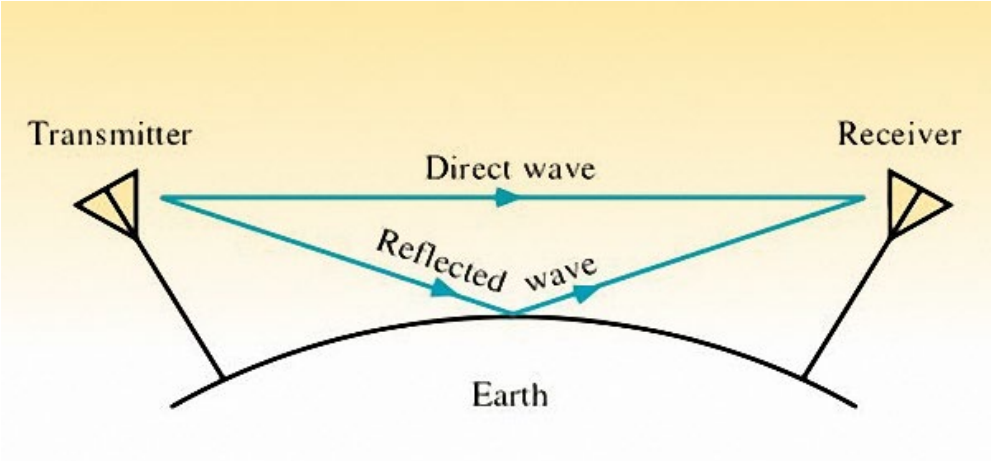

Figure 3. Direct and reflected wave propagation (Bhattacharya, 2019).

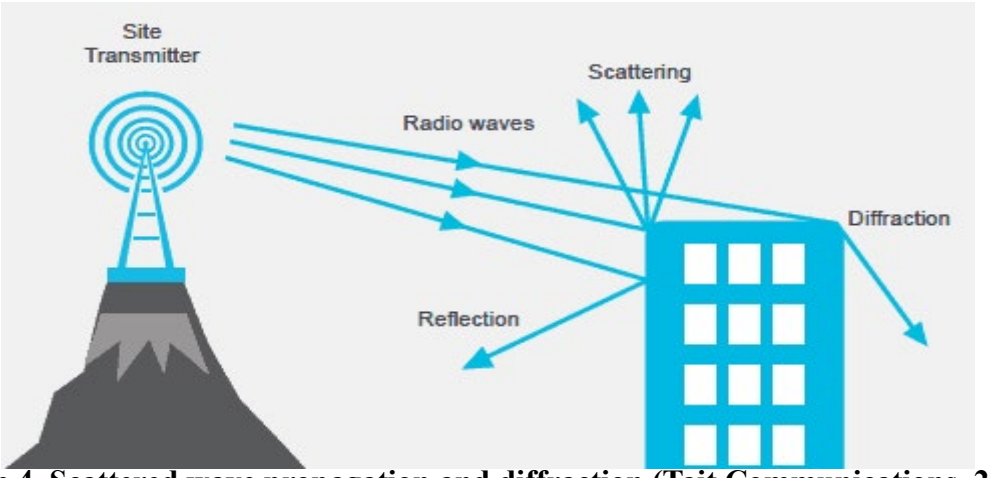

Figure 4. Scattered wave propagation and diffraction (Tait Communications, 2015).

In addition to the above propagation mechanisms, the specific characteristics of the medium through which the radio waves are propagating through, also play a crucial role. Wave factors such as speed, direction and strength are all significantly impacted by the unique properties found in mediums such as vacuums, the Earth's atmosphere, water and solid materials.

Vacuum: In a vacuum, there is an absence of matter which means that radio waves travel at the speed of light, with no attenuation or interference.

Atmosphere: The Earth's atmosphere is made up of several layers of varying densities and compositions. These conditions, along with environmental conditions such as temperature, heat, humidity and atmospheric pressure all influence how signal transmission behaves.

Water: Radio waves experience significant signal strength loss when propagating through water, especially saltwater with its conductive properties.

Solid Materials: Solid materials pose as an obstruction to the radio wave propagation path and typically lead to some form of reflection, diffraction or scattering effect.

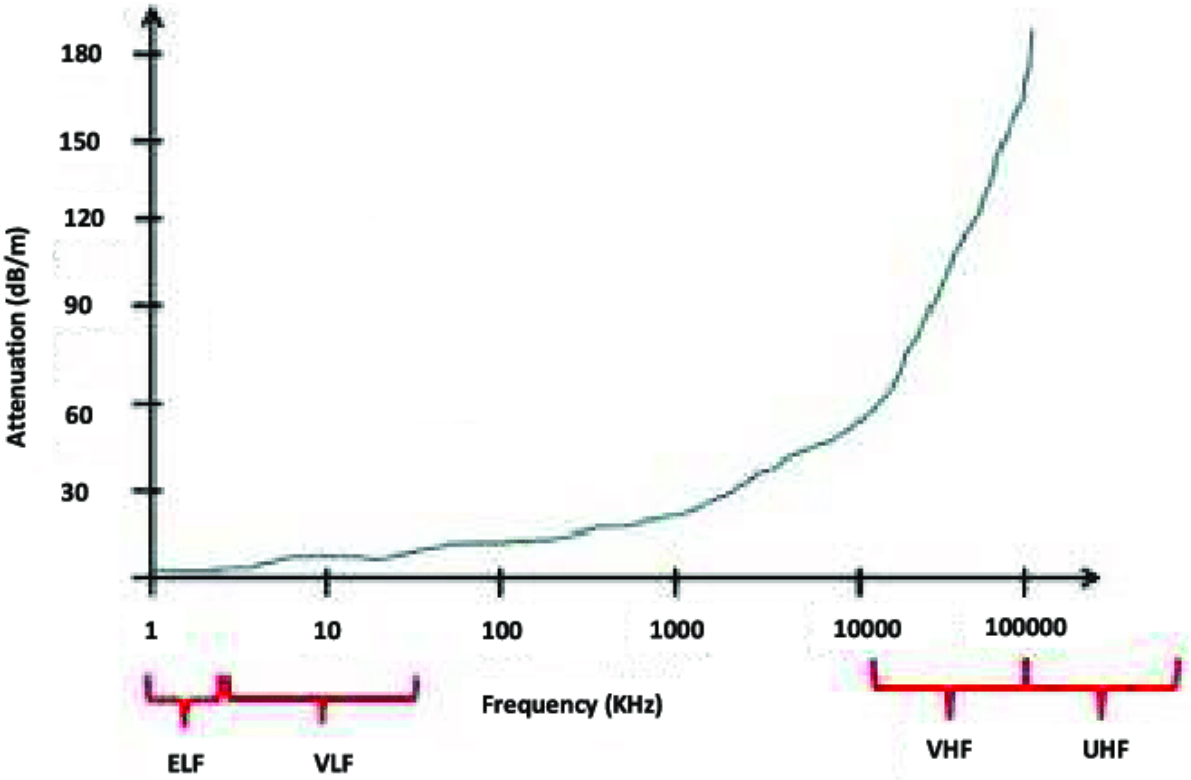

Figure 5. Radio wave attenuation/signal loss in sea water (Kaushal et al. 2016)

Each of these propagation mechanisms along with the mediums through which the wave is propagating through, contribute to a reduction of power of the original source signal by the time it arrives at its intended destination. This decrease in signal strength, commonly referred to as attenuation, is a determining factor in the design and implementation of any wireless communication system and requires suitable consideration to ensure reliable and efficient signal transmission.

2.3 Measuring and Modelling Radio Frequency Attenuation

Understanding and developing suitable means of accurately measuring and modelling radio wave attenuation is critical in ensuring the performance of wireless communication systems – particularly in the ever-changing conditions found in agricultural environments.

A substantial body of research into the measurement of radio wave attenuation currently exists. Early research in this field focused predominately on the development of free-space attenuation models, which only take into consideration the inverse square law of propagation within a vacuum. Despite this 'simplistic' approach, the formulation of the Friis Transmission Equation laid the groundwork for further investigation in attenuation modelling in more complex environments.

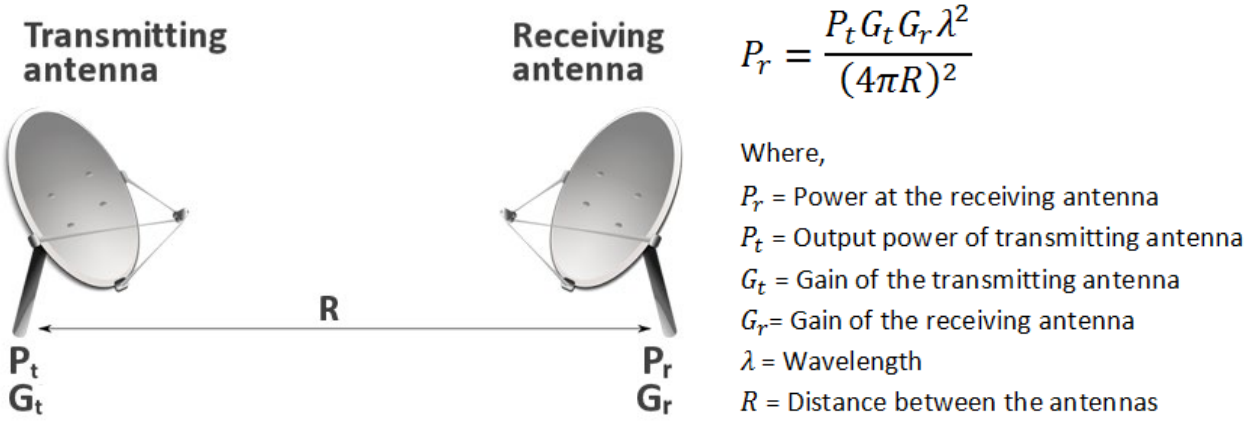

Figure 6. Friis Transmission Equation (everythingRF, nd)

As the need for more reliable and predictable wireless communication systems grew, especially in diverse and challenging environments, researchers sought to understand and quantify various factors that could affect signal quality. These factors include atmospheric conditions, terrain variations, and vegetation density, among others. In response to this growing need, the International Telecommunication Union (ITU) stepped in to provide structured guidance and methodologies through a series of recommendations. One notable publication in this regard is ITU-R P.530-17, which outlines methodologies for integrating complex attenuation factors into predictive models for radio wave propagation.

The ITU-R P.530-17, along with some other recommendations, introduces several key models that have become staples in the design and analysis of wireless communication systems. These include the Free-Space Path Loss Model, Rain Attenuation Model, Multipath Fading Model, Diffraction Over Terrain Model and the Atmospheric Absorption Model.

These models serve as the foundation for many of today's wireless communication systems. They encapsulate a comprehensive body of knowledge concerning radio wave propagation, offering a blend of practical insights and sophisticated mathematical modelling.

Overall, the recommendations and models provided within the ITU-R suite, forms the basis of many of today's wireless communication systems. It encapsulates a wealth of knowledge on radio wave propagation, offering both practical advice and mathematical models to address the dynamic conditions which impacting signal attenuation.

More recently, there has been a shift towards incorporating site-specific measurements into predictive models. This approach leverages advanced techniques to gather data directly from the environment where the communication system will operate. By doing so, it allows for more accurate and tailored predictions, taking into account the unique characteristics of each site. This evolution in methodology underscores the continuous effort to refine and enhance the predictability and reliability of wireless communication systems in the face of ever-changing environmental conditions. studies have focused more on utilising site-specific measurements, using techniques such as ray-tracing simulations and machine learning to model attenuation more accurately.

In an agricultural context, the varying vegetation and terrain presents a unique challenge when trying to accurately predict radio wave attenuation. In this body of research, Barrios-Ulloa's 2022 literature review stands out. Reviewing and assessing the accuracy of existing attenuation models in vegetated environments, Barrios-Ulloa noted that critical factors such as plant geometry, composition and layout had not been captured, despite the obvious impact they have on attenuation rates. Barrios-Ulloa recommended further model developments that encompass machine learning to capture these factors and produce more dynamic modelling methods.

Table 2. Barrios-Ulloa's evaluation of current propagation models

Reference	Models	Environment	Technology	Summary of Results
[16]	FSPL, Two-Ray	Grass	RF equipment	- Two-Ray and FSPL do not adequately represent measurements.
[12]	COST-235, ITU-R, Weissberger	Agricultural fields	Zigbee	- COST-235 was the largest overvaluation of losses in all growth stages of the crop. - Weissberger was the one with the greatest underestimation of losses in all stages of the crop.
[27]	COST-235, FSPL, Weissberger	Agricultural fields	RF equipment	- FSPL, Weissberger, and ITU-R show similar trends and differ from the observed path loss values. - COST 235 features higher precision.
[38]	ITU-R	Agricultural fields	Zigbee	- FITU-R was the most accurate in a setting with no leaves on the trees. - FSPL presented the highest difference concerning the measures.
[40]	FITU-R, ITU-R, Weissberger	Agricultural fields	RF equipment	- FITU-R was more accurate at frequencies below 2 GHz. - COST235 was more accurate at frequencies above 2 GHz.
[39]	FSPL, MED	Agricultural fields	Zigbee	- FSPL, adjusted to the measurements, was the most accurate with grass heights of 15 cm (*RMSE* of 4.5) and 1 m (1.62). - MED, adjusted to measurements, was the least accurate with grass heights of 15 cm (*RMSE* of 4.65) and 1 m (1.9).
[42]	ITU-R, Weissberger	Agricultural fields	Zigbee	- Weissberger was the most accurate with an R2 of 0.62 when adjusted.
[43]	COST-235, FITU-R, FSPL, ITU-R	Agricultural fields	RF equipment	- FITU-R was more accurate at 2.4 GHz. - ITU-R and FITU-R show similar trends at 870 MHz. - FSPL was the one with the greatest difference concerning the measurements.
[44]	COST-235, FITU-R, Weissberger	Agricultural fields	Zigbee	- FITU-R, in all the combinations of the experiment, presented the highest precision (*RMSE* between 3.8 and 13.6). - COST-235, in all the combinations of the experiment, presented the highest overvaluation (*RMSE* between 8.0 and 26.8).
[18]	COST-235, FSPL, ITU-R, Two-Ray, Weissberger	Greenhouse	Zigbee	- Two-Ray presented was more accurate with node antenna height of 0.5 m (% error between 0.65% and 26.25%). - FSPL presented the greatest difference with node antenna height of 0.5 m (% error between 4.52% and 42.84%). - ITU-R added with Two-Ray and Weissberger added with Two-Ray were the most accurate with a node antenna height of 1.5 m.
[46]	COST-235, FSPL, ITU-R, Two-Ray, Weissberger	Forest or jungle	Zigbee	- Two-Ray was more accurate (*MAPE* 25%). - ITU-R was the one with the greatest difference concerning the measurements (*MAPE* of 89%).
[48]	FSPL, Two-Ray	Agricultural fields	Zigbee	- FSPL presented a low performance in all stages of the culture (*RMSE* between 10.33 dB and 18.19 dB). - Two-Ray showed a decrease in *RMSE* when increasing the height of the node antenna.
[53]	COST-235, FITU-R, FSPL, ITU-R, Two-Ray, Weissberger	Greenhouse	Zigbee	- COST-235 added with FSPL was the most accurate (*MAPE* of 10.69%). - Weissberger added with Two-Ray presented the greatest difference concerning the measurements.
[56]	FSPL	Forest or jungle	WiFi	- FSPL presented high overvaluation of the measurements.
[58]	COST-235, FITU-R, FSPL, Weissberger	Forest or jungle	RF equipment	- All models underestimated the measurements (*RMSE* up to 68 dB at 25 m).
[60]	COST-235, FITU-R	Forest or jungle	WiFi	- FITU-R and COST-235 presented high overvaluation of the measurements.

Whilst modelling remains an important tool in network design, an understanding of the actual attenuation rate data is imperative for ensuring the accuracy and reliability of the implemented models. Among the various techniques for quantifying radio wave attenuation, field strength measurement stands out as the most direct and commonly utilised method. This technique entails capturing the intensity of a signal transmitted from a source at different distances, typically using a spectrum analyser.

The measurement of field strength is a measurement of the electronic field in volts/metre as per below:

$$E = \sqrt{120\pi P}$$

Where E = rms value of field strength in volts/metre

P = power density in watts/$metre^2$

120π = impedance of free space in ohms

Whilst the equation above provides the means of calculating the field strength of the transmitted signal, this value is typically determined by measuring the voltage level of the received signal (Receiver Voltage) and factoring in the Antenna gain (K), which is generally supplied by the manufacturer.

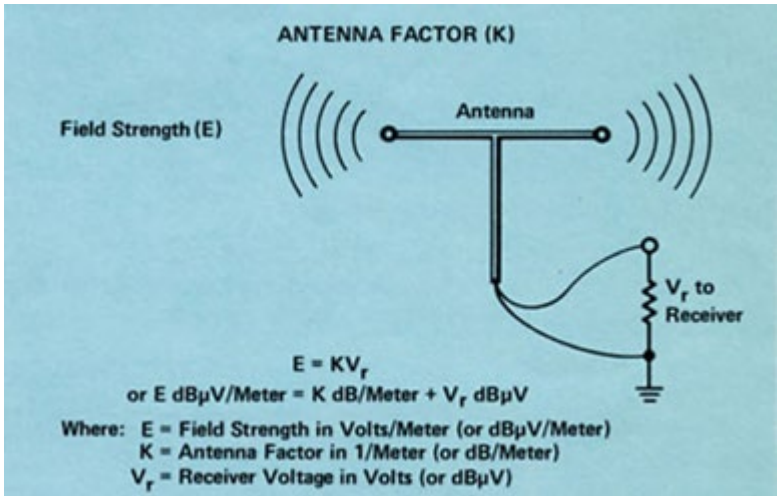

Figure 7. Antenna Factor is used to convert the receiver voltage reading to field strength (Hewlett Packard, 1976).

The Received Signal Strength Indicator (RSSI) is another widely adopted metric for assessing radio wave attenuation. RSSI, an indirect measure of the power level in a received radio signal, offers a practical way to evaluate signal attenuation. It is especially valuable in scenarios where direct measurements pose difficulties, allowing for the estimation of the distance between devices and the overall integrity of a communication link. Despite its practicality, RSSI measurements are not without their limitations. They can be influenced by a range of factors, including interference from other signals and the effects of multipath propagation. Furthermore, the inconsistency in RSSI reporting across different devices and manufacturers complicates the accuracy assessment of these measurements.

Despite significant advancements in measurement techniques, the field continues to face challenges such as environmental variability and the ever-changing nature of many attenuation factors. These complexities make the precise measurement of signal attenuation a daunting task. Consequently, ongoing innovation is essential to overcome these hurdles and improve the accuracy of signal measurements in the evolving landscape of wireless communication systems.

2.4 Radio Wave Propagation in Vegetation

Vegetation impacts radio wave propagation through mechanisms such as absorption, scattering and reflection. These factors all add to attenuation and degrade overall signal transmission quality. Heavily influenced by factors including:

- Frequency of signal
- Density and type of vegetation
- Environmental Conditions (plant moisture content)

As detailed earlier, the frequency at which signals are transmitted at plays a significant role in its propagation characteristics. It is generally understood that higher frequency signals (UHF and above), experience higher attenuation when passing through vegetation compared to that of lower frequency signals. This can largely be attributed to the longer wavelengths found in lower frequency signals, with the longer length being able to diffract around the vegetation, rather than be absorbed or reflected by them.

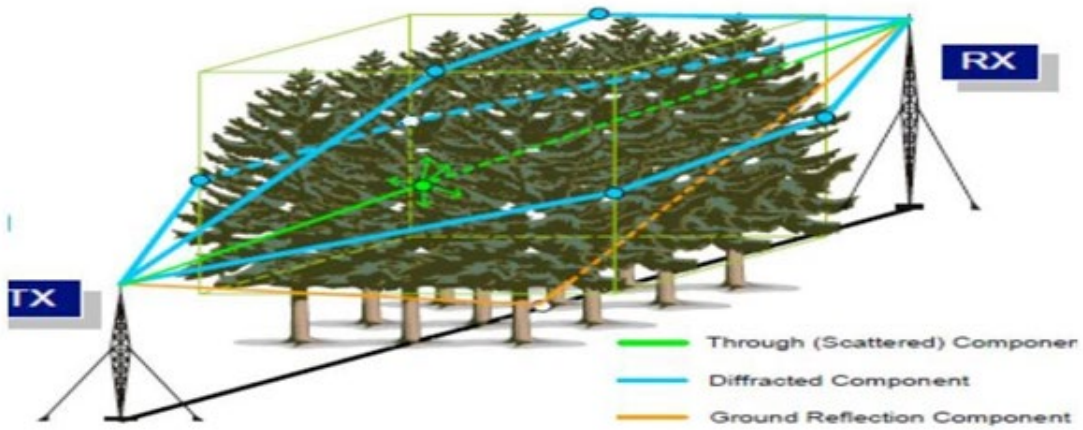

Figure 8. Different Mechanisms of Signal Propagation Through Vegetation (Adegoke and Siddle, 2012).

Vegetation Height and Density

As previously discussed, both the height and relative density of the vegetation dramatically influences the rate of attenuation on radio signals. The ITU-R P.833-10 provides methods to calculate the effective path length of a radio wave as it traverses through vegetation. Taking into account the incidence angle of the wave and the overall thickness of the foliage layer of the vegetation, an estimation of attenuation can be determined.

Representative radio path in woodland with vegetation path length, d, average tree height, h_v, height of the Rx antenna over ground, h_a, radio path elevation, θ, and distance of the antenna to the roadside woodland, d_w

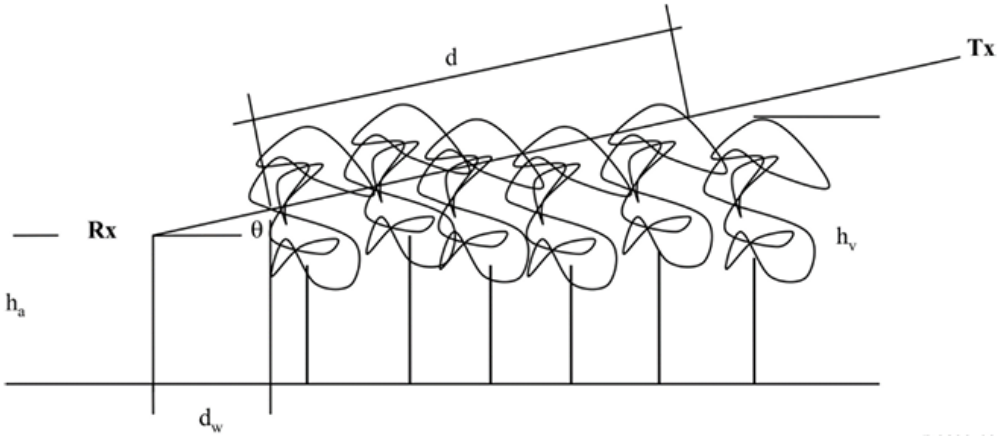

Figure 9. Representative radio path in woodland with vegetation path length, d average tree height, ha, height of the Rx antenna over ground, hv, radio path elevation, θ, and distance of the antenna to the roadside woodland, dw (International Telecommunications Union, 2021)

The attenuation loss, L along both the horizontal and slant foliage path propagation, can be estimated using the following model:

$$L(dB) = A\, f^{\boldsymbol{B}}\, d^{C}\ (\theta + E)^{G}$$

Where:

$f = frequency\ (MHz)$

$d = vegetation\ depth\ (m)$

$\theta = elevation\ (degrees)$

$A, B, C, E\ and\ G = empirical\ found\ parameters$

Along with providing theoretical models and calculations to estimate attenuation rates, the guideline offers practical advice on associated aspects such as antenna placement and selection of transmission frequencies. It also stresses the need for empirical validation when utilising the models to unstudied areas.

Research carried out by Adegoke et al. (2016) analysed the scattering effects found when radio waves encounter discontinuities in the medium through which they are travelling, such as leaves and branches in a vegetated area. They found that more densely vegetated areas caused greater rates of scattering and higher signal attenuation. Another key finding was the correlation between the moisture content found in the sample vegetation and the level of signal attenuation – particularly in the microwave frequency range. This was largely attributed to the dielectric properties of water, which strongly absorb the waves.
These bodies of research demonstrate the complex interaction between radio waves and vegetation, heavily influenced by a multitude of dynamic factors. Whilst nearly impossible to accurately predict the exact effect the specific vegetation will have on signal attenuation, a critical understanding of their effects is vital in the optimal design and integration of wireless

communication systems in vegetated areas.

In a study akin to this research project, Horak et al (2010) conducted an innovative experiment by situating a transmission source within several densely forested locales, effectively obstructing line-of-sight (LOS). They utilized a remotely operated drone, functioning as a makeshift satellite, equipped with a receiving station. The experimental setup involved recording data as the drone operated at various elevation angles, ranging from 20 to 90 degrees, and testing the transmission with carrier signals across a spectrum of frequencies.

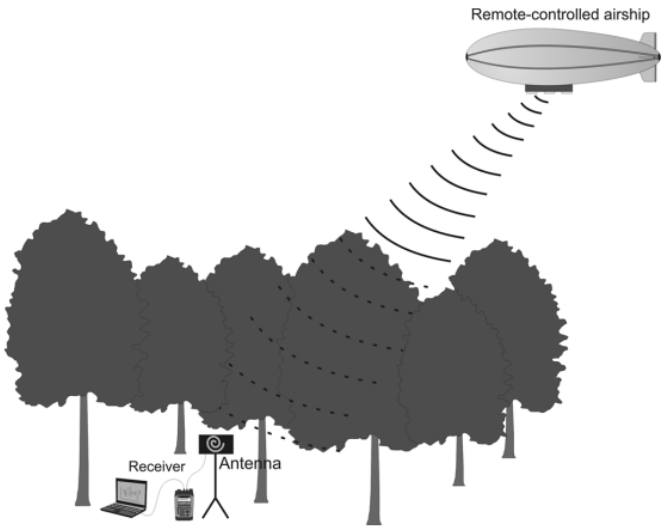

Figure 10. Diagram of Horak's experiment.

The findings from this experiment highlighted the correlation between increased frequency and heightened signal attenuation. Although the study did not delve into detailed data concerning the impact of the satellite's elevation angle on signal attenuation, it acknowledged observable consistencies. Specifically, they noted an attenuation around 10dB at elevation angles spanning 20 to 40 degrees, aligning with findings from Sofos and Contatinou's 2004 study. Their study examined the influence of roadside vegetation on Land Mobile Satellite Systems, particularly at medium and low elevation angles, and introduced a predictive model tailored for rural propagation environments.

This body of work underscores the nuanced interplay between frequency, elevation angle, and environmental factors like vegetation in shaping radio wave propagation, offering valuable insights for enhancing the design and deployment of wireless communication systems in similar settings.

2.5 Cotton Cropping and Radio Frequency Attenuation

Cotton, a perennial crop of significant economic importance, serves as the backbone of the textile industry worldwide. Cultivation practices for cotton tends to vary significantly across growing regions, heavily influenced by local environmental conditions and agronomic practices. Key factors in cotton agriculture include seed selection, soil preparation, irrigation, pest management, and harvesting techniques.
Cotton's growth cycle can be divided into several key stages: planting, irrigating, flowering/boll development, maturation and picking/harvesting. Each stage is critical to the

final yield and quality of the cotton fibre, with environmental factors such as temperature, moisture, and sunlight playing pivotal roles in the plant's overall development.
In recent years, focus has been put on the industry to improve its overall sustainability. A typically heavy user of water and chemicals, there have been numerous studies on the impact the industry has on biodiversity and the environment.
As part of this research, there have been calls for growers to transition their traditional growing practices to more sustainable methods. Some of these practices include the implementation of wireless sensor networks (WSN) throughout the planted crop, facilitating the use of precision agriculture practices.
Despite the push for growers to implement such practices, there has been some reluctance to fully get on board with the technology – predominately due to its lack of reliability. The physical and biological makeup of a cotton crop canopy, including its leaf size, shape and water content, interacts with transmitted signals, leading to attenuation through absorption, scattering and reflection. Studies conducted by Peden et al (2021) have highlighted the correlation between vegetation density and the water content of leaves, playing a crucial role in signal attenuation. With data collected, supporting the theory that a higher moisture content leads to greater absorption and subsequently< higher levels of signal loss (attenuation).

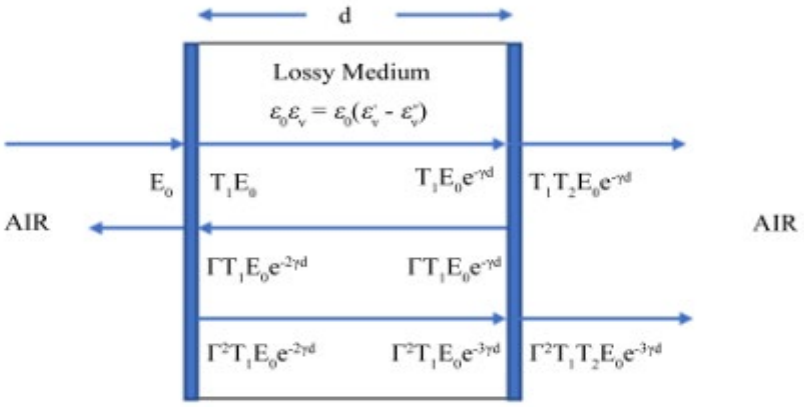

Figure 11. Wave propagation through a lossy homogenous medium, with a complex permittivity (Peden, 2021).

Other factors such as the height of the canopy and the distribution of foliage also have detrimental effects on transmitted signals. Goldhirsh and Vogel's (1989) work on signal attenuation in forests, highlighted the impact that spatial arrangement of vegetation can have on signal path, and how it can introduce multipath propagation issues. Some of their key findings were that worst case fades due to shadowing, occurs at lower elevation angles (<30 degrees). This was put down to the fact that more trees or vegetation would be intercepted by the transmitted signal between the transmitting source and the receiver.

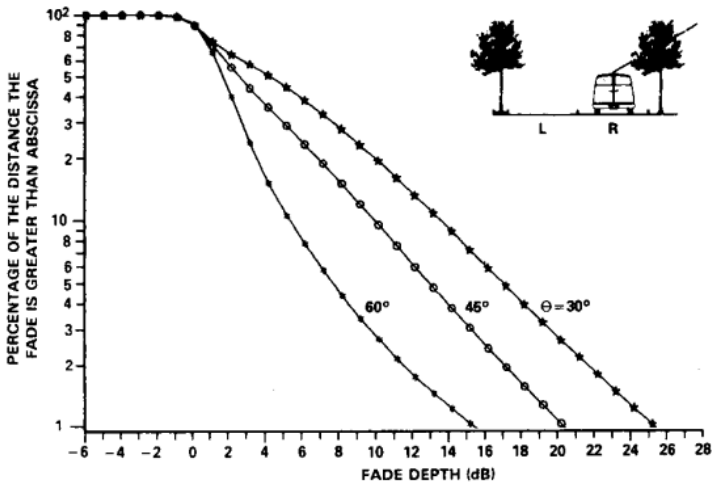

Figure 12. Comparison of cumulative distribution for signal loss for different elevation angles (Goldhirsh and Vogel's, 1989).

Despite the obvious need for widespread adoption of precision agriculture practices, the cotton industry has been slow to get on board – primarily due to their low reliability. Understanding the interactions between cotton crop canopies and radio waves is vital for the effective implementation and operation of WSN's in within a cotton application. Further research in this area should focus on the dynamic conditions specifically found within cotton crops and investigate mitigation techniques to reduce the effects they have on signal attenuation. This may lead to the development of more resilient communication protocols/technologies, improving reliability and increasing grower's confidence.

2.6 Wireless Sensor Networks in Agriculture

Agriculture is one of the economies largest contributors. Driven by a growing population, this industry has witnessed a transformative evolution, particularly since the 1950's, a period often referred to as Agriculture 2.0. This era marked the onset of "Mechanized Agriculture", with the overall scaling of what each farmer was able to produce using modern equipment increasing exponentially. This rapid increase in yield also resulted in a need to integrate advance technologies to combat the challenges posed by unpredictable environmental factors such as droughts and pest infestations. Innovations in more effective irrigation systems and pesticides were crucial in boosting agricultural productivity to meet the demands of the growing population.

Agriculture 3.0 saw the focus shift from machinery-based solutions to information technology. Key advancements in technology such as the introduction of Geographic Information Systems (GIS) and Global Positioning Systems (GPS) allowed farmers to map and monitor fields with unprecedented precision, introducing more efficient and effective ways to utilise their acreage.

The transition into Agriculture 4.0 signified a shift towards a more interconnected farming approach, building on the techniques previously established in Agriculture 3.0. The introduction of Wireless Sensor Networks (WSNs) revolutionised the way farming operations could be carried out. Capturing and relaying real-time data on crucial variables such as soil moisture content, temperature monitoring and nutrient concentrations, allowing growers to

make data- driven decisions, optimising resource allocation, improving crop health and increasing yield rates.

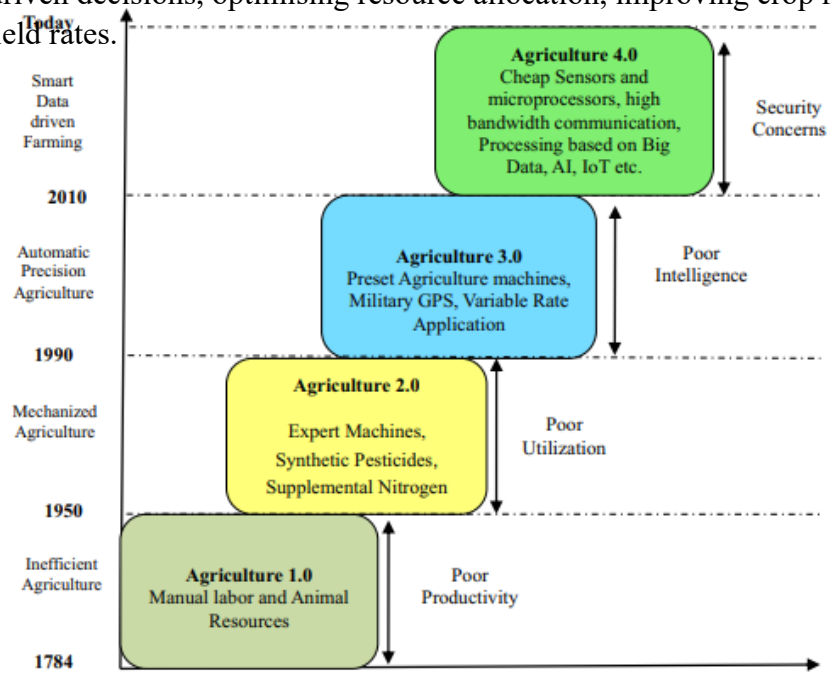

Figure 13. Key transitional periods in agricultural technology (Majumdar et al, 2021).

Some early uses of WSNs within the precision agriculture space include:
Pest and Disease Detection: Gas detection devices deployed in a paddock can pick up key early indicators of various pest or disease infestation. This early warning system allows farmers to take timely intervention and prevent the issue from spreading further.
Soil Analysis: As with Precision Agriculture, in-ground soil sensors can monitor soil conditions such as pH and nutrient levels and moisture content. This data assists famers to determine fertiliser and irrigation application rates, along with a general understanding of the overall soil health. This is crucial for long term strategizing of the property, ensuring the land is not overused.
Livestock Monitoring: GPS trackers and stations installed at watering locations, allowed farmers to track livestock movements and assess the herd's overall health based of key point indicators (lack of movement etc).

These early forms of WSNs have been instrumental in demonstrating the potential of such technologies to improve efficiency and sustainability in a variety of farming practices. However, the widespread adoption within the industry has been hindered by several significant challenges and limitations.

Some of the primary obstacles include:

Limited Battery Life: The early electronics used in WSNs were notorious for their high-power consumption, leading to an extremely limited battery life. Given that these sensors were typically deployed in remote locations, the frequent need for battery replacement rendered the technology impractical for widespread use.

Connectivity Issues: Early wireless networks struggled to provide coverage over extensive areas and tended to be more susceptible to physical obstacles such as dense vegetation. This would lead to frequent service disruptions, data loss or compromised data transmission, severely undermining users' confidence in the technology.

Cost: The initial investment required to set up a WSN was relatively high at the time, with growers generally having to install their own network infrastructure including a base station communication tower, along with multiple servers and other networking equipment. This high upfront cost made it a difficult sell to growers, considering the system's reliability issues.

Interoperability and Lack of Variety: The absence of a standardised communication protocol compounded the difficulty of integrating devices from different manufacturers, with growers often needing to engage a suitable third party to design and implement the WSN. Furthermore, the limited range of devices that were available restricted the type of data that was able to be collected, decreasing the system's usefulness to growers.

By 2024, however, the landscape for WSNs in agriculture has undergone significant transformation, thanks to ongoing advancements in technology. These improvements include extended battery life, a broader range of available sensors, the standardisation of communication protocols, and the integration of Internet of Things (IoT) technologies. These advancements have substantially enhanced the performance, reliability, and versatility of WSNs in the agricultural sector. A 2021 analysis conducted by Abdollahi et al, attributed this progression to an increase in targeted research initiatives and the proliferation of scholarly publications within this field.

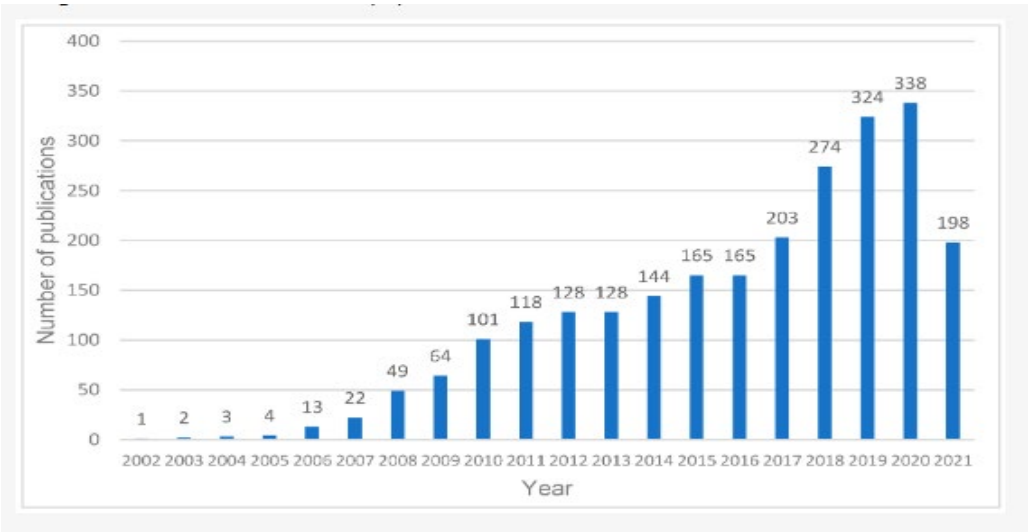

Figure 14. Annual distribution of publications associated with WSN applications in agriculture (Abdollahi et al, 2021).

2.7 Summary

Signal attenuation is an inevitable aspect of wireless communications, one that significantly impacts the performance and reliability of networks. A thorough understanding of the various factors that influence signal propagation is essential for predicting network performance and implementing effective mitigation strategies to protect against undesirable effects. Whilst the concept of signal attenuation modelling is well-established, the persistent recommendation

from current ITU guidelines for the integration of empirical data underscores the importance of site-specific modelling in achieving accurate predictions. Moreover, the existing body of research extensively covers the modelling of signal attenuation through various types of vegetation, particularly forest-type environments. However, there seems to be a notable gap in studies specifically addressing signal attenuation through cotton crop vegetation. Given the unique physical and biological characteristics of cotton plants, it is reasonable to assume that existing models may not adequately capture the nuances of signal attenuation in this agricultural setting. This highlights a potential area for future research, aimed at developing more refined models that takes into account the specific properties of different crop types, specifically cotton.

Additionally, much of the literature reviewed focuses on signal transmission between ground-based transmitters and receivers, a traditional approach in remote communication systems. However, the recent shift towards Low Earth Orbit (LEO) satellite-based systems represents a significant standard change. This transition necessitates a revaluation of existing attenuation models and the development of new frameworks that can accurately account for the unique challenges posed by satellite communication, such as increased path lengths, atmospheric conditions at higher altitudes, and the relative movement between satellites and ground-based devices.

In conclusion, whilst substantial progress has been made in understanding and modelling signal attenuation, the evolving nature of wireless communication technologies and the introduction of new application contexts, such as LEO satellite systems and agricultural settings with unique vegetation types, call for continuous research and innovation. Addressing these emerging challenges will not only enhance the accuracy of signal attenuation models but also contribute to the overall advancement of wireless communication systems, ensuring they meet the demands of precision agriculture.

3. Methodology

3.1 Introduction

The objective of this project is to determine the effect cotton crop canopies and vegetation have on radio frequency signal attenuation. Understanding this interaction is crucial for optimising network communication that relies on RF signals, particularly in an agricultural setting where crop vegetation can significantly degrade signal strength and quality.

Recognising the limitations faced when trying to interface with a Low Earth Orbit (LEO) satellite directly, the data gathering and analysis component of this assignment will focus on three separate cases: simulated modelling, controlled experiments, and finally uncontrolled real-world observations. By integrating these three approaches, this project aims to provide a thorough analysis of RF attenuation due to cotton crop canopies. The simulated models will offer theoretical benchmarks, the controlled experiments will provide detailed insights under specific conditions, and the uncontrolled observations will validate the findings in real-world scenarios. Collectively, these efforts will contribute to a deeper understanding of RF communication challenges in agricultural environments and assist in developing strategies to mitigate signal loss in similar applications.

3.2 Simulated Modelling

To gain a better understanding of the anticipated attenuation rates, this research will firstly use MATLAB to generate baseline data for comparison with the actual obtained experimental results. The simulated models will employ readily available equations, such as those found in ITU-R P.530-17. To maintain generality, only key principles and equations will be utilised, while more specific attenuation factors will be ignored. Consequently, discrepancies between the modelled data and experimental results are expected.

Free-Space Path Loss (FSPL)

FPSL is the reduction of signal strength as it travels through free space. It has been defined as:

$$FPSL(dB) = 20log_{10}(d) + 20log_{10}(f) + 20log_{10}(\frac{4\pi}{c})$$

Where:

3. d is the distance between the transmitter and LEO satellite (in metres)
4. f Is the frequency of the signal (Hz)
5. c is the speed of light ($3 * 10^8 m/s$)

To keep in line with the Myriota equipment, a transmitting/receiving frequency of 400MHz will be used. As LEO satellites can only operate at a maximum altitude of 2000km for them to be considered ‘low orbit’, a range of between 600km and 2000km will be used for the purpose of this simulation.

Atmospheric Absorption

Atmospheric absorption is the absorption of radio-frequency signals by the gases and particles present in the atmosphere. Largely dependent on the transmission frequency and specific atmospheric conditions, the ITU-R 676 has developed a general-purpose MATLAB program to calculate the attenuation coefficient on signals up to 1000GHz. Using this program and considering the typical operating frequencies of the Myriota network, an atmospheric absorption attenuation coefficient will be determined.

Other Important Attenuation Factors

Rain Attenuation: Rain can significantly add to signal attenuation – particularly at higher frequencies. ITU-R P.530 provides methods to accurately determine rain attenuation coefficients. However, this attenuation factor can largely be controlled/eliminated by carrying out the controlled experiments and real-world observations on sunny days.

Multipath Fading: Occurs when the signal takes multiple paths to reach the receiver. This is a difficult attenuation factor to determine before carrying out field measurements. Likely to play a significant role in attenuation in this project – potentially an updated model (after carrying out the field experiments), could provide a coefficient to use here.

Antenna Characteristics: Selection of appropriate equipment with a suitable gain, will assist in minimising any transmission losses.

Whilst considering these additional factors would likely improve the overall comprehensiveness of the model, their inclusion may unnecessarily complicate and slow down the overall process. For this reason, they will not be included in the model.

Even without the inclusion of all the above attenuation factors, the proposed model should provide a useful baseline for understanding the key principles of signal attenuation with LEO satellites. The modelled data will also help establish theoretical expectations and serve as a guide for interpretation of the experimental findings.

3.3 Controlled Experiment

In the controlled experiment, satellite communication will be simulated through a unique setup where an aerial drone substitutes for the LEO satellite. This drone will be equipped with a transmitting antenna and operated at varying heights and angles relative to a receiving antenna strategically placed within the cotton crops. This methodical variation is intended to emulate different satellite positions relative to the ground station.

Setup

A transmitting device and antenna will be suitably fixed to the drone, with the counterpart receiving base station installed within the cotton crop. The drone will then be flown over the cotton crop, altering its angle of transmission from 0 degrees, parallel to the cotton rows, to 90 degrees, perpendicular to the rows, in increments of 10 degrees. The specific altitude/distance at which the drone operates at relative to the receiving base station, will be determined based on baseline testing results. This baseline testing will capture measurements

of RF signal strength and quality between the transmitter and receiver with no obstruction in between. This will assess how different drone heights/distance influences signal attenuation, using the sensitivity range of the spectrum analyser as a guideline. These measurements will be crucial for use as a direct comparison to the attenuation effects observed during the cotton canopy interference tests.

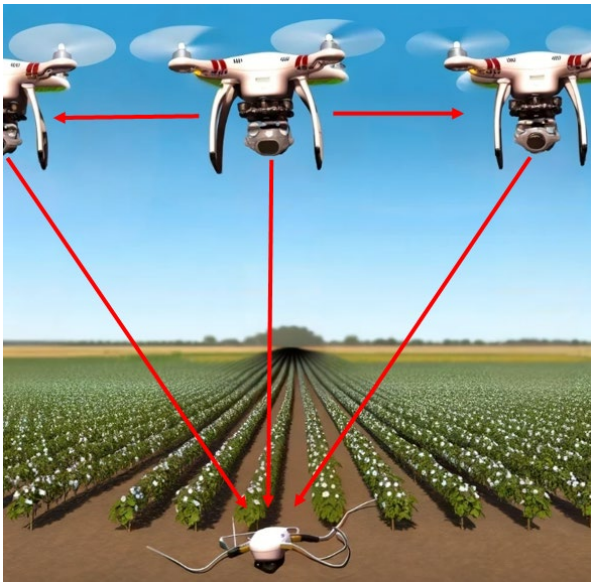

Figure 15. Simulated LEO satellite with different transmission angles.

To mitigate the influence of environmental variables, conditions such as temperature, wind speed, and humidity will be recorded during the tests, ensuring that the experiment's conditions are replicable, and that data integrity is maintained across different test scenarios. In addition to this, repeated measurements will be undertaken to enhance overall data reliability. Each angle will be tested twice, with measurements recorded on both sides of the transmitter (180 degrees apart), ensuring the collected data reflects a complete and unbiased effect of the RF attenuation due to the cotton canopy.

Required Equipment

Drone

- Capable of stable flight at varying altitudes.
- Suitable payload to carry on board transmitting antenna.
- GPS tracking for accurate positioning data.

Transmitting Device

- Operating frequency of 400MHz (to match Myriota equipment).
- TBA gain (aligned with specifications).
- Lightweight, able to be fixed to drone.

Receiving Device

- Operating frequency of 400MHz (to match Myriota equipment).
- TBA gain (aligned with specifications).
- Compatible with data logging software.

Spectrum Analyser

- Suitable resolution to capture RF signal strength and quality.

Weather Station

- To capture suitably accurate temperature, humidity and wind speed readings.

Data Logger

- Interface with spectrum analyser to record signal strength and quality.

Computer/Matlab

- Real-time data processing, angle calculations and presentation of data.

Analysis

Comparison to Baseline: After collecting a robust data set from the repeated measurements, a comparison will be made against the baseline (unobstructed) signal strength measurements. This should identify any significant deviations and quantify the attenuation caused by the cotton canopy.

Environmental Conditions: Determine any correlation between environmental conditions (wind, temperature, humidity) and signal attenuation. These effects should be largely eliminated by conducting the experiment in similar conditions.

Challenges and Considerations

Data Accuracy and Integrity: Obtaining accurate signal strength measurements will be crucial for data analysis. Working within the budget constraints of this project, may result in some equipment having less than optimal accuracy/resolution.

Interpreting Results: Understanding that this project focuses only on key causes of signal attenuation, but other contributing factors may influence the collected data. Acknowledge these limitations whilst using statistical tools to interpret the data.

Time Constraints: Cotton season in the Darling Downs typically runs from October (planting) until June (picking). The crop has a meaningful canopy for around two months, limiting the time to carry out the data collection experiments.

3.4 Uncontrolled Real-World Observations

In the uncontrolled experiment, the setup aims to measure the effect of cotton crop canopies on radio frequency attenuation in a more operational state, compared to the controlled setting. Here, the experiment leverages the natural overhead passes of Low Earth Orbit (LEO) satellites to assess the attenuation without the simulated conditions used in the controlled experiments.

Setup

The Myriota transmitting device is placed within the cotton crop at a fixed location, similar to that of the receiving antenna placement in the controlled experiments. The primary difference is that, in this uncontrolled scenario, the communication and signal strength measurements occur between the ground based Myriota transmitter and the orbiting LEO satellites.

Measurement Process

Satellite Revisit Time Understanding: The typical satellite revisit time, which is the time it takes for the satellite to pass within clear sky view, from the time that a message is queued on the Myriota Module. This cycle rate helps in predicting when the satellite will be in the best position to communicate with the transmitter placed among the cotton crops.

Current data indicates a median latency period of 4 hours or less for at least half of all messages to arrive, with a 90% latency period – that is, 9 out of 10 messages arriving in 9 hours or less. These latency timeframes are measured from when a message is first queued for transmission by the Myriota Module, to the time it has been received by the satellite, processed, sent to the Myriota Cloud and then pushed to its final destination.

Figure 16. Myriota Satellite Path

Data Collection: During each satellite pass, the Myriota device will ‘wake up” and continuously transmit data, including its position and time. This functionality comes built-in, with the orbital model for all Myriota satellites being continually updated and downloaded to the Myriota Modules automatically. The onboard satellite receiver logs the signal strength and quality at various points of its orbit, particularly focusing on when it is closest to the nadir point (directly overhead) over the transmitter.

Angle of Transmission Calculation: For each data point, the angle of transmission relative to the satellite's position will be calculated. This includes computing the elevation angle from the horizon and the azimuth angle, to precisely determine the satellite’s position relative to the transmitter on the ground.

To carry out these complex calculations, it is anticipated that a computational tool such as Matlab will be utilised.

Steps to calculate transmission angles

Conversion of geographic coordinates to ECEF (Earth-Centred, Earth-Fixed).

The latitude, longitude and altitude of both the transmitter and the satellite position will first need to be converted into artesian coordinates in the ECEF system.

Latitude and Longitude into Radians

$$\emptyset rad = \emptyset \frac{\pi}{180}$$

$$\lambda rad = \lambda \frac{\pi}{180}$$

ECEF Coordinates

$$x = (N(\emptyset) + h)\cos(\emptyset rad)\cos(\lambda rad)$$

$$y = (N(\emptyset) + h)\cos(\emptyset rad)\sin(\lambda rad)$$

$$z = [(1 - e^2)N(\emptyset) + h]\ sin(\emptyset rad)$$

Where:

$N(\emptyset) = \frac{\alpha}{\sqrt{1-e^2 sin^2(\emptyset rad)}}$: is the prime vertical radius of curvature.

α : is the Earth's equatorial radius.

e : is the Earth's eccentricity.

Determining the relative position vector

Calculate the relative position vector $\vec{r}$ from the transmitter to the satellite in ECEF.

$$\vec{r} = \vec{r}_{sat} - \vec{r}_{trans}$$

This relative position vector then needs to be converted from ECEF coordinates to the local East-North-Up (ENU) coordinates at the transmitter itself. This will allow for easier calculation of the azimuth and elevation.

Conversion Matrix

$$R = \begin{bmatrix} -sin(\lambda rad) & cos(\lambda rad) & 0 \\ -\sin(\emptyset rad)\, cos(\lambda rad) & -sin(\emptyset rad)\, sin(\lambda rad) & cos(\emptyset rad) \\ \cos(\emptyset rad)\, cos(\lambda rad) & \cos(\emptyset rad)\, sin(\lambda rad) & sin(\emptyset rad) \end{bmatrix}$$

ENU Coordinates

$$\begin{matrix} e \\ n \\ u \end{matrix} = R \cdot \vec{r}$$

Elevation and Azimuth

$$\text{Elevation } (\in) = \arcsin\left(\frac{u}{\sqrt{e^2+n^2+u^2}}\right)$$

$$\text{Azimuth } (\alpha) = arctan2(e, n)$$

Attenuation Measurement: The main variable of interest is the RF signal strength, which will be recorded alongside environmental data such as temperature, wind speed, and humidity, similar to the controlled experiment. This approach ensures that any attenuation can be correlated with the satellite's position and the cotton canopy's influence. The Myriota Module has built-in, timestamped RSSI data recording, which can then be used alongside the calculated elevation and azimuths to determine the satellite's position in relation to the transmitter.

Analysis

Comparison with Baseline: Similar to the controlled setting, baseline measurements of RF signal strength and quality will be made with the transmitter in an open field with no obstructions. These measurements are critical as they provide a reference point for understanding the attenuation effects caused by the cotton canopy.

Attenuation Rates: By comparing the signal strength received during satellite passes with the baseline measurements, the attenuation rates can be calculated. These rates will be analysed to understand how the cotton canopy affects the signal as a function of the satellite's position, particularly the elevation angle.

Statistical Analysis: Statistical methods will be used to analyse the data from multiple satellite passes. This will create a robust data set and help in understanding the consistency of the attenuation effects and in identifying any patterns related to the time of day, satellite position, or environmental conditions.

Challenges and Considerations

Satellite Pass Variability: Since the satellite's path and overhead times vary, measurements must be carefully planned according to the satellite's schedule. Fortunately, the orbital map of the Myriota satellites is readily available and data collection periods will be planned accordingly.

Environmental Variability: As with the controlled experiment, environmental factors that could influence the signal strength need to be recorded and accounted for to ensure the

robustness of the findings. Slightly less in our control, this is where repeating the experiment over several days will hopefully mitigate any environmental effects.

Data Integrity and Replicability: Ensuring that the data reflects the true effects of RF attenuation by the cotton canopy will require careful calibration of the Myriota device and consistent data recording practices.

This uncontrolled approach, by using actual satellite passes, provides a direct and practical measurement of how cotton crop canopies affect RF communication with LEO satellites, complementing the controlled experiment's findings and offering insights into real-world operational conditions.

Summary and Comparison of Obtained Data

By analysing the data obtained from the three different approaches, this project will aim to further understand identified factors which significantly impact attenuation rates.
Some expected factors include:

- Vegetation Density: The height, density and overall structure of the cotton crop.
- Environmental Conditions: Changes in temperature, humidity and wind speed.
- Signal Frequency: Impact transmission frequency has on attenuation.
- Antenna Positioning: Antenna height and orientation. Comparison of results obstructed vs unobstructed.

After identifying exactly what impacts the above factors have on attenuation, suitable mitigation techniques can be proposed and trialled to evaluate their effectiveness. The data obtained from these trails will then be further analysed to assess what improvement is seen. The effectiveness of the trialled mitigation techniques will then be assessed on their practicality to implement. It is presumed that some methods such as a taller antenna, will not be feasible given the application.

By carrying out this comprehensive data collection and analysis, this project aims to develop practical solutions to resolving signal attenuation in agricultural environments. It is hoped that the findings not only further the understanding of signal behaviour in such environments, but also provide practical suggestions for improving communication systems in similar applications.

4. Results and Discussion

4.1 Introduction

This section will delve into the results obtained, carrying out the experiments outlined in chapter three of this research report.

The trial site selected for the data collection was a property approximately 10km east of Dalby, a key agricultural hub in South-East Queensland, Australia. Dalby is well known for its rich farming lands, particularly suited to cotton growing sue to its favourable climate and soil conditions. The trial site cultivates a mixture of both dry-land and irrigated cotton, employing lateral move irrigators as their primary irrigation method.

Figure 17. Trial Site at Dalby, Queensland

The typical growing season in Dalby spans from September to May, with the key phases being:

- Planting (September – October)
- Irrigating (October – January)
- Flowering/Boil Development (December – February)
- Maturation (February – April)
- Picking/Harvest (May – June)

Subsequently, the timing of the data collection was not ideal, occurring in mid-July, when the cotton had already been picked, leaving only vegetation stubble in the field. Whilst collecting during the peak growing season is likely to have provided different insights, the presence of stubble still offered valuable opportunities to study signal attenuation in a post-harvest environment. This scenario is particularly relevant for growers and agronomists who need to carry out post-harvest activities such as soil-monitoring, irrigation planning and preparation for the next planting season.

The timing of data collection also restricted the ability to assess the impacts of factors such as plant moisture content and boll size.

4.1.1 Measurement Equipment

The initial methodology for the experiment called for the use of transceivers operating at 433MHz – similar to that used by the Myriota network. However, due to the unavailability of suitable devices, an alternative approach was adopted and LoRa (Long Range) devices were implemented instead. LoRa is a widely used, wireless communication technology, that enables long-range data transmission, with very low power consumption. Operating in licence-free, sub-gigahertz bands, LoRa has a proven history within the agricultural sector. As detailed previously, despite its successful track record, most LoRa networks require substantial infrastructure including communication towers, gateways, repeaters etc, for them to be adequately implemented on a large scale. This significant capital expenditure has proven to be a deterrent for widespread adoption.

The transceivers utilised for the data collection comprised of a XC4392 LoRa shield module attached to an Arduino Uno, which processed the received signal inputs and outputs. The supplied ANT-RA57-915 vertically polarized antenna is typical of that used in LoRa communication with a centre frequency of 915MHz and a gain of 2dBi. Figure 18 illustrates the radiation of the antenna in both the H-plane and the E-plane. Table 3 summarises the technical specification of the transceivers. For further technical specifications on the equipment used, refer to Appendix C.

Table 3. LoRa Transceiver Parameters

Component	Specifications
XC4392 LoRa Shield **Semtech SX1276/77/78/79**	168dB Maximum Link Budget +20dBm – 100mW constant RF output vs V supply +14dBm high efficiency PA High Sensitivity down to -148dBm Bullet-proof Front End: IIP3 = -11dBm Excellent Blocking Immunity Low RX Current of 9.9mA FSK, GFSK, MSK, GMSK, LoRaTM and OOK 127dB Dynamic Range RSSI Built-in Temperature Sensor and Low Battery Indicator
Antenna **ANT-RA57-915**	890-915MHz, Centre Frequency @ 915MHz 2dBi Gain VSWR <2 Vertical Polarization 50Ω Impedance
Arduino Uno R3	2.7 – 5.5v 32kB Flash 1kB EEPROM 8-bit AVR® RISC-based microcontroller

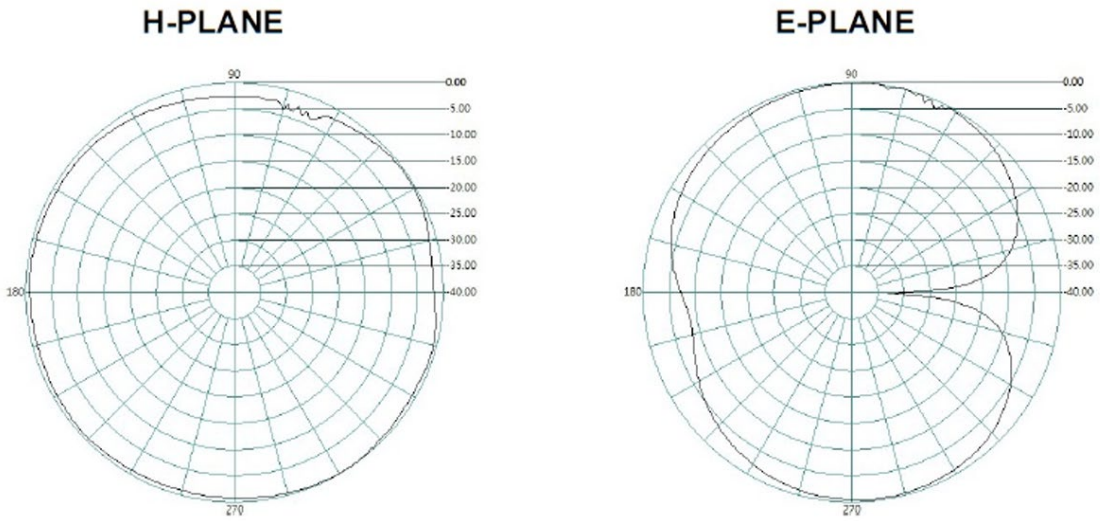

Figure 18 Radiation Pattern of ANT-RA57-915 Antenna

Figure 19. XC4392 Transceivers and Data Logging Equipment

4.1.2 Data Gathering Method

To perform the measurements and collect data, a pair of XC4392 LoRa transceivers were utilised. configured using Arduino software. The transmitter was programmed to send a data packet containing an incrementing “count” beginning at zero, to the receiver once every second. This simple, yet effective communication strategy allowed for continuous monitoring of the signal quality, particularly if any messages were lost. The receiver, upon receiving each data packet, would display the count along with the measured Received Signal Strength Indicator (RSSI) in dBm and the Signal-to-Noise Ratio (SNR) of the received message. These metrics were specifically selected as they provide critical information about the overall quality of the communication link and any attenuation occurring to the signal. The messages were continuously set until which point the receiver had received 20 successful transmission or until a 100 second timeout between received messages had occurred.

This data was subsequently processed using both MATLAB and Excel for pathloss modelling. The receiving device was installed at a fixed location to maintain a consistent reference point, whilst the transmitting device was connected to a portable power bank and moved to the desired position based on the specific test being carried out.

Figure 20 below illustrates the measurement and modelling process.

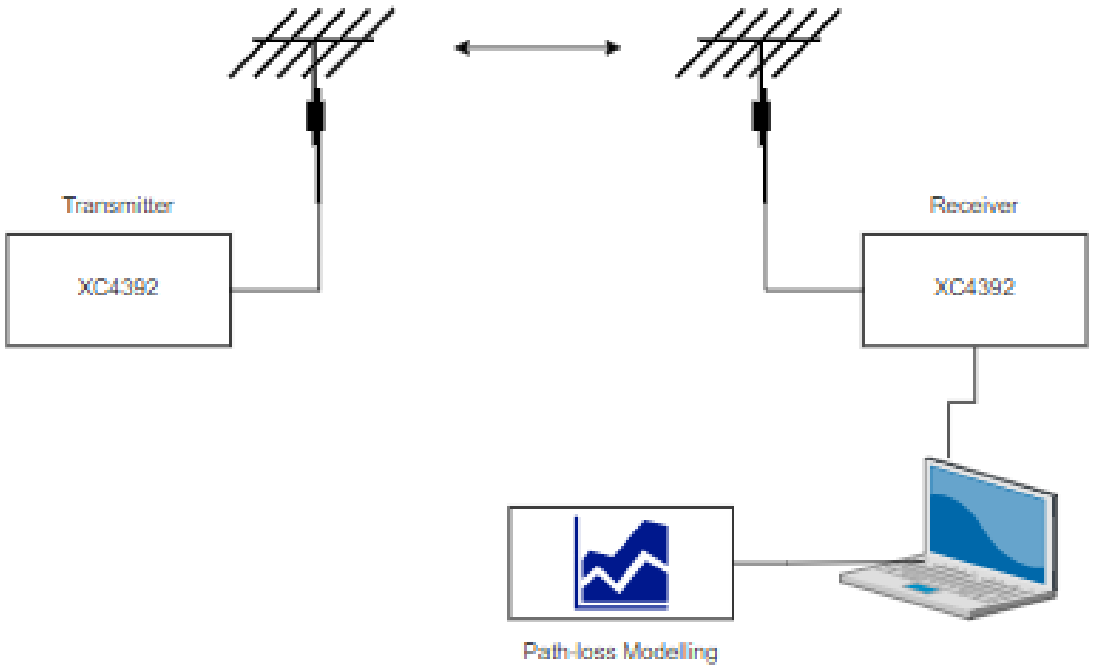

Figure 20. Data Collection and Modelling Process

The initial plan was to carry out measurements at 0m, 1m, 2m, 5, 10m, 20m, 50m, 100m, 200m and 400m under both Line of Sight (LoS) and Non-Line of Sight (NLoS) conditions. These specific distances were chosen to capture a wide range of propagation scenarios, from close proximity to wide separation. However, as the experiments progressed, these distances were adjusted to better suit the actual operating capabilities and environmental conditions encountered during the testing.

In total, over 800 measurements were taken to facilitate the path-loss prediction modelling.

4.1.3 Measurement Geometries

Three main measurement geometries were investigated; Line-of-Sight in “Skipped Rows”, Non Line-of-Sight perpendicular to the ‘Double Skipped” cotton rows and finally, Non Line-of-Sight directly through the cotton row.

Figure 21. Double Skipped Cotton Rows

At each trial site, the receiver was located outside the vegetation and the transmitter was moved along the cotton row at various distances along the direction of signal propagation as shown in Figure 22.

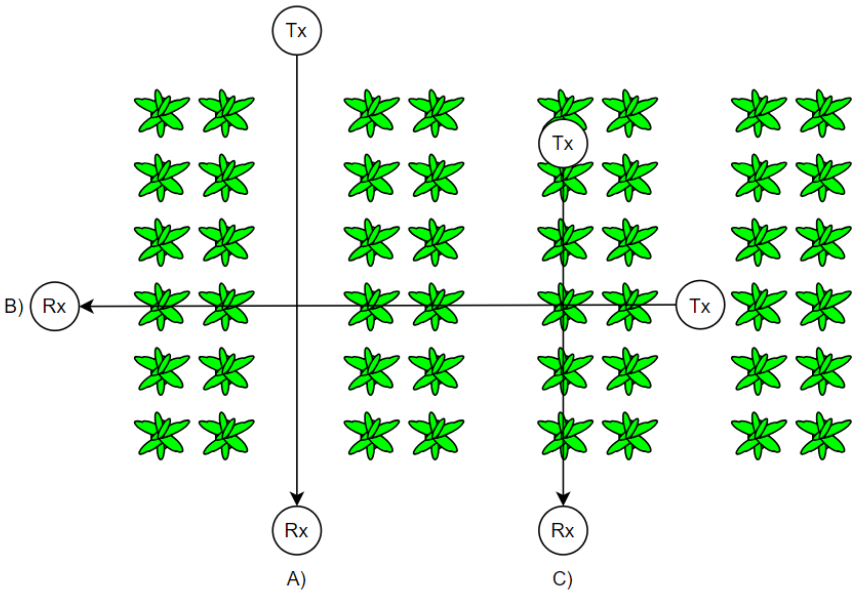

Figure 22. Measurement Geometries. A) LoS, B) NLoS - Double Skipped, C) NLoS - Dense Vegetation

4.2 RSSI

4.2.1 Overview

A key metric required to understand attenuation caused by cotton vegetation stubble, is the actual measured strength of the signal received. Received Signal Strength Indication (RSSI) refers to the metric used in wireless network systems that describes the power level of the received signal at the given receiver. Typically measured in decibels relevant to one milliwatt (dBm), it provides a logarithmic representation of signal power. Ranging from 0dBm, which indicates no loss in signal strength to approximately -130dBm, which signifies an extremely weak signal that is close to the noise floor of the receiver.

RSSI is calculated using the following equation:

$$RSSI\ (dBm) = P_T + G_T + G_R - PL(d)$$

Where:

- P_T is the transmitted power
- G_T is the gain of the transmitting antenna
- G_R is the gain of the receiving antena
- $PL(d)$ is the path loss at distance d

4.2.2 Results

Table 4. Averaged RSSI Measurements

Distance (m)	LOS RSSI (dB)	NLOS RSSI (dB)	Denser NLOS RSSI (dB)
0	-18	-18.05	-19
1	-63.6	-65.6	-80.3
2	-84	-85.2	-86.6
5	-90.15	-99.95	-104
10	-99.5	-101.25	-99.55
20	-117.8	-109.45	-111.4
50	-121.55	-122.15	-121.5
100	-122.9	-123.6	-124.25
115	*-122.915**	*-124.05**	-124.7
125	*-122.925**	-124.35	No Result
200	-123	No Result	No Result
400	-123.8333333	No Result	No Result

*Interpolated data points

4.2.3 Analysis

The results share a common starting RSSI of approximately -18dB, across all test scenarios, indicating high signal strength and the absence of any significant obstructions or attenuation factors at the start of the transmission path. In the LoS scenario, the RSSI consistently decreases with distance – aligning with natural propagation losses described by the inverse square law, where the power density of a radio wave decreases proportionally to the square of the distance from the source. This phenomenon is particularly evident in the substantial drop in RSSI between 0m and 1m, highlighting the rapid attenuation of the signal as it begins to travel through a medium. As the distance increases, the RSSI continues to decay until approximately 50m, where it appears to plateau at 123dB. This plateau suggests that the received signal strength has now reached the noise floor of the receiver and is becoming increasingly more indistinguishable from the background noise. Beyond this point, there is no further reduction in measured RSSI.

In the “Double-Skip” NLoS scenario where obstructions in the form of vegetation was introduced into the signal path, the initial impact of these obstructions appear to be minimal up to 10m, when compared directly to the LoS measurements. Beyond this distance however, the effects of reflections, diffractions and scattering became more pronounced, with a more rapid rate of attenuation. This accelerated signal degradation due to the introduction of vegetation became further evident, with no transmission being successfully received after 125m.

In the scenario involving denser vegetation, which increased the physical depth of vegetation depth in the propagation path, more substantial obstruction to the signal path, however this did not appear to significantly impact the signal strength readings comparatively with the less dense vegetation. The only significant difference was the final successful transmission distance of 115m, which was approximately 10m shorter than that of the Double Skip condition.

The RSSI measurements taken across three different propagation scenarios - LoS, Double Skip NLoS, and Dense Vegetation (NLoS) illustrates the critical impact of environmental factors on signal attenuation. In the LoS condition, signal attenuation is primarily due to free-space loss, following the inverse square law. The two NLoS scenarios demonstrate the impact of obstacles, leading to faster signal degradation due to signal reflections, diffractions and scattering. Understanding these factors is essential for the successful implementation of a reliable and effective communication system in agricultural environments, areas where varying levels of obstruction are expected.

4.3 SNR

4.3.1 Overview

Signal-to-Noise Ratio (SNR) is the ratio between the power of the desired signal and the background noise. A higher SNR indicates a clearer signal with less interference, whilst a lower SNR indicates the signal is more difficult to distinguish from the background noise.

SNR can be described as:

$SNR\ (dB) = P_R - P_N$

Where:

$P_R(dBm)$ is the power of the received signal.

$P_N(dBm)$ is the noise floor

Figures 23 and 24 illustrate the difference between a positive SNR where the RSSI is above the noise floor and a negative SNR where the received signal strength is below the noise floor.

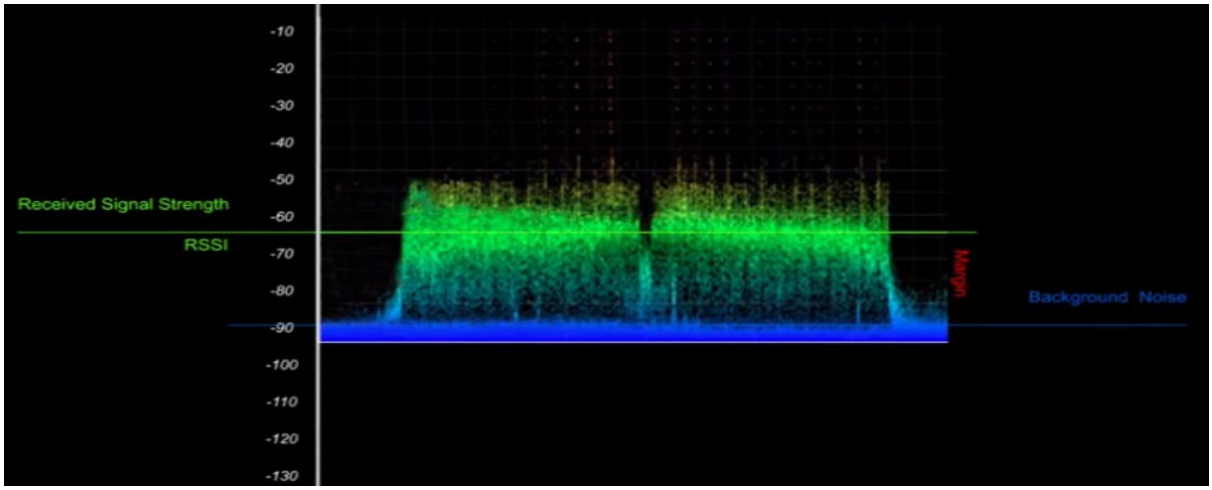

Figure 23. Example of Positive SNR (The Things Network, 2024)

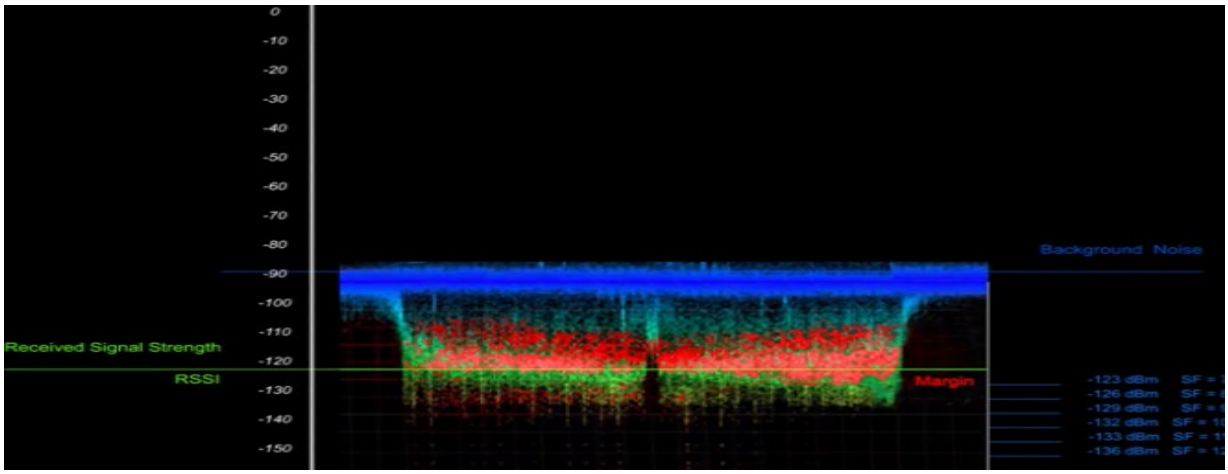

Figure 24. Example of Negative SNR (The Things Network, 2024)

4.3.2 Results

Table 5. Averaged SNR Measurements

Distance - (m)	LOS - (dB)	Double Skip (NLOS) - dB	Dense Vegetation (NLOS) - dB
0	9.00	9.04	9.00
1	8.98	9.04	9.30
2	8.93	9.04	9.09
5	8.98	9.13	9.13
10	8.99	8.75	7.06
20	4.43	8.88	7.24
50	-1.10	-0.19	3.84
100	-2.71	-6.96	-3.55
115	*-3.38**	*-7.56**	-3.98
125	*-3.82**	-7.95	-
200	-7.15	-	-
400	-9.54	-	-

*Interpolated data

4.3.3 Analysis

At distances 10m or less, all scenarios exhibit relatively high SNR values (>7), indicating good signal quality with minimal interference. This high SNR is consistent with expectations for short-range communication, where signal strength is typically strong and any external noise has a limited impact on signal integrity. As the distance increases, the SNR decreases across all three test mediums. Reflecting the anticipated effects of increased path loss and the growing influence of external noise on the signal. In the LoS and Double Skip NLoS scenarios, the transition from a positive SNR to a negative SNR occurs at approximately 50m. This transition coincides with the RSSI measurements beginning to plateau around -120dB, which suggests the signal is approaching the noise floor of the transceiver.

One of the main advantages of LoRa communication is its ability to successfully demodulate signal, even when below the noise floor. Table 6 lists the minimum SNR required for each SF to maintain reliable communications and these values align well with the experimental results. In both the NLoS scenarios, communication was completely once the lost SNR dropped below -7.95dB (Double Skipped) and -3.98dB (Dense Vegetation). Although the LoS scenario did manage to achieve some communication at a SNR of -9.54dB, the reliability of the communication was significantly compromised – with only five messages of the 220 sent successfully demodulated.

Table 6. Minimum SNR for Spreading Factors (Reproduced from Semtech SX1276-7-8-9 Datasheet, nd).

SpreadingFactor (RegModulationCfg)	Spreading Factor (Chips / symbol)	LoRa Demodulator SNR
6	64	-5 dB
7	128	-7.5 dB
8	256	-10 dB
9	512	-12.5 dB
10	1024	-15 dB
11	2048	-17.5 dB
12	4096	-20 dB

A high SNR underpins the foundation of a reliable and efficient wireless communication system. As anticipated, the LoS conditions provided the best SNR results– translating to a more reliable communication system overall. However, both the Double Skip and Dense Vegetation NLoS scenarios encountered significantly worse SNR at distances greater than 100m, ultimately resulting in complete signal loss at 125m and 115m respectively. These results emphasise the need for strategic planning in sensor deployment, minimising any obstructions and maintaining LoS conditions as much as possible.

In addition to this, the use of higher Spreading Factors may enhance the likelihood of successful signal demodulation, even under poor SNR conditions. This does however come with a trade-off, with a reduction in data throughput and an increase in power consumption by the transceiver.

4.4 Transmission Success Rate

4.4.1 Overview

Perhaps a more accurate and meaningful representation on the reliability of the 915MHz transmission system is provided by the actual success rate of the transmitted messages. Representing the percentage of transmitted data packets that are successfully received and demodulated by the receiver without errors.

Transmission success rate can be defined as:

$$TSR(\%) = \left(\frac{Number\ of\ Received\ Packets}{Total\ Number\ of\ Sent\ Packets}\right) * 100$$

Whilst factors such as RSSI and SNR play integral roles in assessing the performance of wireless communication systems, they fail to capture an overall picture of the system's reliability and robustness. TSR on the other hand, provides a clear indication of how effectively the system is operating under varying conditions. It allows for a straightforward means to evaluate the effects of changing transmission parameters such as the Spreading Factor or Bandwidth.

4.4.2 Results

Table 7. Averaged TSR Results

Distance - (m)	LOS – TSR%	Double Skip (NLOS) – TSR%	Dense Vegetation (NLOS) – TSR%
0	100	100	88.2
1	95.28	100	76.92
2	83.33	68.96	44.44
5	71.42	48.78	19.8
10	58.82	37.76	18.34
20	41.66	21.97	26.67
50	27.77	19.6	15.5
100	24.69	11.36	13.33
115	-	-	11.63
125	-	8.47	-
200	17.86	-	-
400	2	-	-

4.4.3 Analysis

As illustrated in Table 7, the three different environments behave in the expected manner with the LoS environment providing higher delivery success rates at nearly every test distance. This data also highlights the fact that both NLoS environments (Double Skip, Dense Vegetation) were unable to transmit reliably at distances greater than 115m and 125m respectively.

The LoS setting demonstrates the highest packet delivery success rate across all distances, achieving approximately a 2% successful transmission rate at 400m (220 messages sent, 5 received). This performance clearly highlights the importance of maintaining LoS conditions for reliable and long-range data transmission. The gradual decline in TSR as distance increases, is consistent with the effects of free-space propagation and its associated attenuation. In contrast, both the Double Skip and Dense Vegetation scenarios exhibit significant drops in TSR at distances greater than 20m, highlighting the impact of vegetative obstructions in the signal path. These drops in transmission success are indicative of the additional signal attenuation caused by reflections, diffractions and scattering in the cotton stubble.

The TSR can provide a direct measurement of the successfully received data packets, presenting a clear indication of the system's ability to operate under varying conditions. RSSI on the other hand, only indicates the strength of the received signal, not accounting for the ability to successfully receive, decode and correctly interpret the transmitted data. It is clear from the data collected, that high RSSI values do not always correlate with successful data delivery, particularly in noisy or obstructed environments, or as the received signal strength approaches the noise floor. In agricultural settings, where having accurate and reliable data available is critical for successful operation, it is crucial that LoS conditions are maximised and obstructions avoided. Even with these factors, consideration should be given to also maximise the number of times signals are transmitted when required. As evident in the data, even with LoS conditions, approximately 220 messages needed to be sent, with only 5 being successfully received at distance of 400m. This kind of failure rate may not be acceptable in all applications and users will need to take this into consideration when selecting a system to implement.

4.5 Combined Analysis of RSSI, SNR and TSR

Through the capture and analysis of three key signal transmission metrics - RSSI, SNR and TSR, across varying propagation mediums, several conclusions can be drawn regarding the effects each condition has on each of the measurements.

The measured RSSI values serve as a direct indicator of the received signal power. The collected experimental data, illustrates the expected decline in signal strength due to a multitude of factors including free-space path loss, along with the attenuation caused by the cotton stubble, which introduces propagation phenomena such as reflections, scattering and diffraction. However, the reliability of RSSI as an indication of transmission quality becomes questionable once the signal strength its noise floor, approximately -123dB. Beyond this point, further signal degradation due to distance or additional obstructions is not accurately reflected in the RSSI, which has effectively plateaued. The captured SNR data demonstrates a

similar correlation between increasing distance and declining signal quality. One unexpected finding from the experiment, was the higher SNR found in NLoS conditions at shorter transmission distances, likely due to phenomena such as constructive multipath interference or shadowing effects. However, as the transmission distance exceeded 10m, the SNR declined more rapidly than its LoS counterpart.

Analysis of the collected data would indicate that high RSSI values coupled with low SNR generally signify that whilst the received signal is strong, it is heavily affected by noise, resulting in a lower overall transmission success rate. Conversely, having both low RSSI and SNR values tends to also lead to lower transmission success rates, as evident in both NLoS scenarios. Whilst RSSI and SNR measurements do provide key details about signal transmission quality, the TSR stands out as being the most practically significant metric as it directly reflects the reliability of the system. Any modification to the system which increases the TSR

Overall, the findings emphasise the need for strategic planning when designing wireless communication systems - particularly in agricultural applications where obstructions are common. Strategic sensor placement, along with appropriate setting of transmission parameters such including Spreading Factor and signal Bandwidth are necessary to ensure robust data transmission. Understanding the interplay between RSSI, SNR and transmission success rates provides the framework for optimisation of radio frequency systems in vegetated environments.

5. Comparison with Theoretical Models

There are several existing methods for predicting Line of Sight attenuation of radio signals as they propagate through space. Two commonly used models include:

- Free-Space Path Loss Model (FSPL)
- Log-Distance Path Loss Model (LDPL)

5.1 Free Space Path Loss Model

Commonly used for modelling satellite communication, the FSPL assumes a clear unobstructed LoS between the Tx and Rx, with the model only accounting for the distance and frequency of the signal. It does not consider a number of atmospheric attenuation factors such as atmospheric absorption, rain attenuation, tropospheric scattering and refraction. However, at frequencies below 1GHz, the attenuation effects caused by these factors are greatly reduced to the point where they can largely be ignored. This simplicity is one of the core reasons why sub 1GHz frequencies are typically used in long-range communication systems such as LoRa and the Myriota network.

The FSPL is expressed as:

$$PL(dB) = 20log_{10}(d) + 20log_{10}(f) + 20log_{10}(\frac{4\pi}{c})$$

Where:

- $PL(dB)$ is the path loss at distance d
- d is the distance between the transmitter and the receiver
- f is the frequency of the signal
- c is the speed of light in a vacuum.

However, to be used in practical applications where signal strength is measured in dBm, it needs to be reverted to the Friis transmission equation. This equation not only factors in the total path loss but also the transmitted power and the gains of the antennas involved.

The equation can be described as:

$$P_R = P_T + G_T + G_R - 20log_{10}(d) - 20log_{10}(\frac{4\pi}{\lambda})$$

Where:

- P_R (dBm) is the received power in decibels relative to 1mW
- P_T(dBm) is the transmitted power in decibels relative to 1mW
- G_T (dBi) is the gain of the transmitting antenna
- G_R(dBi) is the gain of the receiving antenna
- λ (m) is the wavelength of transmitted signal ($\frac{c}{f}$)

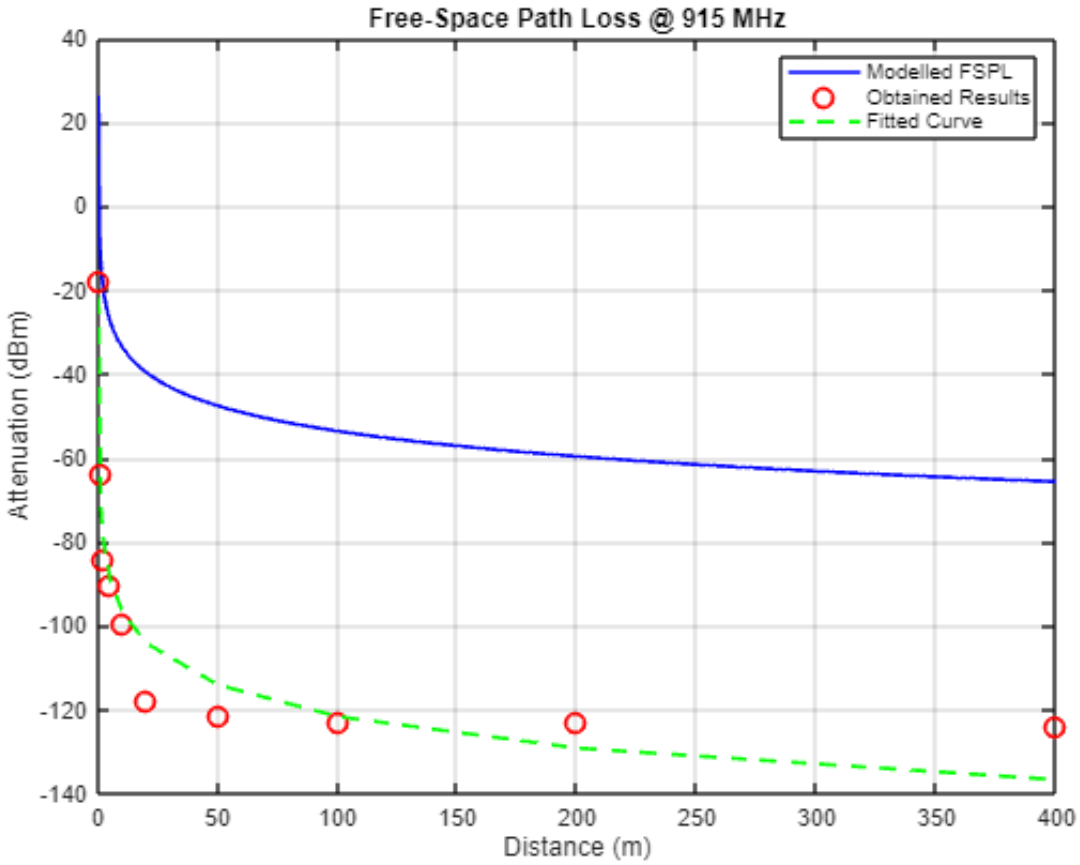

Figure 25. Modelled FSPL against Measured Values

As observed in the graph, the measured readings at each test distance varies significantly from those predicted by the FSPL model. Starting with a discrepancy of approximately 40dB at 0m and quickly growing to around 70dB at 20m. Beyond this point, the discrepancy stabilises and remains at an approximate 40dB offset from the measured values. There are numerous explanations for the discrepancy, with the most likely causes being the characteristics and calibration of the measuring equipment, as well as the introduction of potential obstructions in the test environment. The equipment used for the data collection is hobbyist in nature, and not necessarily going to provide scientifically precise results. However, it does produce replicable and reasonably consistent results, which align with the general behaviour of radio frequency signal attenuation.

The original methodology had also called for the atmospheric absorption attenuation factor to be taken into account. However, at frequencies <1GHz, the attenuation caused by atmospheric absorption is negligible and as such, was ignored.

The FSPL model itself is an idealised representation of signal propagation, assuming a perfectly unobstructed and homogeneous environment. In reality, the test environment was significantly more complex, with varying conditions such as partial obstructions (caused by blowing weeds) and changes in soil elevation not accounted for in the model. These findings highlight the importance of using more comprehensive models or empirical data to predict signal attenuation in environments where factors not captured by the FSPL model are present. This approach ensures a more accurate and reliable communication system design.

5.2 Log Distance Path Loss Model

In contrast, the Log-Distance Path Loss (LDPL) Model generalises the FSPL model by incorporating additional factors including the effects of obstructions, reflections and other environmental conditions. Whilst the LDPL is more generalised and adaptable than the FSPL model, one of its major downsides is that it is somewhat empirical in nature. This means it relies on field measurements to accurately determine the path loss exponent (n), which varies based on the specific environment.

The Log-Distance Path Loss Model is expressed as:

$$PL(d) = PL(d_0) + 10 * n * log_{10}\left(\frac{d}{d_0}\right) + X_\sigma$$

Where:

- $PL(d)\ is\ the\ path\ loss\ at\ distance\ d$
- $PL(d_0)$ is the path loss at the reference distance d_0
- n is the path loss exponent
- d is the distance between the transmitter and the receiver
- d_0 is the reference distance
- X_σ is a normal (Gaussian) random variable with zero mean, reflecting the shadowing effect

The path loss exponent is a critical parameter in the LDPL model, as it characterises how rapidly the signal attenuates through the environment. Table 8 illustrates typical values of path loss exponent in different propagation environments.

Table 8. Typical Path Loss Exponents in Varying Propagation Environments

Environment	Path Loss Exponent
Free Space	2
Urban Area Cellular Radio	2.7 – 3.5
Shadowed Urban Cellular Radio	3 – 5
In Building Line-of-Sight	1.6 – 1.8
Obstructed in Buildings	4 – 6
Obstructed in Factories	2 -3

Substituting the recorded LoS measurements at 1m and 400m:

$$n = (123.8 - 63.6)/10\log\left(\frac{400}{1}\right)$$

$$= 2.31$$

$$PL(d) = 63.6 + 10 * 2.31 * log_{10}\left(\frac{d}{1}\right)$$

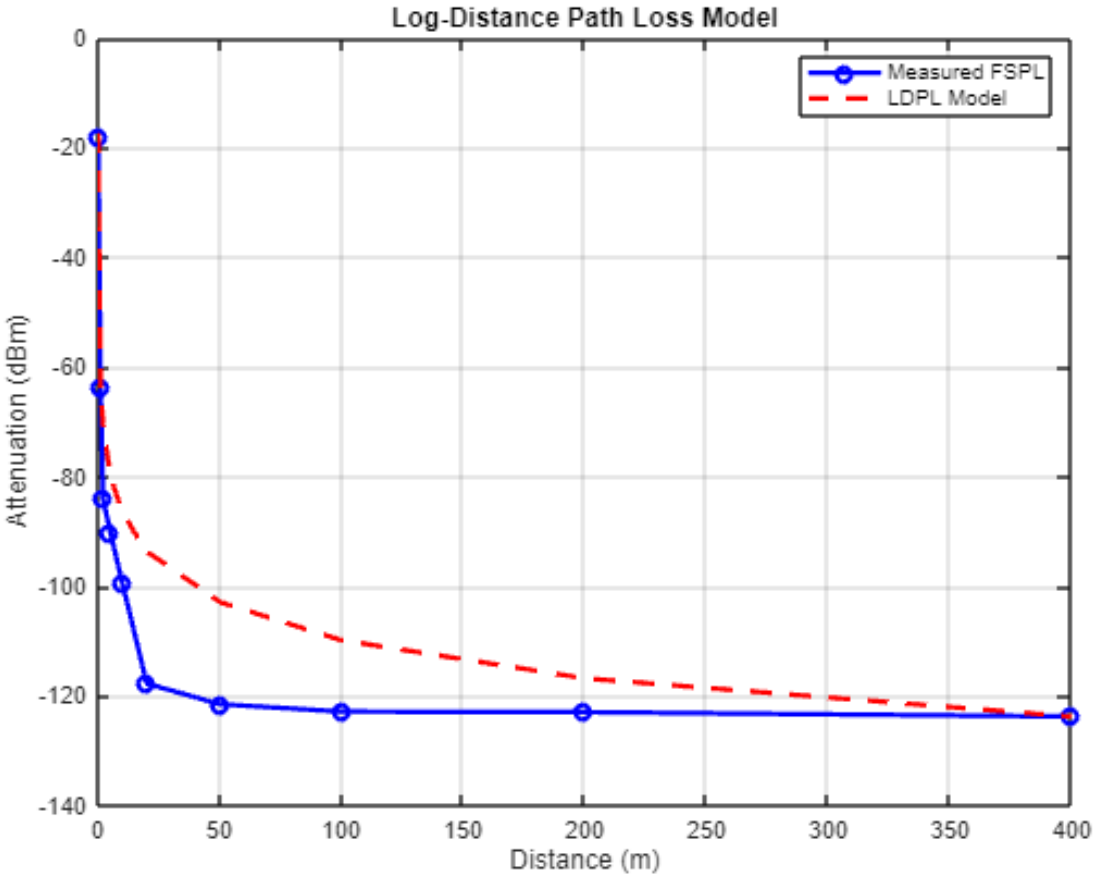

Figure 26. LDPL Attenuation Model; n = 2.31

The determined path loss exponent of n = 2.31 is consistent with typical values when measuring signal loss in free space, which has an exponent of 2. Adding in the intermittent obstructions due to moving weeds, 2.31 is perfectly reasonable. The Log-Distance Path Loss (LDPL) provides a generally good fit with the measured data, particularly at distances >150m, however there is a noticeable deviation between modelled attenuation and measured values at distances between 20m and 100m. This discrepancy can likely be attributed to near-field effects or other propagation factors not captured by the basic LDPL model.

Given the RSSI measurements appeared to find a noise floor at approximately -123dB after 50m, the accuracy of the model may be improved by instead using a multi-slope path loss model which varies the path loss exponent (n) for different distance ranges.

Readjusting for measurements at 1m and 50m:

$$n1 = (121.55 - 63.6)/10\log\left(\frac{50}{1}\right)$$

$$= 3.41$$

And between 50m and 400m:

$$n2 = (123.8 - 121.55)/10\log\left(\frac{400}{50}\right)$$

= 0.249

Total Path Loss: d < 50m:

$PL(d) = 63.6 + 10 * 3.41 * log_{10}(d)$

Total Path Loss: 50 < d < 400m

$PL(d) = 121.55 + 10 * 0.249 * log_{10}\left(\frac{d}{50}\right)$

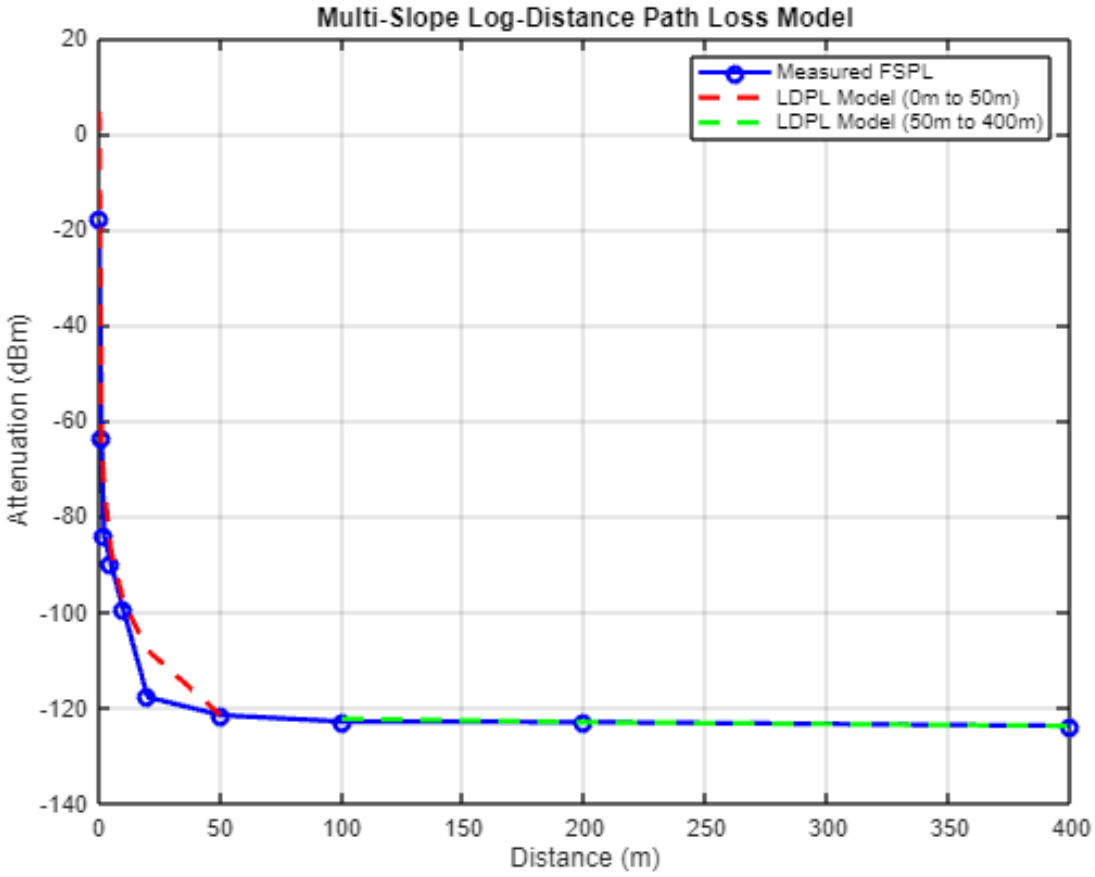

Figure 27. Multi-Slope LDPL Attenuation Model; n1 = 3.41, n2 = 0.249

5.3 Assessment of Data Collection Equipment

5.3.1 Overview

To assess the reliability of the gathered data and subsequently the accuracy of the test equipment, the standard deviation and span of each set of measurements was calculated. This provided a clear indication of the consistency and variability of the collected data.

Table 9. Standard Deviation and Overall Span of Recorded Measurements

(m)	LOS				Double Skip (NLOS)				Dense Vegetation (NLOS)			
	RSSI	Span	SNR	Span	RSSI	Span	SNR	Span	RSSI	Span	SNR	Span
0	0.224	1	0.247	1.25	0.224	1	0.247	1.25	0.224	1	0.247	1.25
1	2.683	14	0.197	1	0.821	3	0.327	1.5	0.657	3	0.276	0.75
2	2.974	14	0.345	1.5	0.894	3	0.392	1	1.429	6	0.186	0.75
5	0.933	4	0.242	1.25	0.759	3	0.329	1.5	1.076	4	0.293	1
10	2.013	10	0.250	1.25	0.851	3	0.380	1.25	1.317	5	0.323	1
20	3.270	17	0.460	1.25	0.887	4	0.565	2.5	1.188	5	0.319	1
50	0.887	3	0.308	1	0.875	4	0.525	2	0.889	3	0.383	1.25
100	0.641	2	0.233	0.75	0.598	2	0.233	1	0.639	2	0.394	1
115									0.571	2	0.280	1.25
125					0.813	3	0.402	1.75				
200	0.725	2	0.582	2								
400	0.408	1	0.368	1								

Reviewing the results obtained, it is clear that the LoS RSSI measurements had the highest level of variability – particularly within distances less than 20m. This variance could be attributed to several propagation factors such as multipath interference, near-field effects, environmental factors and the inherent characteristics of the test equipment.

In stark contrast, both sets of NLoS measurements appear to be significantly more stable, with much lower swings in both standard deviation and overall span in recorded measurements. This stability may be due to the signal paths being more diffused, reducing the impact of any sharp variations caused by specific obstructions. Whilst it is difficult to determine the exact extent to which each of these factors contributed to overall signal attenuation, they collectively caused fluctuations in the signal strength, making the RSSI less stable compared the measurements obtained at longer distances. At longer distances, the signal path tended to be more straightforward and less influenced by the immediate surroundings. Further experimentation/data collection could provide a better understanding of the impact of each factor and how better RSSI measurements could be obtained.

5.3.2 Factors impacting Equipment Performance

As stated previously, the test equipment used for the data collection was not scientific or professional-grade and as such, its performance was likely influenced by several factors specific to the experimental setup. The most significant factor causing detrimental impact to the accuracy of the measurements was multipath interference, particularly in the LoS scenario. The LoS measurements were taken within the “Skipped” rows of the cotton cultivation, meaning the signal was essentially funnelled between the transmitter and the receiver, with the adjacent cotton stubble potentially reflecting the transmitted signals. At shorter transmission distances, these reflections may have created multiple signal paths to the receiver. The multiple paths may interfere constructively or destructively, leading to significant fluctuations in signal strength, which could explain high variance in the recorded LoS RSSI measurements at distances less than 20m.

Another important consideration is the near-field effects experienced by the receiver when placed close to the transmitter. In the near-field region, the electromagnetic fields are typically far more complex compared to the far-field region, where the fields are generally more orthogonal and propagate as plane waves. At close range, the electric and magnetic fields can be out of phase, with peaks and troughs subsequently not coinciding. This appears to have created highly localised patterns of field strength, resulting in the measured RSSI to fluctuate significantly. As the transmission distance increased and it transitioned out of the near-field region, the electric and magnetic waves typically become more aligned and propagate as electromagnetic waves, creating the more stable and consistent RSSI measurement.

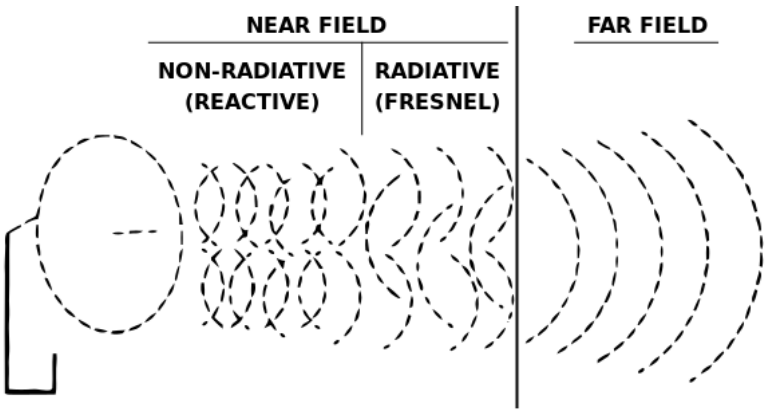

Figure 28. Near Field vs. Far Field Effects (Djukric, 2003)

Environmental factors undoubtedly contributed to the variability observed in the measured data. At shorter transmission distances, the transmitted signal exhibited increased susceptibility to the adverse weather conditions present during the data collection period, such as higher humidity levels and excessive wind speed. The heightened concentration of water molecules in the atmosphere may have absorbed some of the signal energy, further adding to the attenuation associated with FSPL. As noted previously, the excessive wind speeds encountered during the experiment likely induced movement within the cotton vegetation. Such movement would have created temporary obstructions, intermittently blocking the LoS transmissions or varying the overall foliage depth in the signal path.

The characteristics of the test equipment and the specific parameters used for signal transmission likely had a significant impact on the accuracy and reliability of the recorded measurements. Both transceivers were equipped with the standard 2dBi antenna that were included as part of the device package. These antennas are designed to be used with these devices operating on the LoRa network, which is specifically engineered for long-range, low-power communication. However, given the LoRa network is designed for long range data transmission, the specific gain and associated radiation pattern of these antenna appears to not provide ideal conditions for short-range transmissions. With a narrower transmission beam, a slight misalignment in antenna orientation could have caused substantial fluctuations, leading to the inconsistencies in measured attenuation. All signals were sent from the transmitting device using the maximum power setting of 10mW/14dBm. Whilst this high transmission power, typically assists in maintaining long-range communication, it appears to have overwhelmed the receiver, saturating the circuitry and resulting in the inaccurate and unstable measurements captured in Table 4.

In addition to these hardware influences, the transmission parameters used such as spreading factor and signal bandwidth may have played some role in overall capabilities of the test equipment. The experiment used factory set parameters of Spreading Factor (SF) 7 and Bandwidth (BW) 125kHz. Upon reflection, these may not have been optimal for the specific conditions of the experiment. Given the received signal was clearly weak at times, using a higher spreading factor may have improved the receiver's sensitivity and allowed signals to be transmitted further and with less error. However, it's important to note that having a higher Spreading Factor also reduce the data transmission rate and increases overall power consumption – a critical consideration in battery-powered devices.

Table 10. Spreading Factor versus Receiver Sensitivity @ 125kHz (The Things Network, 2024)

Spreading factor	Receiver sensitivity for bandwidth fixed at 125 kHz
SF7	-123 dBm
SF8	-126 dBm
SF9	-129 dBm
SF10	-132 dBm
SF11	-134.5 dBm
SF12	-137 dBm

The default bandwidth of 125kHz is standard in LoRa communications, maintaining a balance between range and data throughput. The narrower bandwidth improves receiver sensitivity and acts as a natural filter, reducing noise from any adjacent channels. This parameter as deemed suitable for the experiment as it provided the optimal balance between sensitivity and noise rejection but may have also contributed to some of the erratic readings observed at shorter transmission distances.

5.4 Comparison of Results with Existing Vegetation Path-Loss Models

Generating an accurate vegetation attenuation model, be that either empirical or analytical, requires numerous inputs which can be difficult to obtain. These include parameters such as the height of vegetation, leaf state, vegetation density, trunk size, leaf size and canopy height (Welch and Lemark, 1995).

To provide a baseline comparison, three well-established empirical path-loss models were used: the ITU early vegetation model, the Weissberger Model and the ITU-R Maximum Attenuation Model (MA).

Since these empirical models have been created using previous measurements, they model the combined effects of different propagation modes, not only through the vegetation. Please note, that these are not the only models available for vegetation attenuation modelling, there are also several analytical models which attempt to predict attenuation only through the vegetation. These models are typically much more mathematically intensive and as such, have not been evaluated in this report.

All models require some empirical data about the vegetation, with a key variable being the actual depth of vegetation through which the signal will be propagates.

As stated previously, the cotton plant had already been picked, leaving behind only stubble with an average height of 1100mm. The cotton had been planted using a ‘Double Skip’ configuration, where two consecutive rows are planted and then two rows are skipped. According to Cotton Australia’s definition, “Double Skip” cotton cultivation occupies approximately 50% of the total area. Given the timing of the measurements and the current state of the cotton plant, a conservative vegetation depth of 30% between the transmitter and receiver was assumed for the perpendicular Double Skip (NLoS) measurements. This estimation was reached on the reduced biomass present post-picking. In addition to this, another set of NLoS measurement were collected, directly along the cotton row. This represented a higher depth of foliage than its ‘Double Skip’ counterpart and provided opportunity to compare the effects of different vegetation. It was assumed to have a foliage depth of 50%.

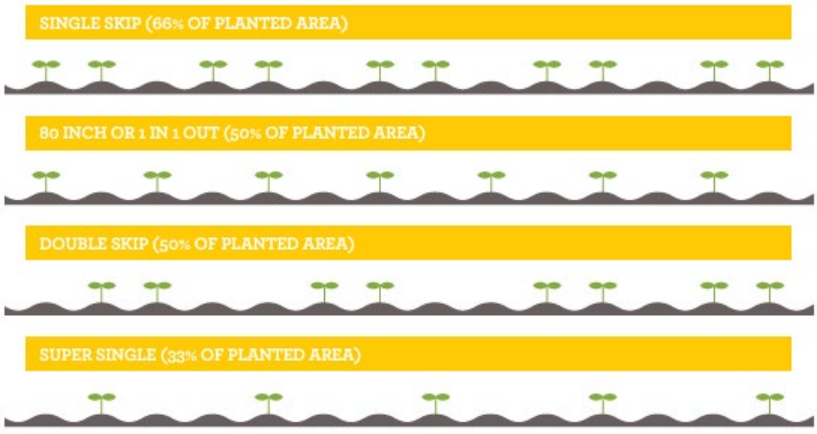

Figure 29. Cotton Row Configurations (Cotton Australia, nd).

5.4.1 ITU Vegetation Model

The ITU (International Telecommunication Union) Vegetation Model developed in 1988 is a widely recognised tool for predicting signal attenuation in vegetated areas. Developed using empirical data and methodologies similar to those employed in the Weissberger Model. The ITU model provides a generalised approach for estimating attenuation, making it applicable across a wide range of scenarios.

The ITU model is particularly useful at frequencies less than 1GHz, where he complexities of signal attenuation is somewhat reduced. The model is based on the depth of foliage and the frequency of transmission, with the total path loss (L) expressed as:

$L = 0.2 * f^{0.3} * d^{0.6}$

Where:

$L = Vegetation\ Attenuation\ (dB)$

$f = Frequency\ (MHz)$

$d = Depth\ of\ Foliage\ (m)$

The model captures the essential factors influencing signal attenuation, allowing a straightforward calculation that can be applied easily to a wide range of vegetated environments, making it a versatile tool in signal propagation studies.

5.4.2 Weissberger Model

The Weissberger Model, developed earlier in 1982, is another empirical model designed to predict signal attenuation in vegetated environments. It is generally considered as more accurate than the ITU model, offering more precise predictions under certain conditions. The Weissberger Model is particularly applicable in cases where total foliage depth is less than 400m and the transmission frequency is below 1GHz.

The Weisberger Model has two distinct formulas depending on the depth of foliage:

1. For Foliage depths of $14m < d < 400m$
   $L = 1.33 * f^{0.284} * d^{0.588}$

2. For Foliage depths of $d < 14m$
   $L = 0.45 * f^{0.284} * d$

Where:

$L = Vegetation\ Attenuation\ (dB)$

$f = Frequency\ (GHz)$

$d = Depth\ of\ Foliage\ (m)$

5.4.3 ITU-R Maximum Attenuation Model

The ITU-R maximum attenuation model calculates excess attenuation for signals passing through vegetative paths, using the maximum excess attenuation (Am) and the specific attenuation for very short vegetative paths as inputs. The model is represented by the following equation:

$$A_{ev} = A_m\left(1 - \exp\left(-\frac{dy}{A_m}\right)\right)$$

Where:

$A_{ev} = Total\ Excess\ Attenation\ (dB)$

$A_m = Maximum\ Excess\ Attenuation$

$y = Specific\ Attenuation\ for\ Very\ Short\ Vegetative\ Path\ (dB/m)$

$d = Length\ of\ Path\ Within\ Foliage\ (m)$

A_m has a frequency dependency of the form $A_m = A_L f^{\alpha}$.

The ITU-R P.833-6 provides a derived set values of A_L and α for frequencies ranging from 900 to 1800MHz. Specifically:

$A_L = 0.18dB$

$\alpha = 0.752$

Whilst not specifically designed for use in cotton vegetation attenuation modelling, it is anticipated that these values will provide a reasonable comparison against the measured readings in this context.

It is important to note that the attenuation calculated in all above models, is defined as excess to all other mechanisms. However, for simplicity, this research report only considers attenuation related to Free Space Path Loss as the other mechanisms.

$Total\ Attenuation = Vegetation\ Attenuation + FSPL\ Attenuation$

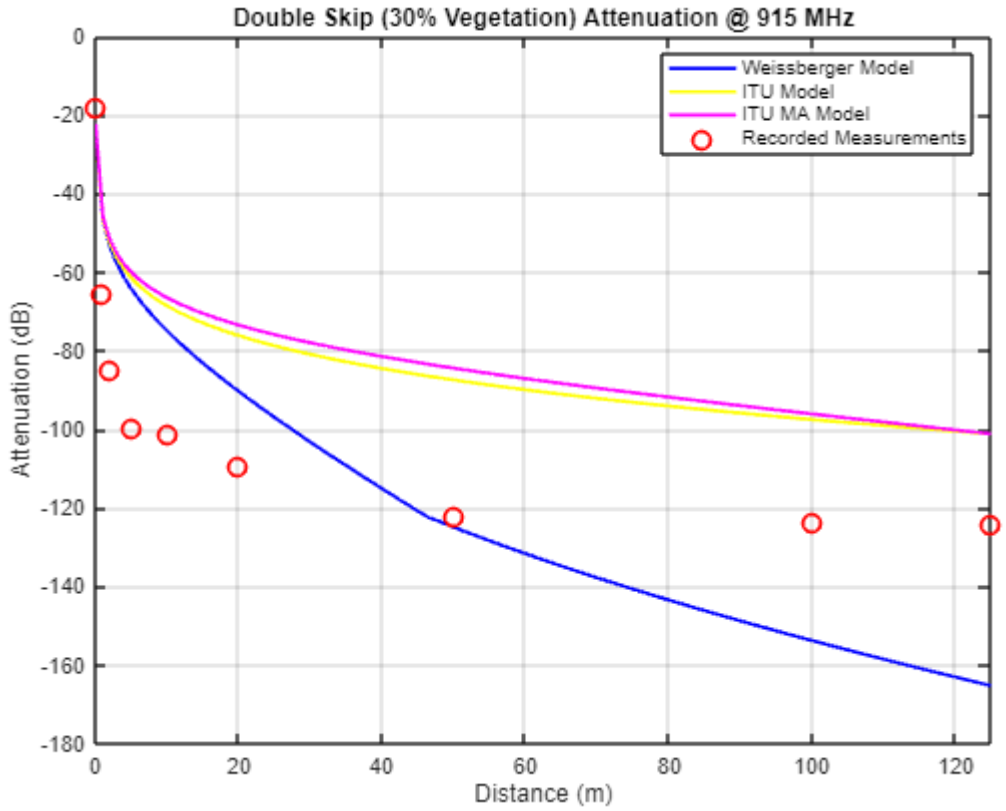

Figure 30. Existing Vegetation Models against Measured Values at 30% Foliage Depth

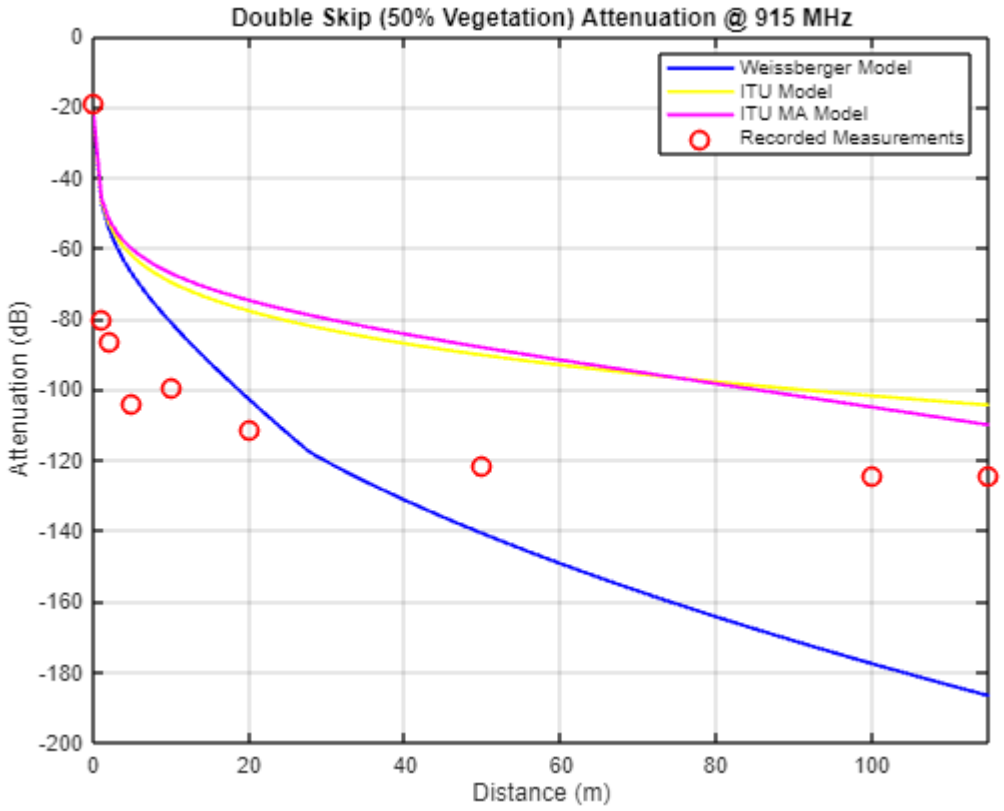

Figure 31. Existing Vegetation Models against Measured Values at 50% Foliage Depth

5.5 Assessment of Existing Empirical Models

To evaluate the accuracy of the three existing empirical models against the obtained results, the Root Mean Square Error (RMSE) formula has been used:

$$RMSE = \sqrt{(\sum P_m - P_r)^2/(N-1)}$$

Where:

Pm: Measured Path Loss (dB)

Pr: Predicted Path Loss

N: Number of Measured Data Points

A RSME within the range of 6 – 10dB is generally accepted as adequate for signal modelling (Faruk eta al, 2013).

Table 11. Accuracy of Existing Vegetation Models against Measured Values

	ITU Vegetation Model		Weissberger Model		ITU MA Model	
Foliage Depth	**30%**	**50%**	**30%**	**50%**	**30%**	**50%**
RMSE (dB)	28.75	29.51	26.35	34.80	28.75	30.40
Maximum Error (dB)	38.22	41.51	40.95	62.08	39.75	41.56
Average Error (dB)	27.01	27.60	23.23	29.51	28.38	27.92

Assessment of three existing empirical models – the ITU Vegetation Model, Weissberger Model and the ITU MA Model; against the measured values of attenuation has identified significant discrepancies. Using the RMSE as the primary metric for evaluating each model's accuracy, the analysis showed that all three models exhibited significantly higher RMSE than the required 6 – 10dB target, ranging from 26.35dB to 34.8dB. The ITU Vegetation Model and the ITU MA model provided the closer fits to the measured data, with the Vegetation Model yielding slightly better performance, with the lowest RMSE, maximum and average errors across both foliage depths. In contrast, as illustrated in figures 30 and 31, the Weissberger Model, had the worst performance, severely overestimated attenuation at longer distances, exacerbated with a higher foliage density.

Whilst none of the existing models met the 6 – 10dB RMSE criteria, the ITU Vegetation Model provided the closest fit among the three, having the lowest RMSE, maximum and average error. However, the general inadequacy of all models, highlights the need for the development of a new model, using empirical data specific to cotton stubble.

5.6 Optimised Path Loss Model

Given the large discrepancies between exiting empirical models and the recorded measurements, a new empirical model is proposed.

Using the LDPL model determined earlier and the existing ITU Vegetation model,

Total Path Loss: d < 50m

$$L = (0.2 * f^{0.3} * Fd^{0.6}) + (63.6 + 23.1 * log_{10}(d))$$

Total Path Loss: 50m < d < 400m

$$L = (0.2 * f^{0.3} * Fd^{0.6}) + (121.55 + 2.49 * log_{10}\left(\frac{d}{50}\right))$$

Where:

L = Total Attenuation (dB)

f = frequency (GHz)

Fd = Depth of Foliage (m)

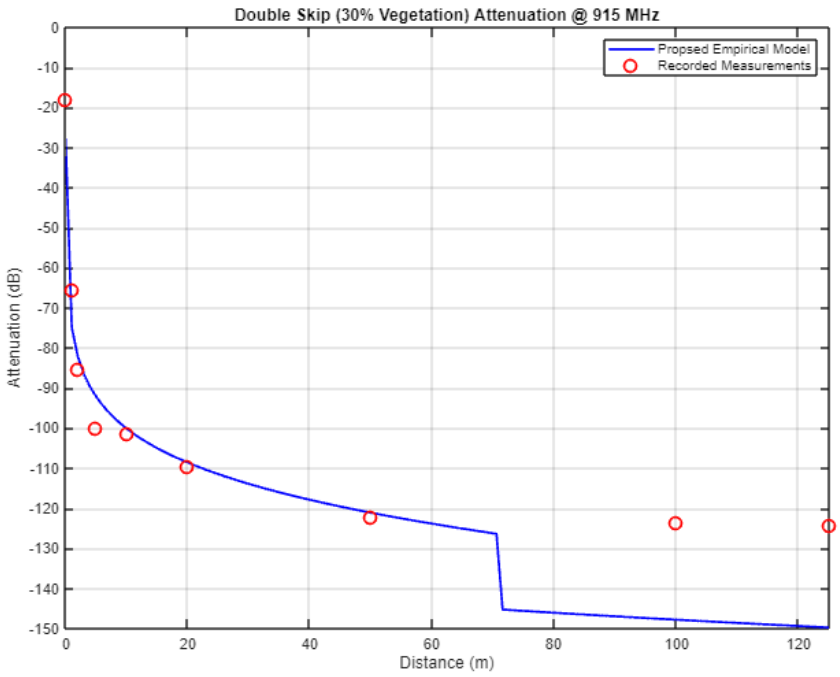

Figure 32. Proposed Cotton Vegetation Attenuation Model

One of the most significant issues identified during the data collection, was the RSSI behaviour as the signal strength approached the noise floor. Despite the signal continuing to attenuate (as evident with lower SNR and higher overall packet loss), the signal's RSSI 'flattened' out at approximately -125dB, at which point the transceiver did not appear to be able to distinguish between the signal and the background noise.

The noise floor represents the inherent background noise apparent in the wireless communication system or environment. This noise typically comes from a variety of sources including thermal noise, ambient radio frequency interference (from other nearby devices) and electronics components contained within the transceiver itself. Given the manufacturer has specified a noise floor of 127dB, the obtained results would now indicate an actual value of 125dB. Once the RSSI fell below this threshold, the measurement becomes unreliable and plateaus.

Incorporating the noise floor into the proposed empirical model was crucial for accurately predicting the RSSI behaviour, particularly as it approached its maximum operating distance. Most existing models do not incorporate any sort of noise floor, typically resulting in unrealistically low attenuation values that the receiver would be unable to detect.

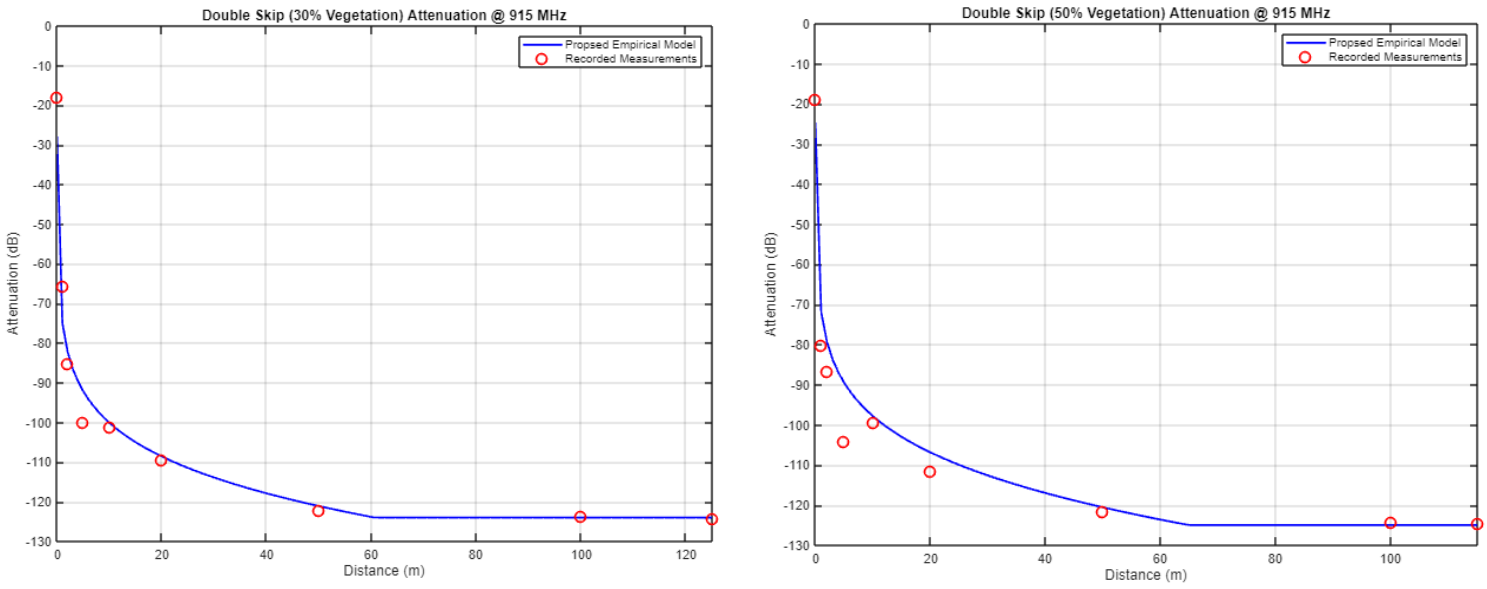

Figure 33. Proposed Attenuation Model with -125dB Noise Floor at 30% and 50% Foliage Depths

Table 12. Accuracy of Attenuation Model

	30% Vegetation	50% Vegetation
RMSE (dB)	6.5dB	5.2dB
Maximum Error (dB)	14.4dB	10.4dB @ 5m
Average Error (dB)	+/- 4.8dB	+/- 4.3dB

The proposed empirical model demonstrates a significantly improved accuracy compared to both the existing ITU Vegetation and Weissberger models. This success can be largely attributed to the incorporation of a noise floor and the tailored Log Distance Path Loss calculations. By integrating a realistic noise floor into the model, the limitations of the transceiver have been accounted for, ensuring the model does not predict unrealistic low RSSI values that would never be detected. Additionally, the use of a dual-slope LDPL model

While these results are promising, it is important to understand that further analysis and data collection must be undertaken in a range of different environments and with varying foliage depths, to fully validate the model's accuracy.

5.7 Verification of Path Loss Model – Satellite Simulation

The Myriota network, which utilises LEO satellites to provide low power, wide-area communication for IoT devices, faces similar challenges to those observed in the 915MHz LoRa experiments. Although operating at 433MHz (as opposed to the experiment's 915MHz), the fundamental principles of RF propagation remain the same. The network's low-power transmission strategy is key in maintaining long battery life for IoT devices. However, this approach can limit the device's ability to operate effectively in NLoS environments, typically resulting in a reduced RSSI, higher error rates and complete packet loss. Therefore, positioning devices to maximise their LoS conditions with the Myriota satellites is imperative for performance. Even with optimised LoS conditions, devices will still experience significant periods of NLoS operation due to the satellite's orbit.

To further understand the effects of these conditions, an additional experimentation was carried out. In this experiment, the transmitter was attached to a drone operated at various elevations and positions to simulate the movements of a Low-Earth-Orbit (LEO) satellite orbiting the earth. This method aimed to examine the impact transmission elevation and the associated propagation path through the cotton stubble had on overall attenuation. The XC4392 LoRa Transceiver was attached to a lightweight DJI Mini 3 Drone and flown at varying altitudes and distances as indicated in Table 13. The actual transmission distance between the transmitter and receiver was fixed at 50m.

In line with the other experiments, 20 RSSI measurements were taken at each transmission angle and averaged for an end result.

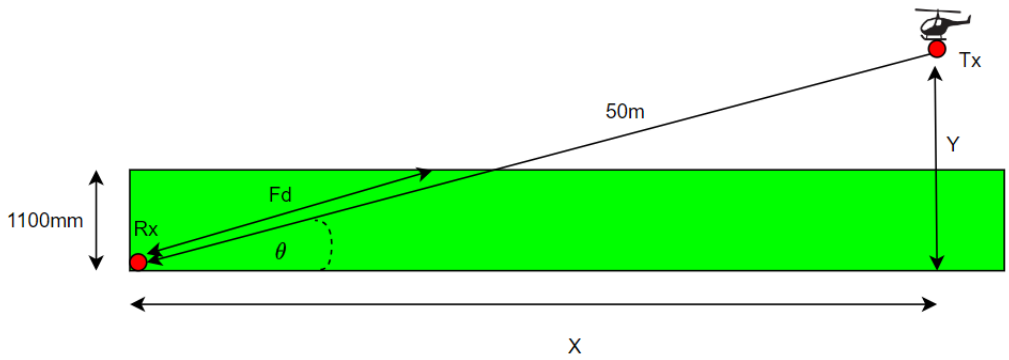

Figure 34. Satellite Simulation Experiment

Table 13. Transmission Angles and Drone Coordinates

Transmission Angle (Degrees)	X Plane (m)	Y Plane (m)
0	50	0
10	48	8
20	46	17
30	43	25
40	38	32
50	32	38
60	25	43
70	17	46
80	8	48
90	0	50

Table 14. Transmission Angle vs. RSSI

Transmission Angle (Degrees)	RSSI (dB)
0	-120.25
5	-97.4
10	-93.7
20	-86.9
30	-85.35
40	-83.45
50	-85
60	-84.95
70	-83.3
80	-80.05
90	-79.7

The ITU-R P.833-7 does provide an alternative model to use when predicting attenuation in situations where there is both horizontal and vertical path propagation, described as:

$$L\ (dB) = Af^{B}d^{C}(\theta + E)^{G}$$

Where:

f: Frequency (MHz)

d: Foliage Depth (m)

θ: Elevation (Degrees)

A, B, C, E, G: Empirically Found Parameters

Using the measured data from the drone experiment and subtracting the attenuation attributed to FSPL, the results were fitted to the equation, giving it the form:

$$L\ (dB) = 90.5245\ \ f^{-0.4383}\ \ d^{0.9185}\ \ (\theta + 1.1236)^{0.6528}$$

Figure 35 shows the comparison between the ITU-R Foliage Slant Model and the measured results. The modelled data closely aligns with the recorded data, except for deviations at extreme angles (at θ = 0 and θ = 90), illustrating a generally accurate prediction.

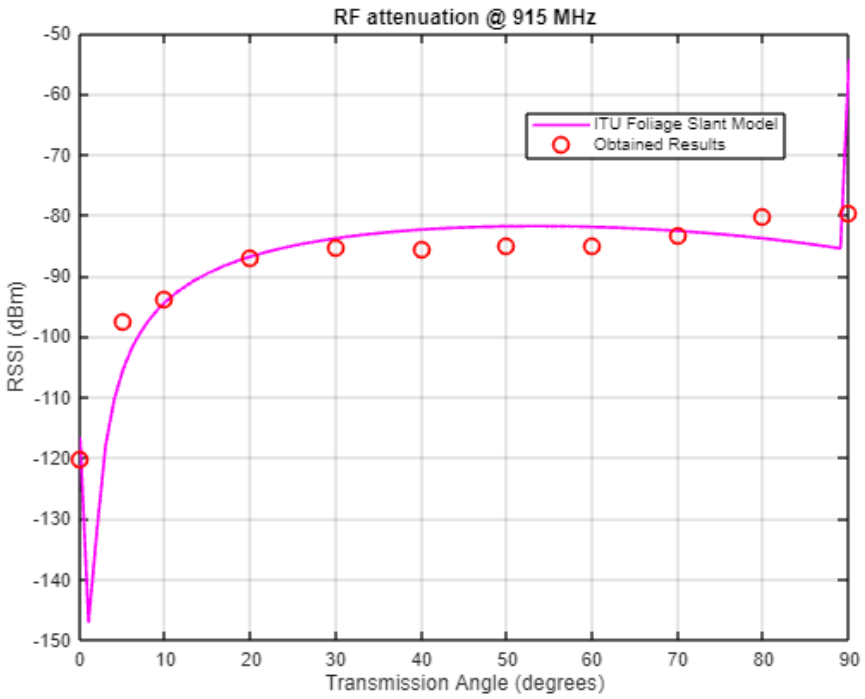

Figure 35. ITU Foliage Slant Model

Table 15. Accuracy of Model

RMSE (dB)	8.35dB
Maximum Error (dB)	25.35dB
Average Error (dB)	+ / - 4.82dB

In contrast, applying the same model to the NLoS with 50% Foliage depth scenario resulted in much less accurate predictions.

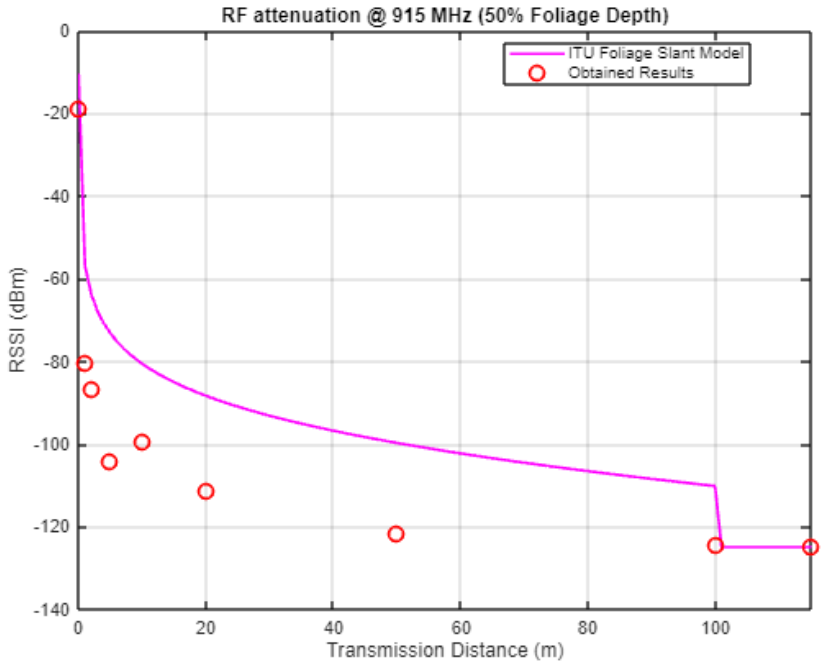

Figure 36. ITU Foliage Slant Model with LDPL Attenuation

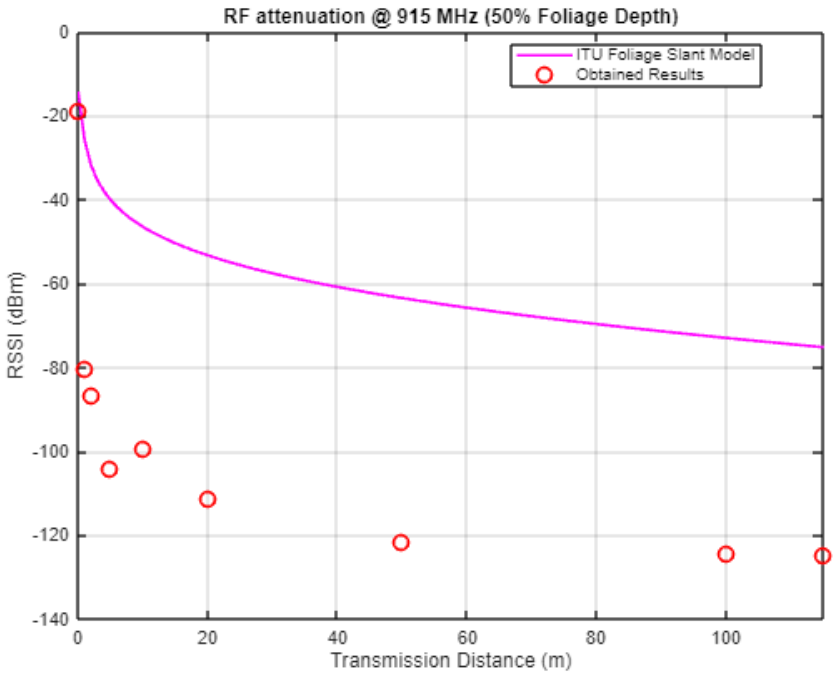

Figure 37. ITU Foliage Slant Model with FSPL Attenuation

The issue appears to arise due to the significant difference in attenuation attributed to free space path loss measured in the field experimentations versus what was measured when using the drone. During the field experiment, the LoS scenario recorded a RSSI of approximately -120dBm at a distance of 50m, whereas when the drone was flown directly overhead of the receiver at an altitude of 50m (essentially an identical LoS measurement), the measured RSSI was approximately 80dB. This 40dB is significant and highlights the challenge in creating a model which can be used interchangeably between land-based transmissions and satellite-based transmissions. The misalignment likely stems from the different polarization and radiation characteristics of the antennas attached to both the transmitter and the receiver. The results from the drone experiment suggest a more optimal alignment between the two antennas, leading to reduced attenuation. This is interesting, because both antennas are vertically polarized, which typically does not provide ideal transmission conditions from satellite-to-earth transmission. Vertical polarization is generally more suitable for static, ground-based transmissions, where the relative orientation of the antennas remains consistent. For satellite-to-earth communications, circular polarization is the preferred antenna orientation. This is due to it being less sensitive to the orientation of the transmitting antenna, a crucial factor in satellite communication where the satellite's orientation may change as it orbits. This aspect makes it extremely difficult to maintain alignment with any sort of linearly polarized antenna.

Given the limitations of the ITU's foliage slant path model, particularly in accurately attenuation within the cotton stubble environment, the original proposed path loss model from Chapter 4 proved to be significantly more accurate, as illustrated in Figure 38.

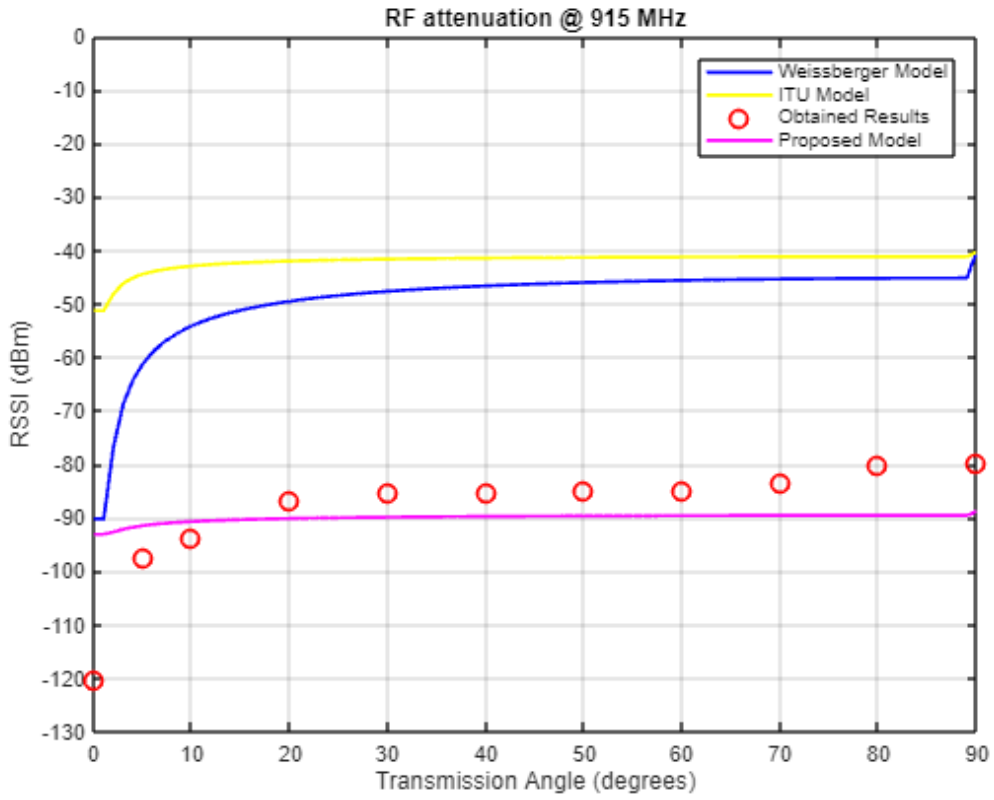

Figure 38. Satellite Simulation - Model Validation against Measured Values

Table 16. Accuracy of Models

	Weissberger Model	ITU Vegetation Model	Proposed Model
RMSE (dB)	37.35	47.31	9.94
Maximum Error (dB)	39.55	68.95	27.12
Average Error (dB)	37.25	46.6	7.5

The results indicate that the proposed model not only aligns better with the observed data but also has a reduced overall error margin, with a RMSE of 9.94dB – within the acceptable range for path loss modelling. The model's maximum error of 27.12dB, though still notable, is much lower than that of the alternative models. Again, this significant discrepancy occurs at a transmission elevation of 90 degrees – when free space attenuation is at its greatest. As noted earlier, the LoS free space attenuation measured varied significantly (40dB) between ground-to-ground based transmissions and those measured using satellite-to-earth propagation. This suggests that whilst the proposed model is not perfect, it does provide a more refined framework for understanding signal behaviour in complex vegetative environments. Further refinement of this model could be achieved by resolving the discrepancies found between the various free space LoS measurements.

6. Conclusion and Future Work

This report investigated the effects of vegetation on radio frequency signal attenuation, specifically focusing on a post-harvest cotton field near Dalby, Queensland. The research aimed to assess how cotton vegetation impacts signal propagation, particularly in the context of satellite-based agricultural communication networks, such as the Myriota network. The study utilised LoRa transceivers operating at 915MHz with data collected under various Line of Sight (LoS), Non-Line of Sight (NLoS) conditions, demonstrating the significant effect residual cotton stubble has on signal attenuation. The results highlighted the limitations of existing empirical models, such as the ITU's Vegetation and Maximum Attenuation models and the Weissberger model, in accurately predicting attenuation within a cotton vegetation environment. Consequently, a new empirical model was proposed, better reflecting the specific conditions found in a cotton field. This model achieved reasonable accuracy in predicting attenuation across varying foliage densities, with a RMSE of 6.4dB for 30% foliage depth and 5.2dB for 50% foliage depth. The model also performed suitably when used in slant path applications, achieving a RMSE of 9.94dB.

The study also acknowledges its own limitations. Whilst the gathered data does offer valuable insights, it cannot be considered comprehensive, as it was collected post-cotton picking and under unfavourable weather conditions. Future work should focus on collecting a substantially bigger data set, with measurements taken throughout the cotton growth cycle and under varying weather conditions. This additional data is likely to assist in refining the proposed model and make it a more robust tool for predicting attenuation.

More specifically, further research should extend to conducting similar experiments during the irrigation and maturation cycles of the cotton growing season, prior to picking. Data collection during these key phases would offer a more accurate representation of signal attenuation behaviour in the devices typical operational environment – insights which would be invaluable to the cotton research industry. Additionally, the measurements taken during this period are likely to align more closely with the existing path loss models, offering a more robust validation of these models with a cotton farming context.

Future studies should also investigate how different transmission parameters impact attenuation. Understanding the effects these parameters have will be key for optimising wireless network systems and ensuring network reliability. There is also extensive research still to be carried out using the Myriota equipment itself, however due to its associated security protocols, it is unclear how much can be carried out in an external research capacity.

Finally, expanding the scope of this research to include different types of crops such as sorghum and wheat, could provide a broader understanding of how different plant structures and genetic makeup affect signal attenuation. Pursuing these additional areas of research, would further the understanding of how to optimise wireless communication systems within an agricultural context, ultimately leading to more effective and reliable systems to support modern farming practices.

References

Abdollahi, A., Rejeb, K., Rejeb, A., Mostafa, M. M., and Zailani, S. (2021). Wireless sensor networks in agriculture: Insights from bibliometric analysis. *Sustainability, 13*(21), 12011.

Adegoke, A. S., Siddle, D. R., and Salami, S. O. (2016). Vegetation attenuation and its dependence on foliage density. In *Proceedings of the X Conference on Environmental Communications*.

Adegoke, S., and Siddle, D. (2012). Investigation into vegetation effects on propagating radio waves. *International Journal of Communication Studies, 5*(2), 87–95.

Appleyard, R. (1927). Pioneers of electrical communication part 5 – Heinrich Rudolph Hertz. *Electrical Communication, 6*(2), 45–57.

Bhattacharya, B. (2019). Ground wave propagation. *Amazing Amateur Radio, 12*(3), 45-50.

Borrelli, P., Robinson, D. A., Fleischer, L. R., et al. (2017). An assessment of the global impact of 21st-century land use change on soil erosion. *National Library of Medicine*. https://www.ncbi.nlm.nih.gov/pmc/articles/PMC5722879/

Djuknic, G. M. (2003, December 2). *Far and near fields* [Image]. US Patent 6657596. https://en.wikipedia.org/wiki/Near_and_far_field#/media/File:FarNearFields-USP-4998112-1.svg/2

Everything RF. (n.d.). Friis transmission equation calculator. *Everything RF*. https://www.everythingrf.com/rf-calculators/friis-transmission-calculator

Faruk, N., Ayeni, A., Adediran, Y. A., and Surajudeen–Bakinde, N. T. (2013). On the study of empirical path loss models for accurate prediction of TV signal for secondary users. *Progress in Electromagnetic Research*, 155–176.

Goldhirsch, J., and Vogel, W. J. (1989). Mobile satellite system fade statistics for shadowing and multipath from roadside trees at UHF and L-band. *IEEE Transactions on Antennas and Propagation*.

Hewlett Packard. (1976). *Spectrum analysis – Field strength measurement* (Application Note 150-10). Hewlett Packard.

Horak, P., Kvicera, M., and Pechac, P. (2010). Frequency dependence of attenuation due to vegetation for satellite services. *IEEE Antennas and Wireless Propagation Letters, 9*, 142-144. https://doi.org/10.1109/LAWP.2010.2045150

Kaushal, H., and Kaddoum, G. (2016). Underwater optical wireless communication. *IEEE Communications Magazine, 54*(2), 40–46.

Majumdar, P., Mitra, S., and Bhattacharya, D. (2021). IoT for promoting Agriculture 4.0: A review from the perspective of weather monitoring, yield prediction, security of WSN protocols, and hardware cost analysis. *Journal of Biosystems Engineering, 46*, 440–461. https://doi.org/10.1007/s42853-021-00118-6

Myriota. (2023). FAQs. *Myriota*. https://myriota.com/faqs/.

Nuccitelli, D. (2022, January 6). UN report: The world's farms stretched to a breaking point. *Yale Climate Connections*. https://yaleclimateconnections.org/2022/01/un-report-the-worlds-farms-stretched-to-a-breaking-point/

Pätzold, M. (2017). *Graphical models and simulation for THz-imaging* (Doctoral dissertation). University of Bonn.

Peden, S., Dearden, R., Davies, B., and Jones, D. (2021). A model for RF loss through vegetation with varying water content. *Proceedings of the X Conference on Wireless Propagation*. https://rune.une.edu.au/web/handle/1959.11/45311

Richards, J. A. (2008). Fundamental concepts: Propagation in free space. In J. A. Richards (Ed.), *Radio wave propagation* (pp. 123-150). Springer.

Saakian, A. (2020). *Radio wave propagation fundamentals* (2nd ed.). Artech House. Available from: ProQuest Ebook Central.

Seneviratne, C. (2023, January 6). What are LEO satellites and how do they work? *Telstra Exchange*. https://www.telstra.com.au/exchange/what-are-leo-satellites-and-how-do-they-work--

Sofos, T., and Constantinou, P. (2004). Propagation model for vegetation effects in terrestrial and satellite mobile systems. *IEEE Transactions on Antennas and Propagation, 52*(7), 1917–1920. https://doi.org/10.1109/TAP.2003.818789

Tait Communications Blog. (2015, September 23). 9 channel concepts every system designer needs to understand. *Tait Communications Blog*. https://blog.taitcommunications.com/2015/09/23/9-channel-concepts-every-system-designer-needs-to-understand/

The Things Network. (2021). Spreading factors. *The Things Network*. https://www.thethingsnetwork.org/docs/lorawan/spreading-factors/

The Things Network. (n.d.). RSSI and SNR. *The Things Network*. https://www.thethingsnetwork.org/docs/lorawan/rssi-and-snr/

Appendix A – Raw Data (Field Measurements)

LOS @ 1m				LOS @ 2m				LOS @ 5m			
Count	RSSI	SNR		Count	RSSI	SNR		Count	RSSI	SNR	
1	-65	9		3	-83	9		1	-90	9	
2	-60	9		4	-82	9		2	-90	8.25	
3	-63	9		5	-85	8.75		6	-89	9	
4	-65	9		6	-85	9		7	-89	9	
5	-65	9		7	-85	8.25		8	-92	9	
6	-64	8.75		8	-85	9		9	-90	9	
7	-54	8.5		9	-72	9		10	-90	8.75	
8	-63	9		11	-85	9.25		14	-90	9	
9	-64	8.75		14	-86	9		15	-90	9	
10	-64	9		15	-85	9		16	-91	8.75	
11	-64	9		16	-85	9		17	-88	9.25	
12	-65	8.75		17	-84	9		18	-90	9	
13	-65	9.5		18	-85	9		19	-90	9.5	
14	-68	9		19	-85	9		20	-90	9	
15	-64	9		20	-85	8.25		23	-90	9	
17	-64	9.25		21	-85	9.75		24	-91	9	
18	-64	9		22	-83	9		25	-91	9	
19	-64	9		23	-85	8.25		26	-90	8.75	
20	-63	9		25	-85	9		27	-92	9	
21	-64	9		26	-85	9		28	-90	9.25	
95.2381	-63.6	8.975	AVG	83.33333	-84	8.925	AVG	71.42857	-90.15	8.975	AVG
	-64	9	MED		-85	9	MED		-90	9	MED
	2.683282	0.197017	STD		2.973568	0.345078	STD		0.933302	0.241977	STD
	14	1	RANGE		14	1.5	RANGE		4	1.25	RANGE

LOS @ 10m				LOS @ 20m				LOS @ 50m			
Count	RSSI	SNR		Count	RSSI	SNR		Count	RSSI	SNR	
4	-97	9		8	-118	5		4	-120	-1	
5	-101	9		9	-118	4.5		5	-122	-1.5	
6	-100	9		12	-117	5.25		6	-122	-1.5	
7	-101	9		13	-119	4		12	-122	-1	
10	-101	8.75		14	-118	4		20	-120	-1	
11	-99	9.25		15	-118	4		22	-121	-1	
12	-99	8.75		22	-118	4		23	-121	-1	
15	-98	9		23	-117	5		24	-122	-1.5	
16	-93	9.25		24	-117	4.5		29	-122	-1.5	
17	-100	9		29	-105	4		37	-122	-0.5	
18	-99	9		30	-119	4		38	-120	-1	
19	-103	8.25		31	-118	4		39	-120	-1	
24	-101	9		32	-118	4.5		53	-123	-1	
25	-101	9.25		33	-120	5.25		54	-122	-1.5	
26	-100	9		43	-118	4		55	-122	-1.5	
30	-100	9.5		44	-119	4		56	-122	-1	
31	-99	8.75		45	-121	4.5		62	-122	-1	
32	-99	9		46	-122	4.5		68	-122	-0.5	
33	-100	9		54	-118	5		74	-122	-1	
37	-99	9		55	-118	4.5		75	-122	-1	
58.82353	-99.5	8.9875	AVG	41.66667	-117.8	4.425	AVG	27.77778	-121.55	-1.1	AVG
	-100	9	MED		-118	4.5	MED		-122	-1	MED
	2.013115	0.249671	STD		3.270281	0.459548	STD		0.887041	0.307794	STD
	10	1.25	RANGE		17	1.25	RANGE		3	1	RANGE

LOS @ 100m				LOS @ 200m				LOS @ 400m			
Count	RSSI	SNR		Count	RSSI	SNR		Count	RSSI	SNR	
32	-122	-3		22	-123	-6		72	-124	-10	
33	-123	-2.5		23	-123	-7		95	-123	-9	
34	-123	-2.75		24	-123	-7.5		136	-124	-9.25	
41	-122	-3		25	-123	-6.75		137	-124	-9.75	
42	-123	-3		52	-123	-7		185	-124	-9.5	
46	-123	-2.25		53	-123	-7		220	-124	-9.75	
47	-123	-2.5		82	-122	-6.5					
64	-123	-2.75		83	-123	-6.25					
65	-122	-2.75		84	-122	-7					
66	-123	-2.75		85	-122	-7					
67	-124	-2.5		86	-124	-7					
68	-124	-3		110	-122	-7					
69	-123	-3		111	-123	-6.75					
70	-122	-2.25		112	-124	-8					
92	-122	-2.75		113	-124	-8					
93	-123	-2.75		114	-124	-7					
102	-124	-2.5		114	-124	-7.75					
103	-123	-2.75		130	-123	-8					
104	-123	-2.75		132	-122	-7.75					
112	-123	-2.75		133	-123	-7.75					
24.69136	-122.9	-2.7125	AVG	17.85714	-123	-7.15	AVG	-28.169	-123.833	-9.54167	AVG
	-123	-2.75	MED		-123	-7	MED		-124	-9.625	MED
	0.640723	0.233326	STD		0.725476	0.581513	STD		0.408248	0.36799	STD
	2	0.75	RANGE		2	2	RANGE		1	1	RANGE

DS_NLOS @ 0m

Count	RSSI	SNR	
1	-18	9	
2	-18	9	
3	-19	8.25	
4	-18	9.25	
5	-18	9.5	
6	-18	9	
7	-18	9	
8	-18	9	
9	-18	9	
10	-18	9	
11	-18	9	
12	-18	9	
13	-18	9	
14	-18	9	
15	-18	9	
16	-18	9	
17	-18	9	
18	-18	9.5	
19	-18	9.25	
20	-18	9	
100	-18.05	9.0375	AVG
	-18	9	MED
	0.223607	0.247022	STD
	1	1.25	RANGE

DS_NLOS @ 1m

Count	RSSI	SNR	
1	-65	9	
2	-65	9	
3	-66	9	
4	-65	9.25	
5	-66	9	
6	-65	9.25	
7	-66	9	
8	-66	9	
9	-65	9.5	
10	-65	8.75	
11	-66	8.75	
12	-65	9	
13	-66	9	
14	-67	9.25	
15	-68	9.5	
16	-66	9	
17	-65	9	
18	-65	9.5	
19	-65	8	
20	-65	9	
100	-65.6	9.0375	AVG
	-65	9	MED
	0.820783	0.327219	STD
	3	1.5	RANGE

DS_NLOS @ 2m

Count	RSSI	SNR	
4	-86	9	
5	-86	9	
6	-85	9	
7	-85	9	
8	-85	8	
11	-87	8.25	
12	-86	8.25	
13	-86	8.25	
14	-85	8.75	
15	-84	8.75	
16	-84	8	
20	-84	8	
21	-84	8	
22	-85	8	
27	-85	8	
28	-84	8.25	
29	-86	8.25	
30	-86	8.25	
31	-85	8.75	
32	-86	8.25	
68.96552	-85.2	8.4	AVG
	-85	8.25	MED
	0.894427	0.392361	STD
	3	1	RANGE

DS_NLOS @ 5m

Count	RSSI	SNR	
2	-100	9	
3	-100	9	
4	-99	9.75	
6	-98	9	
7	-100	9.25	
12	-100	9	
13	-101	9	
14	-101	8.25	
15	-100	9.25	
16	-100	9	
26	-100	9.75	
29	-99	9	
30	-99	9	
31	-100	9.5	
32	-100	9	
33	-100	9.25	
34	-101	9	
38	-100	9	
39	-101	9.5	
42	-100	9	
48.78049	-99.95	9.125	AVG
	-100	9	MED
	0.759155	0.329473	STD
	3	1.5	RANGE

DS_NLOS @ 10m

Count	RSSI	SNR	
1	-101	9	
2	-101	8.5	
3	-102	9	
5	-101	9	
6	-101	9	
7	-102	8.75	
10	-102	9.25	
11	-101	8	
12	-100	8	
25	-101	8.75	
26	-101	8.75	
27	-100	9.25	
33	-101	9	
34	-103	9	
42	-103	9	
43	-102	9	
44	-101	8.25	
45	-100	8.25	
52	-101	8.75	
53	-101	8.5	
37.73585	-101.25	8.75	AVG
	-101	8.875	MED
	0.850696	0.380443	STD
	3	1.25	RANGE

DS_NLOS @ 20m

Count	RSSI	SNR	
8	-109	9	
9	-109	9	
10	-110	9	
11	-110	8.25	
12	-109	7	
21	-108	9	
22	-109	9	
23	-109	9.5	
37	-110	9	
38	-110	9	
42	-109	8.25	
43	-111	8.25	
56	-109	9	
68	-109	9.25	
69	-110	9.25	
70	-112	9.25	
71	-109	9	
93	-109	9	
94	-109	9.5	
98	-109	9	
21.97802	-109.45	8.875	AVG
	-109	9	MED
	0.887041	0.564871	STD
	4	2.5	RANGE

DS_NLOS @ 50m

Count	RSSI	SNR	
15	-120	1	
16	-122	1	
17	-122	0	
18	-122	-0.5	
35	-123	0	
36	-124	0	
52	-122	-0.25	
55	-121	-0.25	
56	-121	0	
57	-123	0	
58	-122	0	
63	-122	-0.5	
64	-122	-0.5	
65	-122	-0.5	
93	-122	-1	
94	-122	0	
112	-123	0	
114	-123	-1	
115	-123	-0.5	
116	-122	-0.75	
19.60784	-122.15	-0.1875	AVG
	-122	-0.125	MED
	0.875094	0.524875	STD
	4	2	RANGE

DS_NLOS @ 100m

Count	RSSI	SNR	
5	-124	-7.5	
6	-124	-7	
23	-123	-7	
24	-122	-7	
25	-124	-7	
26	-123	-7	
75	-123	-7.25	
76	-124	-6.5	
77	-124	-7	
78	-124	-7	
79	-123	-7	
80	-123	-7	
134	-124	-7	
135	-124	-6.5	
136	-124	-6.5	
137	-123	-7	
151	-124	-7	
165	-124	-7	
166	-124	-7	
180	-124	-7	
11.36364	-123.6	-6.9625	AVG
	-124	-7	MED
	0.598243	0.233326	STD
	2	1	RANGE

DS_NLOS @ 125m

Count	RSSI	SNR	
39	-125	-8	
40	-125	-8	
41	-124	-8.5	
83	-122	-7.75	
84	-124	-8	
103	-125	-8	
104	-125	-7.75	
144	-124	-8	
145	-125	-7	
146	-125	-7	
147	-124	-8	
168	-124	-8.25	
207	-124	-8	
208	-125	-8	
209	-125	-8	
210	-125	-7.75	
220	-124	-8.75	
257	-123	-8	
258	-125	-8.25	
274	-124	-8	
8.474576	-124.35	-7.95	AVG
	-124.5	-8	MED
	0.812728	0.402296	STD
	3	1.75	RANGE

V_NLOS @ 1m

Count	RSSI	SNR	
4	-80	9	
5	-80	9.25	
6	-80	9.25	
7	-81	9	
9	-81	9	
10	-80	9	
11	-80	9.5	
12	-80	9.5	
13	-80	9.25	
14	-81	9.75	
15	-79	9.75	
19	-80	9.75	
20	-80	9	
21	-81	9	
22	-81	9.25	
23	-80	9.5	
26	-80	9.5	
27	-80	9.25	
28	-82	9.5	
29	-80	9	
76.92308	-80.3	9.3	AVG
	-80	9.25	MED
	0.656947	0.276253	STD
	3	0.75	RANGE

V_NLOS @ 2m

Count	RSSI	SNR	
3	-87	9	
4	-87	9.25	
5	-85	9	
6	-85	9.5	
14	-85	9.5	
15	-88	9	
23	-87	9	
24	-87	9	
25	-87	9	
37	-87	9.25	
38	-86	8.75	
39	-87	9	
40	-88	9	
41	-88	9	
42	-87	9	
43	-87	9.25	
44	-82	9.25	
45	-88	9	
46	-87	9	
47	-87	9	
44.44444	-86.6	9.0875	AVG
	-87	9	MED
	1.429022	0.18629	STD
	6	0.75	RANGE

V_NLOS @ 5m

Count	RSSI	SNR	
9	-101	9	
10	-104	9	
11	-105	9	
12	-105	8.75	
13	-105	9.5	
35	-105	8,25	
36	-102	9	
37	-104	9.5	
38	-104	9.75	
39	-104	9	
40	-105	8.75	
41	-103	9.25	
57	-104	9	
58	-104	9.5	
67	-104	9.5	
83	-104	9	
84	-105	9.25	
85	-104	9	
105	-103	8.75	
109	-105	9	
19.80198	-104	9.131579	AVG
	-104	9	MED
	1.076055	0.293073	STD
	4	1	RANGE

V_NLOS @ 10m

Count	RSSI	SNR	
12	-100	6.5	
13	-103	7	
14	-98	7.25	
15	-99	7.5	
45	-100	7	
46	-100	7	
47	-100	7.5	
67	-99	7.25	
68	-98	7.25	
69	-99	7	
70	-99	7	
89	-100	7	
90	-101	7	
91	-98	7.5	
92	-98	7.5	
93	-100	6.5	
94	-101	6.5	
118	-98	6.75	
119	-99	7	
120	-101	7.25	
18.34862	-99.55	7.0625	AVG
	-99.5	7	MED
	1.316894	0.323173	STD
	5	1	RANGE

V_NLOS @ 20m

Count	RSSI	SNR	
22	-112	7	
23	-111	7	
24	-110	7	
25	-110	7.5	
26	-112	7.25	
27	-111	7.5	
43	-111	7.75	
44	-112	7	
45	-114	7	
74	-112	7	
75	-113	7.25	
76	-110	7.25	
77	-112	7.75	
78	-112	7.75	
91	-112	7.25	
92	-111	6.75	
93	-109	7.75	
94	-110	7	
95	-112	7	
96	-112	7	
26.66667	-111.4	7.2375	AVG
	-112	7.125	MED
	1.187656	0.319076	STD
	5	1	RANGE

V_NLOS @ 50m

Count	RSSI	SNR	
17	-122	4	
18	-120	4	
19	-120	3.25	
39	-122	3.5	
40	-122	3.25	
64	-122	3.25	
65	-122	3.25	
66	-123	3.75	
67	-120	4	
68	-122	3.75	
74	-121	3.75	
75	-120	4.25	
99	-122	4	
100	-122	4	
101	-121	4	
122	-121	4	
123	-122	3.75	
124	-122	4.5	
125	-122	4.5	
145	-122	4	
15.50388	-121.5	3.8375	AVG
	-122	4	MED
	0.888523	0.382813	STD
	3	1.25	RANGE

V_NLOS @ 100m

Count	RSSI	SNR	
55	-124	-3	
56	-123	-3	
57	-124	-3.25	
58	-125	-3	
59	-124	-3.5	
88	-124	-3.5	
89	-125	-3.5	
121	-125	-3.5	
122	-124	-3.5	
123	-123	-4	
124	-124	-4	
132	-124	-4	
133	-124	-4	
134	-125	-4	
135	-125	-3.25	
136	-125	-3.25	
185	-124	-3.75	
185	-125	-3	
202	-124	-4	
204	-124	-4	
13.33333	-124.25	-3.55	AVG
	-124	-3.5	MED
	0.638666	0.394034	STD
	2	1	RANGE

V_NLOS @ 115m

Count	RSSI	SNR	
84	-125	-4	
85	-125	-4	
86	-125	-4	
87	-125	-4	
104	-124	-4.25	
105	-125	-3.75	
134	-123	-4	
135	-125	-3.25	
136	-125	-4.25	
137	-125	-4.5	
172	-125	-4	
173	-125	-3.75	
177	-124	-3.75	
178	-125	-3.75	
209	-124	-4	
210	-124	-4	
211	-125	-4	
212	-125	-4.5	
245	-125	-4	
259	-125	-3.75	
11.36364	-124.7	-3.975	AVG
	-125	-4	MED
	0.571241	0.279803	STD
	2	1.25	RANGE

Drone @ 0deg				Drone @ 5deg				Drone @ 10deg			
Count	RSSI	SNR		Count	RSSI	SNR		Count	RSSI	SNR	
23	-120	0.5		18	-96	-2		6	-96	-1	
24	-119	0.75		19	-96	-2.5		7	-96	-1	
25	-120	0		20	-99	-2.25		8	-95	0	
26	-121	0		21	-100	-3		9	-93	0	
32	-122	0.75		33	-100	-2.5		10	-90	0	
33	-120	0.75		34	-99	-2		11	-90	0	
40	-120	0.75		39	-98	-2		12	-90	0.5	
45	-120	0		40	-95	-2		13	-95	-0.25	
46	-121	0		41	-92	-2		21	-96	-0.25	
68	-118	0		42	-93	-2		22	-92	-0.5	
69	-119	0		43	-96	-2.5		23	-90	-0.5	
70	-119	0.5		44	-99	-2.75		24	-92	-1	
81	-120	-0.5		45	-98	-2		38	-92	-1	
82	-120	-1		61	-100	-2.5		39	-94	-0.5	
95	-119	0		62	-101	-2.5		40	-94	-1	
96	-121	0		73	-98	-2.5		41	-95	-2	
97	-122	0.5		74	-98	-2.75		44	-99	0	
109	-122	0.5		75	-95	-2.75		45	-96	-1.5	
110	-120	-1		76	-100	-2		46	-95	-1.5	
123	-122	0.25		80	-95	-2		47	-94	-1	
19.80198	-120.25	0.1375	AVG	31.74603	-97.4	-2.325	AVG	47.61905	-93.7	-0.625	AVG
	-120	0	MED		-98	-2.375	MED		-94	-0.5	MED
	1.164158	0.522362	STD		2.521487	0.33541	STD		2.515217	0.641236	STD
	4	1.75	RANGE		9	1	RANGE		9	2.5	RANGE

Drone @ 20deg				Drone @ 30deg				Drone @ 40deg			
Count	RSSI	SNR		Count	RSSI	SNR		Count	RSSI	SNR	
3	-86	-1		7	-86	-1		14	-85	-1	
4	-87	-1		8	-87	0.5		15	-84	-0.25	
5	-87	-1		13	-85	0		16	-88	-1	
6	-87	-1		14	-87	0		17	-87	-1	
12	-88	0.5		15	-82	0.25		24	-83	-0.25	
13	-86	-0.75		16	-86	-0.75		25	-85	-0.25	
14	-87	-1		17	-87	-0.75		35	-89	-1	
15	-87	-0.5		18	-85	-0.5		36	-87	-0.5	
16	-85	-0.25		24	-85	-0.25		37	-88	-0.25	
18	-87	0		25	-87	-1		52	-88	-0.25	
19	-89	-0.5		28	-86	0.25		53	-83	-1	
20	-88	-0.5		29	-88	0.25		54	-84	-1	
25	-88	-0.5		30	-87	-0.75		55	-85	-0.5	
26	-87	-1		31	-87	-1		56	-88	-0.25	
27	-86	-0.25		32	-82	-1		57	-86	-1	
28	-87	0		33	-82	0.75		61	-85	-0.25	
36	-86	-0.5		35	-85	-1		62	-84	-0.25	
37	-87	-1		36	-83	-0.5		63	-83	-0.25	
38	-87	-0.5		37	-84	-0.25		64	-83	-0.5	
39	-86	-0.5		38	-86	-0.5		65	-84	-0.25	
54.05405	-86.9	-0.5625	AVG	62.5	-85.35	-0.3625	AVG	38.46154	-85.45	-0.55	AVG
	-87	-0.5	MED		-86	-0.5	MED		-85	-0.375	MED
	0.91191	0.420487	STD		1.871532	0.55887	STD		2.012461	0.349812	STD
	4	1.5	RANGE		6	1.75	RANGE		6	0.75	RANGE

Drone @ 50deg				Drone @ 60deg				Drone @ 70deg			
Count	RSSI	SNR		Count	RSSI	SNR		Count	RSSI	SNR	
6	-85	0		23	-88	1		9	-83	0.5	
7	-84	-0.5		24	-86	0.25		10	-82	0.25	
8	-86	-0.25		25	-86	0.25		11	-83	0.75	
9	-85	-1		31	-83	1		12	-83	1	
15	-84	-0.5		32	-84	-0.5		13	-81	0	
16	-85	-0.5		38	-84	-0.5		14	-80	0	
17	-85	-0.5		39	-84	-0.25		29	-81	0	
18	-85	-0.5		40	-88	0.75		30	-84	0.5	
19	-85	-0.5		41	-87	-0.5		32	-85	0.25	
20	-85	-1		41	-85	-0.25		33	-84	0	
21	-85	0		47	-86	-1		34	-87	0.5	
22	-87	0		48	-87	0.5		35	-84	-0.75	
23	-86	-0.25		50	-87	-0.25		36	-83	0	
29	-83	-0.25		51	-83	-0.25		37	-83	0	
30	-84	-0.25		52	-84	0.5		38	-84	-1	
31	-87	-0.75		53	-82	0.25		39	-84	0.25	
32	-85	0		54	-85	0		40	-84	0.5	
45	-85	0		58	-81	0.5		41	-83	-0.5	
46	-84	0		59	-84	0.25		44	-85	0.25	
47	-85	-0.75		62	-85	0.5		45	-83	0.25	
47.61905	-85	-0.375	AVG	50	-84.95	0.1125	AVG	54.05405	-83.3	0.1375	AVG
	-85	-0.375	MED		-85	0.25	MED		-83	0.25	MED
	0.973329	0.329473	STD		1.932411	0.540924	STD		1.559352	0.476245	STD
	4	1	RANGE		7	2	RANGE		7	2	RANGE

Drone @ 80deg				Drone @ 90deg			
Count	RSSI	SNR		Count	RSSI	SNR	
3	-78	1		19	-79	1	
7	-80	1.5		21	-79	1	
8	-79	1		22	-81	1	
9	-80	1.5		23	-80	1	
10	-82	1.25		29	-81	0.5	
11	-82	0.75		30	-81	0.25	
12	-79	1		31	-80	0.5	
13	-77	1		32	-77	1	
14	-80	1.25		33	-77	0.25	
47	-82	1.25		34	-83	0.75	
48	-81	1.5		38	-80	1.75	
49	-81	0.75		39	-80	2	
50	-78	1		40	-80	2	
64	-78	1		41	-79	1.75	
65	-80	0.75		42	-79	1	
66	-82	0.5		45	-76	0.75	
67	-82	1.5		46	-81	1	
68	-83	1.5		47	-80	1	
83	-80	1		49	-80	1.75	
84	-77	1.25		54	-81	1.5	
24.39024	-80.05	1.1125	AVG	55.55556	-79.7	1.0875	AVG
	-80	1	MED		-80	1	MED
	1.820208	0.297744	STD		1.625455	0.539706	STD
	6	1	RANGE		7	1.75	RANGE

Appendix B - Matlab Code

Free Space Path Loss Model

```
%%
%FSPL Modelling
%Author: Nicholas Manns
%USQ
%u1092436

%
clear;
clc;

% Obtained results and corresponding distances
obtained_distances = [0.01 1 2 5 10 20 50 100 200 400]; % (m)
obtained_fspl = [-18 -63.6 -84 -90.15 -99.5 -117.8 -121.55 -122.9 -123 -123.8]; % dBm


% Parameters
frequency = 915e6; % Frequency in Hz (915 MHz)
speed_of_light = 3e8; % Speed of light in m/s
d_min = 0.01; % Minimum distance to the transmitter in meters
d_max = 400; % Maximum distance to the transmitter in meters
num_points = 1000; % Number of points for distance sampling
transmitted_power_dBm = 14;
Antenna_Gain = 4; %Factor in 2dBi Gain for each antenna

% Generate distance array
distances = linspace(d_min, d_max, num_points);

% Calculate Free-Space Path Loss (FSPL)
fspl = transmitted_power_dBm + Antenna_Gain - 20*log10(distances) -
20*log10(4*pi/(speed_of_light/frequency));

% Logarithmic curve fitting with bounds
ft = fittype('a*log10(x) + b', 'independent', 'x', 'dependent', 'y');
opts = fitoptions(ft);
opts.Lower = [-Inf, -Inf]; % Set lower bounds
opts.Upper = [Inf, Inf]; % Set upper bounds
opts.Robust = 'Bisquare'; % Use robust fitting to reduce the influence of outliers
[fitresult, gof] = fit(obtained_distances', obtained_fspl', ft, opts);

% Generate fitted values
fitted_values = feval(fitresult, obtained_distances);

% Plot the results
figure;
plot(distances, fspl, 'b', 'LineWidth', 1.5); % Plot calculated FSPL in blue
hold on;
plot(obtained_distances, obtained_fspl, 'ro', 'LineWidth', 1.5, 'MarkerSize', 8); % Plot obtained
results in red circles
plot(obtained_distances, fitted_values, 'g--', 'LineWidth', 1.5); % Plot fitted curve in green dashed
line
xlabel('Distance (m)');
ylabel('Attenuation (dBm)');
title('Free-Space Path Loss @ 915 MHz');
legend('Modelled FSPL', 'Obtained Results','Fitted Curve');
grid on;
```

LDPL Model

```
%%
%Log Distance Path Loss Modelling
%Author: Nicholas Manns
%USQ
%u1092436

%
clear;
clc;

% Given data
distances = [0.01 1 2 5 10 20 50 100 200 400]; % m
fspl = [-18 -63.6 -84 -90.15 -99.5 -117.8 -121.55 -122.9 -123 -123.8]; % dB

% Define the reference distance
d0 = distances(2); % reference distance
L0 = fspl(2); % path loss at reference distance d0


% Calculate the path loss exponent (n)
n = (fspl(end) - L0) / (10 * log10(distances(end) / d0));

% Calculate the theoretical path loss values using the Log-Distance Path Loss model for each segment
L_model = L0 + 10 * n * log10(distances / d0);

% Plot the measured and theoretical path loss values
figure;
plot(distances, fspl, 'bo-', 'LineWidth', 2); % Plot measured data
hold on;
plot(distances, L_model, 'r--', 'LineWidth', 2); % Plot theoretical model
grid on;
xlabel('Distance (m)');
ylabel('Attenuation (dBm)');
title('Log-Distance Path Loss Model');
legend('Measured FSPL', 'LDPL Model');
```

Multi-Slope LDPL Model

```
%%
%Multi-slope Log Distance Path Loss Modelling
%Author: Nicholas Manns
%USQ
%u1092436

%
clear;
clc;

% Given data
distances = [0.01 1 2 5 10 20 50 100 200 400]; % m
fspl = [-18 -63.6 -84 -90.15 -99.5 -117.8 -121.55 -122.9 -123 -123.8]; % dB

% Define the reference distance
d0 = distances(2); % reference distance
L0 = fspl(2); % path loss at reference distance d0

% Separate the distances into two segments
distances_1 = distances(distances <= 50); % 0m to 50m
distances_2 = distances(distances > 50);  % 50m to 400m

% Corresponding FSPL values for the two segments
fspl_1 = fspl(1:length(distances_1));
fspl_2 = fspl(length(distances_1)+1:end);

% Calculate the path loss exponent (n) for each segment
n1 = (fspl_1(end) - L0) / (10 * log10(distances_1(end) / d0)); % 0m to 50m
n2 = (fspl_2(end) - fspl_1(end)) / (10 * log10(distances_2(end) / distances_1(end))); % 50m to 400m

% Calculate the theoretical path loss values using the Log-Distance Path Loss model for each segment
L_model_1 = L0 + 10 * n1 * log10(distances_1 / d0);
L_model_2 = fspl_1(end) + 10 * n2 * log10(distances_2 / distances_1(end));

% Plot the measured and theoretical path loss values
figure;
plot(distances, fspl, 'bo-', 'LineWidth', 2); % Plot measured data
hold on;
plot(distances_1, L_model_1, 'r--', 'LineWidth', 2); % Plot theoretical model for 0m to 50m
plot(distances_2, L_model_2, 'g--', 'LineWidth', 2); % Plot theoretical model for 50m to 400m
grid on;
xlabel('Distance (m)');
ylabel('Attenuation (dBm)');
title('Multi-Slope Log-Distance Path Loss Model');
legend('Measured FSPL', 'LDPL Model (0m to 50m)', 'LDPL Model (50m to 400m)');
% Remove logarithmic scale from x-axis
hold off;
```

Existing Empirical Models

```
%%
%Vegetation Attenuation Modelling
%Author: Nicholas Manns
%USQ
%u1092436

%
clear;
clc;

% Parameters
frequency = 915e6; % Frequency in Hz (915 MHz)
speed_of_light = 3e8; % Speed of light in m/s
d_min = 0.01; % Minimum distance to the transmitter in meters
d_max = 125; % Maximum distance to the transmitter in meters
num_points = 125; % Number of points for distance sampling
transmitted_power_dBm = 14;
Vegetation_Factor = 0.3; % 30% Foliage

% Obtained results
Recorded_Distances = [0.01 1 2 5 10 20 50 100 125]; % m
Recorded_Measurements = [-18.05 -65.6 -85.2 -99.95 -101.25 -109.45 -122.15 -123.6 -124.35]; %dBm

% Generate distance array
distances = linspace(d_min, d_max, num_points);

% Calculate Free-Space Path Loss (FSPL)
fspl = 20*log10(distances) + 20*log10(frequency) + 20*log10(4*pi/speed_of_light);
fspl = -abs(fspl);

%
Vegetation_Travel = zeros(size(distances));
Free_Space_Travel = zeros(size(distances));
Vegetation_Travel = distances * Vegetation_Factor;
Free_Space_Travel = distances - Vegetation_Travel;

% Initialize attenuation array
Weissberger_Vegetation_Attenuation = zeros(size(Vegetation_Travel));

% Calculate attenuation using the Weissberger model
for i = 1:length(Vegetation_Travel)
    d = Vegetation_Travel(i);
    if d <= 14
        Weissberger_Vegetation_Attenuation(i) = 0.45 * (frequency/1e6)^0.284 * d;
    else
        Weissberger_Vegetation_Attenuation(i) = 1.33 * (frequency/1e6)^0.284 * d^0.588;
    end
end

Weissberger_Vegetation_Attenuation = -abs(Weissberger_Vegetation_Attenuation);
Weissberger_TotalAttenuation = Weissberger_Vegetation_Attenuation + fspl;
Weissberger_dBm = Weissberger_TotalAttenuation - transmitted_power_dBm;

% Calculate attenuation using the ITU model
for i = 1:length(Vegetation_Travel)
    d = Vegetation_Travel(i);
    ITU_Vegetation_Attenuation(i) = 0.2 * (frequency/1e6)^0.3 * d^0.6;
end

ITU_Vegetation_Attenuation = -abs(ITU_Vegetation_Attenuation);
ITU_TotalAttenuation = ITU_Vegetation_Attenuation + fspl;
ITU_dBm = ITU_TotalAttenuation - transmitted_power_dBm;

%ITU Maximum Attenuation Model
Am = 0.18 * 915^0.752;
R = 0.3;
Excess_Att = Am * (1 - exp(R*Vegetation_Travel/Am));
Total_Att = Excess_Att + fspl;
MA_dBm = Total_Att - transmitted_power_dBm;
```

```
% Find the closest distances in the modeled array
ITU_Modeled_Values = zeros(size(Recorded_Distances));
for i = 1:length(Recorded_Distances)
    [~, idx] = min(abs(distances - Recorded_Distances(i)));
    ITU_Modeled_Values(i) = ITU_dBm(idx);
end

% Calculate the error
ITU_Error = ITU_Modeled_Values - Recorded_Measurements;
ITU_Max_Error = max(abs(ITU_Error));
ITU_Avg_Error = mean(abs(ITU_Error));
ITU_RMSE = sqrt(mean((ITU_Modeled_Values - Recorded_Measurements).^2));

% Find the closest distances in the modeled array
Weissberger_Modeled_Values = zeros(size(Recorded_Distances));
for i = 1:length(Recorded_Distances)
    [~, idx] = min(abs(distances - Recorded_Distances(i)));
    Weissberger_Modeled_Values(i) = Weissberger_dBm(idx);
end

% Calculate the error
Weissberger_Error = Weissberger_Modeled_Values - Recorded_Measurements;
Weissberger_Max_Error = max(abs(Weissberger_Error));
Weissberger_Avg_Error = mean(abs(Weissberger_Error));
Weissberger_RMSE = sqrt(mean((Weissberger_Modeled_Values - Recorded_Measurements).^2));

% Find the closest distances in the modeled array
ITU_MA_Modeled_Values = zeros(size(Recorded_Distances));
for i = 1:length(Recorded_Distances)
    [~, idx] = min(abs(distances - Recorded_Distances(i)));
    ITU_MA_Modeled_Values(i) = MA_dBm(idx);
end

% Calculate the error
ITU_MA_Error = ITU_MA_Modeled_Values - Recorded_Measurements;
ITU_MA_Max_Error = max(abs(ITU_MA_Error));
ITU_MA_Avg_Error = mean(abs(ITU_MA_Error));
ITU_MA_RMSE = sqrt(mean((ITU_MA_Modeled_Values - Recorded_Measurements).^2));


% Plot the results
figure;
plot(distances, Weissberger_dBm, 'b', 'LineWidth', 1.5);
hold on;
plot(distances, ITU_dBm, 'y','LineWidth', 1.5);
plot(distances, MA_dBm,'m','LineWidth', 1.5);
plot(Recorded_Distances, Recorded_Measurements, 'ro', 'LineWidth', 1.5, 'MarkerSize', 8); % Plot
recorded measurements in red circles
xlabel('Distance (m)');
xlim ([0 125]);
ylabel('Attenuation (dB)');
title('Double Skip (30% Vegetation) Attenuation @ 915 MHz');
legend('Weissberger Model', 'ITU Model', 'ITU MA Model','Recorded Measurements' ,'Fitted Curve');
grid on;
hold off;
```

Proposed Path Loss Model

```
%%
%Proposed Empirical Model
%Author: Nicholas Manns
%USQ
%u1092436

%
clear;
clc;


% Obtained results
Recorded_Distances = [0.01 1 2 5 10 20 50 100 115];
Recorded_Measurements = [-19 -80.3 -86.6 -104 -99.55 -111.4 -121.5 -124.25 -124.7];

% Parameters
frequency = 915e6; % Frequency in Hz (915 MHz)
speed_of_light = 3e8; % Speed of light in m/s
d_min = 0.01; % Minimum distance to the transmitter in meters
d_max = 115; % Maximum distance to the transmitter in meters
num_points = 115; % Number of points for distance sampling
transmitted_power_dBm = 14; % Transmitted power in dBm
Vegetation_Factor = 0.5; % Vegetation Factor


% Generate distance array
distances = linspace(d_min, d_max, num_points);

%Determine hoe much propagation in veg or free space
Vegetation_Travel = zeros(size(distances)); % Propagation length through vegetation
Free_Space_Travel = zeros(size(distances)); % Propagation length through free space
Vegetation_Travel = distances * Vegetation_Factor;
Free_Space_Travel = distances - Vegetation_Travel;


% Calculate attenuation using the ITU model
for i = 1:length(Vegetation_Travel)
    d = Vegetation_Travel(i);
    ITU_Vegetation_Attenuation(i) = 0.2 * (frequency/1e6)^0.3 * d^0.6;
end


% Calculate LDPL attenuation
for i = 1:length(Free_Space_Travel)
    d = Free_Space_Travel(i);
    if d <= 50
        LDPL_Attenuation(i) = 63.6 + 23.1 * log10(d);
    else
        LDPL_Attenuation(i) = 121.55 + 2.49 * log10(d/50);
    end
end

ITU_Vegetation_Attenuation = -abs(ITU_Vegetation_Attenuation);
LDPL_Attenuation = -abs(LDPL_Attenuation);

% Define the noise floor level
noise_floor = -125; % Noise floor in dB

TotalAttenuation = ITU_Vegetation_Attenuation + LDPL_Attenuation;
ITU_dBm = TotalAttenuation - transmitted_power_dBm;

for i = 1:length(ITU_dBm)% Apply noise floor limit
 if ITU_dBm(i) < noise_floor
    ITU_dBm(i) = noise_floor;
 end
end



% Find the closest distances in the modelled array
Modelled_Values = zeros(size(Recorded_Distances));
```

```
for i = 1:length(Recorded_Distances)
    [~, idx] = min(abs(distances - Recorded_Distances(i)));
    Modelled_Values(i) = ITU_dBm(idx);
end

% Calculate the error
Error = Modelled_Values - Recorded_Measurements;
Max_Error = max(abs(Error));
Avg_Error = mean(abs(Error));
Empirical_Model_RMSE = sqrt(mean((Modelled_Values - Recorded_Measurements).^2));


% Plot the results
figure;
plot(distances, ITU_dBm, 'b', 'LineWidth', 1.5);
hold on;
plot(Recorded_Distances, Recorded_Measurements, 'ro', 'LineWidth', 1.5, 'MarkerSize', 8); % Plot
recorded measurements in red circles
xlabel('Distance (m)');
xlim ([0 115]);
ylabel('Attenuation (dB)');
ylim([-130 0])
yticks([-130 -120 -110 -100 -90 -80 -70 -60 -50 -40 -30 -20 -10 0])
title('Double Skip (50% Vegetation) Attenuation @ 915 MHz');
legend('Propsed Empirical Model', 'Measured Values');
grid on;
hold off
```

Satellite Simulation Modelling

```
%%
%Satellite Simulation Signal Attenuation Modelling
%Author: Nicholas Manns
%USQ
%u1092436


%%
clear;
clc;

%Measured Results
Test_Angles = [0 5 10 20 30 40 50 60 70 80 90];
obtained = [-120.25 -97.4 -93.7 -86.9 -85.35 -85.45 -85 -84.95 -83.3 -80.05 -79.7];%dBm

% Define parameters
Transmission_Distance = 50; % Distance between Tx & Rx
Cotton_Height = 1.1; % Height of stubble (m)
Transmission_Angle = 0:1:90; % Angles in degrees
speed_of_light = 3e8; % Speed of light in m/s
transmitted_power_dBm = 14 % Transmitted power in dBm
frequency = 915; % Frequency in MHz
Foliage_Depth = 0.3; % Vegetation Factor

% Convert angles from degrees to radians
Transmission_Angle_Rad = deg2rad(Transmission_Angle);
% Calculate X and Y coordinates based on the transmission angle
Transmission_X = Transmission_Distance * cos(Transmission_Angle_Rad);
Transmission_Y = Transmission_Distance * sin(Transmission_Angle_Rad);
%
Vegetation_Travel = zeros(size(Transmission_Angle));% Propagation length through vegetation
Free_Space_Travel = zeros(size(Transmission_Angle));% Propagation length through free space
%%
Vegetation_Travel = Transmission_Distance - ((Transmission_Y - Cotton_Height) ./
sin(Transmission_Angle_Rad));
old = [Inf];
new = [Transmission_Distance];
Vegetation_Travel = changem(Vegetation_Travel,new,old);
Vegetation_Travel(end) = 0;
% Set Vegetation_Travel to 0 if Transmission_Y is less than Cotton_Height
Vegetation_Travel(Transmission_Y < Cotton_Height) = Transmission_Distance;
Vegetation_Travel = Vegetation_Travel .* Foliage_Depth;
Free_Space_Travel = Transmission_Distance - Vegetation_Travel;

%Model 1
% Initialize Weissberger attenuation array
Weissberger_Vegetation_Attenuation = zeros(size(Vegetation_Travel));

% Calculate attenuation using the Weissberger model
for i = 1:length(Vegetation_Travel)
    d = Vegetation_Travel(i);
    if d <= 14
        Weissberger_Vegetation_Attenuation(i) = 1.33 * frequency^0.284 * d^0.588;
    else
        Weissberger_Vegetation_Attenuation(i) = 0.45 * frequency^0.284 * d;
    end
end

Weissberger_Vegetation_Attenuation = -abs(Weissberger_Vegetation_Attenuation);
fspl = 20*log10(Free_Space_Travel) + 20*log10(frequency) + 20*log10(4*pi/speed_of_light);
Weissberger_TotalAttenuation = Weissberger_Vegetation_Attenuation + fspl;
Weissberger_Received_dBm = transmitted_power_dBm + Weissberger_TotalAttenuation

%Model 2
% Calculate attenuation using the ITU model
for i = 1:length(Vegetation_Travel)
    d = Vegetation_Travel(i);
    ITU_Vegetation_Attenuation(i) = 0.2 * frequency^0.3 * d^0.6;
end

ITU_Vegetation_Attenuation = -abs(ITU_Vegetation_Attenuation);
```

```
ITU_TotalAttenuation = ITU_Vegetation_Attenuation + fspl;
ITU_Received_dBm = transmitted_power_dBm + ITU_TotalAttenuation;

%Proposed Model
% Calculate LDPL attenuation
for i = 1:length(Free_Space_Travel)
    d = Free_Space_Travel(i);
    if d <= 50
        LDPL_Attenuation(i) = 63.6 + 23.1 * log10(d);
    else
        LDPL_Attenuation(i) = 121.55 + 2.49 * log10(d/50);
    end
end
LDPL_Attenuation = -abs(LDPL_Attenuation);
Attenuation = ITU_Vegetation_Attenuation + LDPL_Attenuation + transmitted_power_dBm;
% Define the noise floor level
noise_floor = -125; % Noise floor in dB
for i = 1:length(Attenuation)% Apply noise floor limit
 if Attenuation(i) < noise_floor
    Attenuation(i) = noise_floor;
 end
end

% Plot the results
figure;
plot(Transmission_Angle, Weissberger_Received_dBm, 'b', 'LineWidth', 1.5); % Plot calculated FSPL in
blue
hold on;
plot(Transmission_Angle, ITU_Received_dBm, 'y','LineWidth', 1.5);
plot(Test_Angles, obtained, 'ro', 'LineWidth', 1.5, 'MarkerSize', 8); % Plot obtained results in red
circles
plot(Transmission_Angle, Attenuation, 'm', 'LineWidth',1.5);
%plot(Transmission_Angle, fitted_values, 'g--', 'LineWidth', 1.5); % Plot fitted curve in green dashed
line
xlabel('Transmission Angle (degrees)');
ylabel('RSSI (dBm)');
ylim([-130 0])
yticks([-130 -120 -110 -100 -90 -80 -70 -60 -50 -40 -30 -20 -10 0])
title('RF attenuation @ 915 MHz');
legend('Weissberger Model', 'ITU Model','Obtained Results', 'Proposed Model', 'Location', 'best');
grid on;
hold off;
```

XC4392 Data Receiving/Processing

```
%%
%%XC4392 Receiver Processing
%Author: Nicholas Manns
%USQ
%u1092436

clear;
clc;

% Define serial port
serialPort = 'COM4';

% Set up serial connection
baudRate = 115200;
device = serialport(serialPort, baudRate);

% Initialize arrays to store data
countArray = [];
timestampArray = [];
rssiArray = [];
snrArray = [];

% Set the timeout for reading the serial data
device.Timeout = 100; % Maximum 100 secs between messages

% Specify the number of readings to collect
numReadings = 20;

disp('Reading data from Arduino...');

for i = 1:numReadings
    try
        % Read a line of data from the serial port
        data = readline(device);

        % Split the data string by comma
        dataSplit = split(data, ',');

        % Check if the data contains four parts
        if length(dataSplit) == 4
            % Extract the count, timestamp, RSSI, and SNR values
            count = str2double(dataSplit{1});
            timestamp = str2double(dataSplit{2});
            rssi = str2double(dataSplit{3});
            snr = str2double(dataSplit{4});

            % Check for NaN values and only append valid data
            if ~isnan(count) && ~isnan(timestamp) && ~isnan(rssi) && ~isnan(snr)
                % Append the values to their respective arrays
                countArray = [countArray; count];
                timestampArray = [timestampArray; timestamp];
                rssiArray = [rssiArray; rssi];
                snrArray = [snrArray; snr];

                % Display the read values (optional)
                fprintf('Count: %d, Timestamp: %d, RSSI: %d dBm, SNR: %.2f dB\n',
count, timestamp, rssi, snr);
```

```
            end
        else
            disp('Incorrect data format received');
        end
    catch
        disp('Error reading data');
    end

    % Short pause to allow data accumulation
    pause(0.1);
end

disp('Data collection complete.');

% Close the serial connection
clear device;

% Display the collected data
disp('Count Array:');
disp(countArray);
disp('Timestamp Array:');
disp(timestampArray);
disp('RSSI Array:');
disp(rssiArray);
disp('SNR Array:');
disp(snrArray);

dataTable = table(countArray, timestampArray, rssiArray, snrArray, ...
                  'VariableNames', {'Count', 'Timestamp', 'RSSI', 'SNR'});

% Save data to Excel spreadsheet
filename = 'received_data.xlsx';
writetable(dataTable, filename);

disp(['Data saved to ', filename]);
```

Appendix C – Arduino Code

XC4392 Transmitter

```
#include <SPI.h>
#include <LoRa.h> // Include the LoRa library

#define TXADDR 0xE7E7E7E7 // Address of the receiving device
#define SEND_INTERVAL 1000 // Delay in milliseconds between each send

struct Message {
  unsigned long count;
  unsigned long timestamp;
};

unsigned long messageCount = 0;

void setup() {
  Serial.begin(115200); // Initialize serial communication for debugging

  // Initialize SPI
  SPI.begin();

  // Initialize the LoRa transceiver
  if (!LoRa.begin(915E6)) { // Initialise the transceiver at 915 MHz
    Serial.println("Initilisation LoRa failed!");
    while (1);
  }

  LoRa.setSyncWord(0xF3); // Set the sync word
  LoRa.setPreambleLength(8); // Set the preamble length
}

void loop() {
```

```
  static unsigned long lastSendTime = 0;
  unsigned long currentTime = millis();

  // Send a message at intervals
  if (currentTime - lastSendTime >= SEND_INTERVAL) {
    lastSendTime = currentTime;

    // Create a new message
    Message message;
    message.count = messageCount++;
    message.timestamp = millis();

    // Start the packet
    LoRa.beginPacket();

    // Write the message structure to the packet
    LoRa.write((uint8_t*)&message, sizeof(message));

    // End the packet and send it
    LoRa.endPacket();

    // Print the sent message to the serial monitor
    Serial.print("Sent message: Count = ");
    Serial.print(message.count);
    Serial.print(", Timestamp = ");
    Serial.println(message.timestamp);
  }
}
```

XC4392 Receiver

```
#include <SPI.h>

#include <LoRa.h> // Include the LoRa library


#define RXADDR 0xE7E7E7E7 // Address of the device to listen to (same as TXADDR for communication)

#define POLLING_INTERVAL 100 // Delay in milliseconds between each poll


struct Message {
  unsigned long count;
  unsigned long timestamp;
  int rssi;
  float snr;
};
`

void setup() {
  Serial.begin(115200); // Initialize serial communication for debugging


  // Initialize SPI
  SPI.begin();


  // Initialize the LoRa transceiver
  if (!LoRa.begin(915E6)) { // Initialise the transceiver at 915 MHz
    Serial.println("Initilisation LoRa failed!");
    while (1);
  }


  LoRa.setSyncWord(0xF3);
  LoRa.setPreambleLength(8); // Set the preamble length
}
```

```
void loop() {
  static unsigned long lastPollTime = 0;
  unsigned long currentTime = millis();

  // Polling mode to check if a new message has been received at intervals
  if (currentTime - lastPollTime >= POLLING_INTERVAL) {
    lastPollTime = currentTime;

    // Check if there is a packet available
    int packetSize = LoRa.parsePacket();
    if (packetSize) {
      Message message;
      int i = 0;

      // Read the packet into the message structure
      while (LoRa.available() && i < sizeof(Message)) {
        ((uint8_t*)&message)[i++] = LoRa.read();
      }

      // Get RSSI and SNR values
      message.rssi = LoRa.packetRssi();
      message.snr = LoRa.packetSnr();

      // Print the received message to the serial monitor
      Serial.print("Count: ");
      Serial.print(message.count);
      Serial.print(", Timestamp: ");
      Serial.print(message.timestamp);
      Serial.print(", RSSI: ");
      Serial.print(message.rssi);
      Serial.print(" dBm, SNR: ");
```

```
        Serial.print(message.snr);
        Serial.println(" dB");

        // Send data in format: count,timestamp,rssi,snr
        Serial.print(message.count);
        Serial.print(",");
        Serial.print(message.timestamp);
        Serial.print(",");
        Serial.print(message.rssi);
        Serial.print(",");
        Serial.println(message.snr);
      }
    }
}
```

Appendix D - Hardware Datasheets

SX1276/77/78/79 - 137 MHz to 1020 MHz Low Power Long Range Transceiver

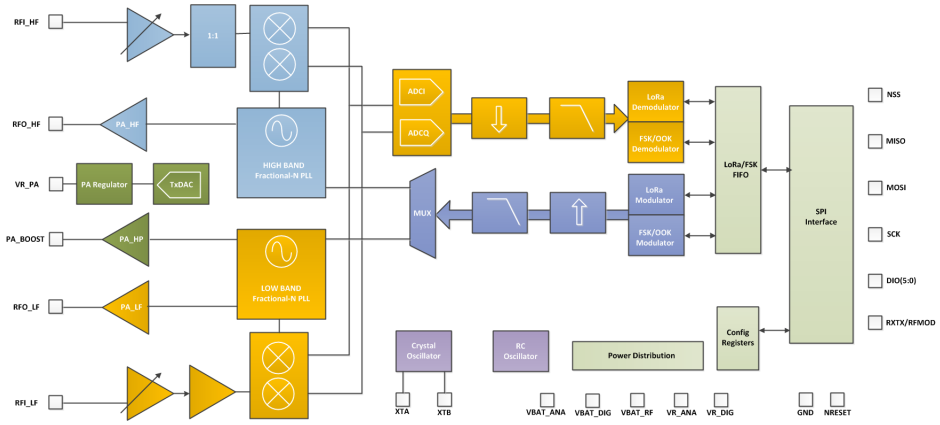

GENERAL DESCRIPTION

The SX1276/77/78/79 transceivers feature the LoRa® long range modem that provides ultra-long range spread spectrum communication and high interference immunity whilst minimising current consumption.

Using Semtech's patented LoRa modulation technique SX1276/77/78/79 can achieve a sensitivity of over -148dBm using a low cost crystal and bill of materials. The high sensitivity combined with the integrated +20 dBm power amplifier yields industry leading link budget making it optimal for any application requiring range or robustness. LoRa provides significant advantages in both blocking and selectivity over conventional modulation techniques, solving the traditional design compromise between range, interference immunity and energy consumption.

These devices also support high performance (G)FSK modes for systems including WMBus, IEEE802.15.4g. The SX1276/77/78/79 deliver exceptional phase noise, selectivity, receiver linearity and IIP3 for significantly lower current consumption than competing devices.

ORDERING INFORMATION

Part Number	Delivery	MOQ / Multiple
SX1276IMLTRT	T&R	3000 pieces
SX1277IMLTRT	T&R	3000 pieces
SX1278IMLTRT	T&R	3000 pieces
SX1279IMLTRT	T&R	3000 pieces
SX1276WS[1]	Wafer Form	1 Wafer (2000 dies)

1. For Wafer deliveries, refer to the corresponding "Wafer Delivery Specification"

- QFN 28 Package - Operating Range [-40;+85°C]
- Pb-free, Halogen free, RoHS/WEEE compliant product

KEY PRODUCT FEATURES

- LoRa® Modem
- 168 dB maximum link budget
- +20 dBm - 100 mW constant RF output vs. V supply
- +14 dBm high efficiency PA
- Programmable bit rate up to 300 kbps
- High sensitivity: down to -148 dBm
- Bullet-proof front end: IIP3 = -11 dBm
- Excellent blocking immunity
- Low RX current of 9.9 mA, 200 nA register retention
- Fully integrated synthesizer with a resolution of 61 Hz
- FSK, GFSK, MSK, GMSK, LoRa® and OOK modulation
- Built-in bit synchronizer for clock recovery
- Preamble detection
- 127 dB Dynamic Range RSSI
- Automatic RF Sense and CAD with ultra-fast AFC
- Packet engine up to 256 bytes with CRC
- Built-in temperature sensor and low battery indicator

APPLICATIONS

- Automated Meter Reading.
- Home and Building Automation.
- Wireless Alarm and Security Systems.
- Industrial Monitoring and Control
- Long range Irrigation Systems

XC4392 LoRa™ Shield

LoRa™:

LoRa™ is a powerful new technology enabling secure wireless data communications over long distances even several kilometres without the need of a mobile GSM network. LoRa™ can be used in many outdoor or indoor applications, such as building automation, weather monitoring, irrigation systems control, smart metering, smart cities, and much more. For more information about LoRa™ visit https://www.lora-alliance.org/.

The XC4388 LoRa™ Shield is based on the Semtech SX1276 IC. More information can be found on the datasheet at http://www.semtech.com/images/datasheet/sx1276_77_78_79.pdf, but is not necessary for basic usage. This version operates at 915MHz.

Software:

The library at https://github.com/sandeepmistry/arduino-LoRa (or simply search for 'lora' in the Library Manager) provides most basic functionality. Also see the examples for applications. Detailed information about this library can be found in the API description at https://github.com/sandeepmistry/arduino-LoRa/blob/master/API.md

The LoRa™ Remote Relay project at https://www.jaycar.com.au/lora-remote also has some example code.

Hardware:

The antenna is provided loose and should be attached before operation.

It's also recommended to disconnect the three jumpers labelled J_DIO5, J_DIO2 and J_DIO1, as they connect pins on the shield to the Arduino board underneath, and are usually not necessary.

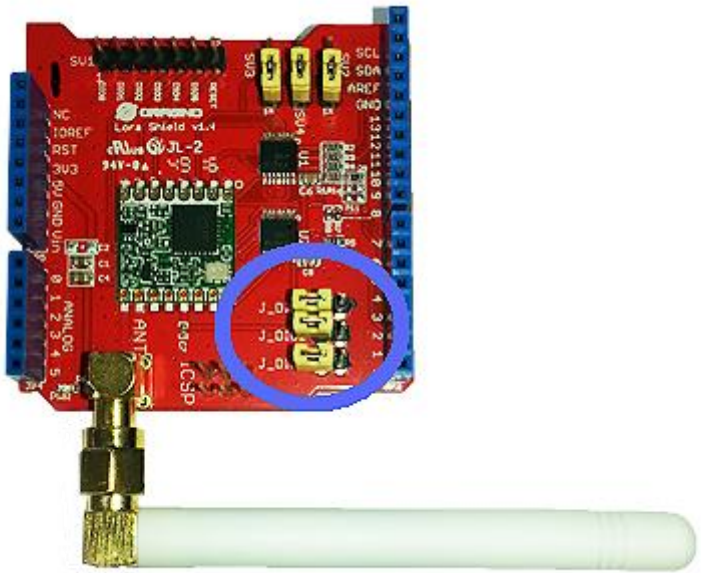

The LoRa™ Shield uses SPI for communication, and these pins are routed to the ICSP header. As such, any R3 board (including duinotech Uno, Leonardo or Mega) should work using hardware SPI directly.

ANT-RA57-915 Compact Right Angle 915MHz Antenna

890-960MHz(Center Frequency 915MHz) 1/4 wave 2dBi FOR SMA MALE R/A

RoHS

Specifications/Special Features :

This antenna is designed for 890-960MHz wireless Communications

Specification	
Model No.	
Frequency	890-960MHz(Center Frequency 915MHz)
Gain	2 dBi
V.S.W.R	<=2.0 (Center Frequency 915MHz <=1.5)
Polarization	Vertical
Connector	SMA Male Right Angle
Impedance	50Ω
Operation temperature	-20°C ~+60°C
Storage temperature	-30°C ~+75°C
Dimensions	L57 x W16.5 x H8 mm

1/4wave 2 dBi FOR SMA MALE R/A

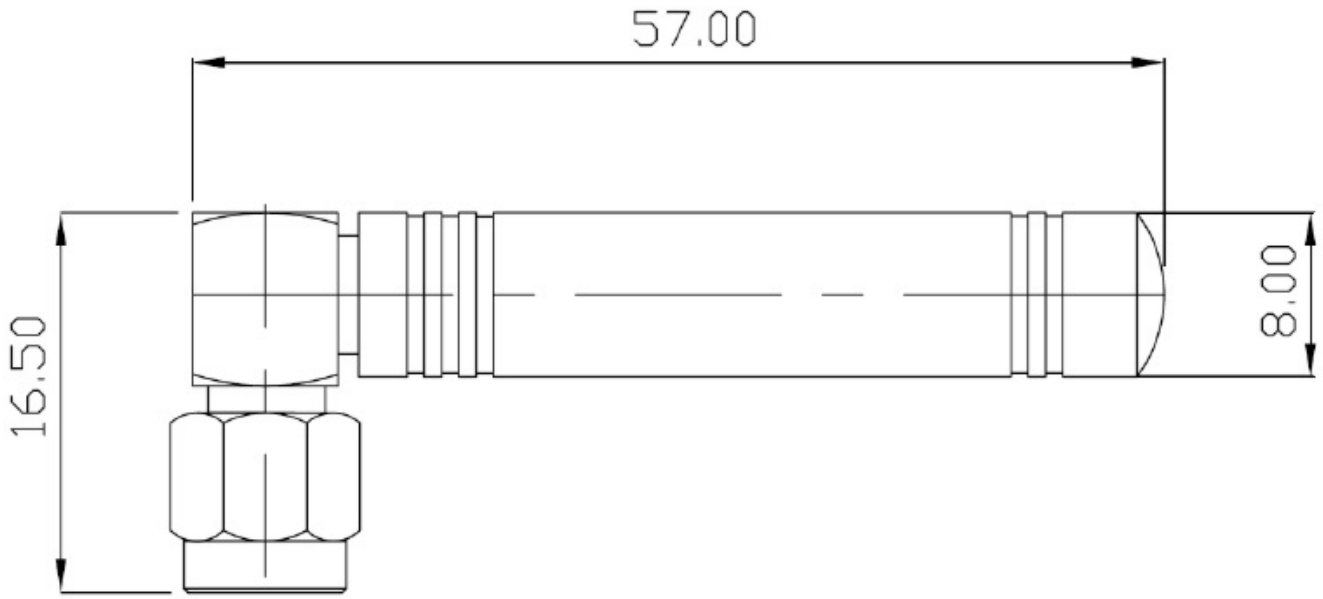

SMA MALE RIGHT ANGLE

1		6	IMPEDANCE : 50Ω
2	GAIN : 2dBi	7	
3	V.S.W.R : <=2:1	8	
4	LENGTH : 57mm	9	
5	CONNECTOR : SMA MALE R/A	10	

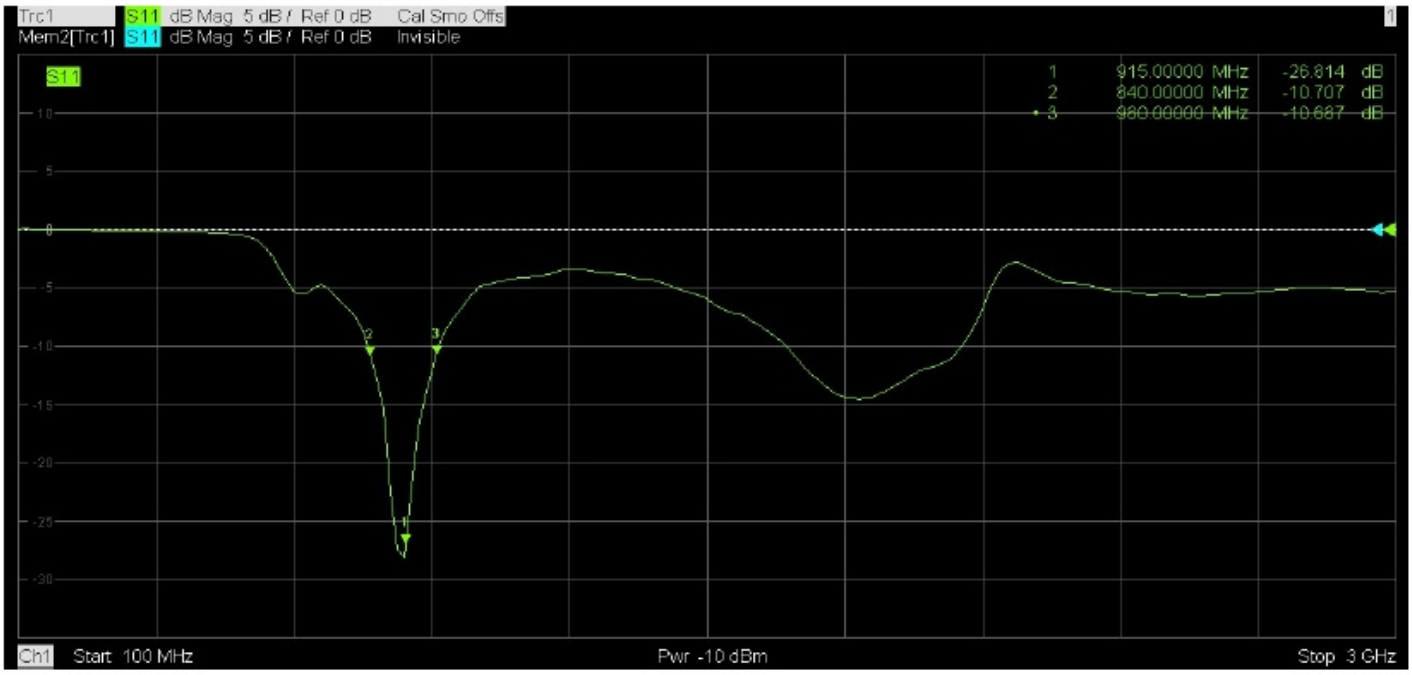

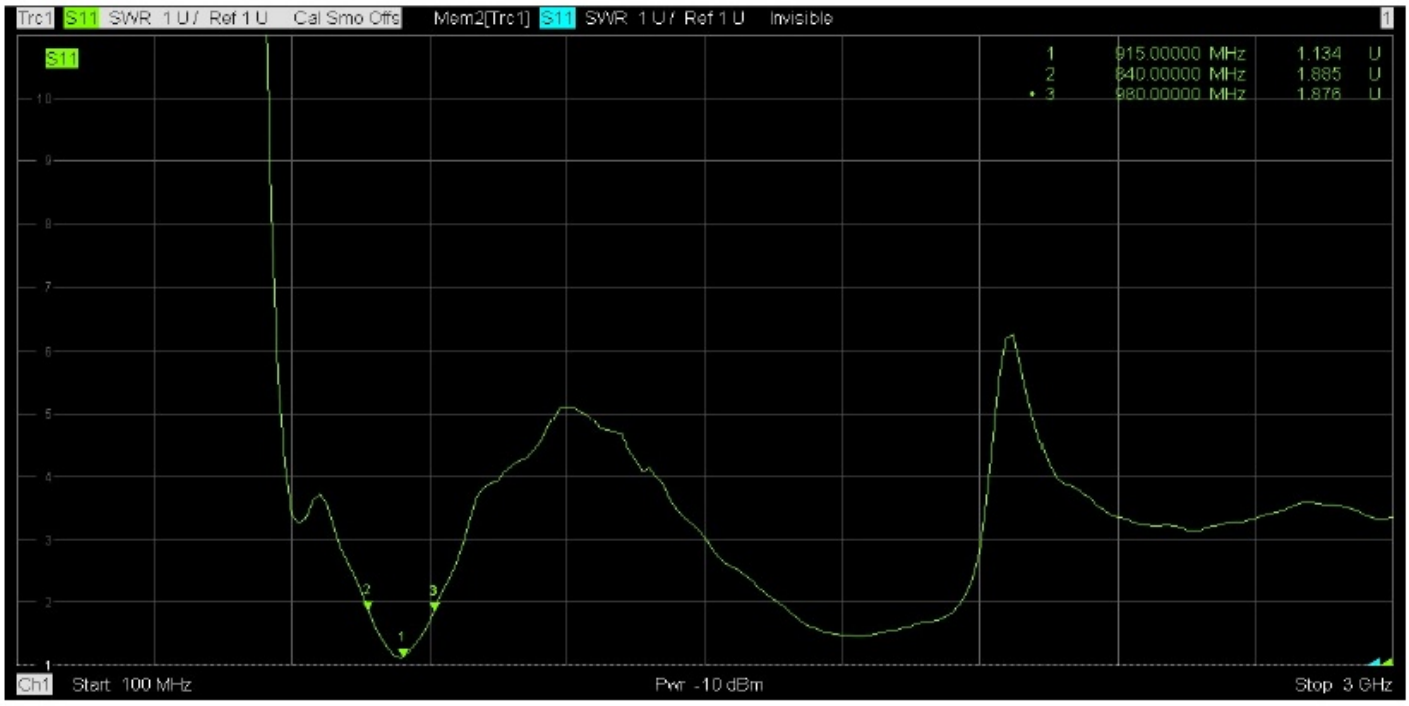

H-PLANE

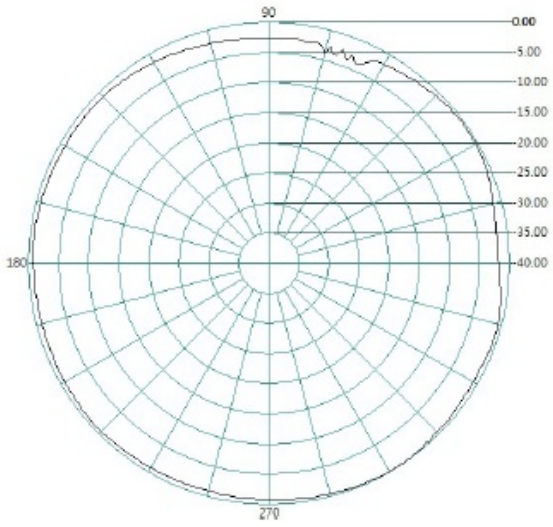

E-PLANE

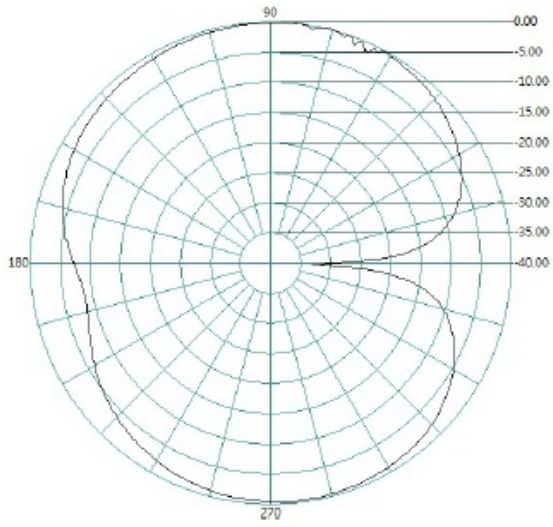

Appendix E – Weather Conditions

Dalby, Queensland
July 2024 Daily Weather Observations

Australian Government
Bureau of Meteorology

Date	Day	Temps		Rain	Evap	Sun	Max wind gust			9am						3pm					
		Min	Max				Dirn	Spd	Time	Temp	RH	Cld	Dirn	Spd	MSLP	Temp	RH	Cld	Dirn	Spd	MSLP
		°C	°C	mm	mm	hours		km/h	local	°C	%	eighths		km/h	hPa	°C	%	eighths		km/h	hPa
1	Mo	13.9	14.9	9.8			SSW	26	11:13	14.2	96		WSW	7	1020.6	13.7	91		SSW	9	1020.0
2	Tu	11.2	15.4	3.6			SE	30	13:53	13.0	97		SSE	9	1023.3	14.6	93		SSE	13	1021.2
3	We	9.7	18.5	2.6			E	54	13:14	13.1	86		SE	13	1025.6	17.0	62		ESE	30	1023.8
4	Th	8.4	19.4	0			ESE	57	10:40	12.7	81		SSE	17	1028.0	18.1	49		ESE	30	1026.0
5	Fr	1.8	19.9	0			ESE	48	11:46	11.1	82		SE	13	1030.5	17.5	56		ESE	28	1028.6
6	Sa	5.3	20.5	0			ESE	57	10:31	12.9	81		SE	17	1031.1	19.2	50		E	30	1028.3
7	Su	6.8	19.8	0			ESE	50	10:50	13.8	78		ESE	19	1029.3	17.5	56		ENE	30	1026.2
8	Mo	6.2	19.9	0			E	37	10:52	14.0	86		ESE	20	1026.4	18.3	69		ENE	20	1022.7
9	Tu	11.5	21.4	1.6			NW	28	11:58	14.8	96		ESE	2	1023.7	20.0	71		WNW	15	1020.8
10	We	11.1	19.7	0			SSW	28	12:00	14.0	77		S	15	1023.6	19.1	48		SW	15	1020.6
11	Th	1.4	22.2	0			W	19	16:40	9.0	87		SSW	9	1022.2	22.0	49		W	9	1016.5
12	Fr	2.1	21.9	0			W	43	14:39	11.6	89		WSW	6	1015.8	21.0	38		WSW	24	1011.2
13	Sa	5.2	17.2	0			WSW	46	14:01	12.0	76		WSW	20	1014.9	16.4	49		SW	30	1012.0
14	Su	0.1	16.5	0			SW	41	14:42	6.8	92		W	9	1017.6	15.4	48		WSW	22	1013.2
15	Mo	-1.1	15.3	0			W	37	13:44	8.2	81		WSW	9	1014.9	13.9	45		WSW	28	1011.2
16	Tu	0.6	15.5	0			WSW	57	12:03	9.5	78		WNW	17	1014.3	15.2	38		W	35	1010.7
17	We	-1.2	11.5	0			W	39	14:54	8.0	77		W	22	1015.1	11.1	63		W	30	1012.8
18	Th	1.2	14.5	0			SW	48	14:49	9.0	90		WSW	24	1017.7	10.5	91		SSW	28	1015.8
19	Fr	-0.7	17.4	0.6			WSW	50	12:59	8.7	89		NW	7	1023.1	16.8	42		WSW	15	1017.8
20	Sa	-1.9	21.4	0			W	50	11:38	11.4	69		NW	20	1019.1	21.1	27		W	30	1014.6
21	Su	-1.7	17.6	0			SW	48	11:08	10.0	59		SW	26	1023.9	17.1	29		SW	28	1021.3
22	Mo	-2.5	19.1	0			SSW	22	15:40	9.0	74		W	6	1028.0	18.8	28		W	11	1024.4
23	Tu	-1.6	21.4	0			E	24	19:50	8.7	71		SE	7	1028.6	20.4	31		W	6	1024.4
24	We	0.0	22.9	0			E	31	10:33	13.0	82		ESE	11	1026.7	22.3	35		NE	15	1021.7
25	Th	6.9	22.4	0			N	43	12:19	17.1	78		NE	15	1024.4	21.0	42		N	19	1020.6
26	Fr	9.5	23.7	0			N	44	09:51	18.7	60		N	22	1023.9	22.8	45		NW	19	1020.4
27	Sa	6.6	21.8	0			SW	41	21:46	17.7	80		N	11	1023.6	20.3	60		NW	17	1019.3
28	Su	10.6	18.0	3.4			SW	46	14:38	13.1	85		SW	20	1022.9	16.8	42		SW	30	1020.8
29	Mo	-4.0	16.2	0			WSW	41	13:58	6.5	74		SW	13	1027.3	16.0	29		SW	28	1024.2
30	Tu	-4.4	17.2	0			SSW	31	14:37	6.2	77			Calm	1030.6	16.6	25		S	19	1027.2
31	We	-2.5	19.0	0			SW	30	13:42	9.1	60		SSE	4	1032.0	18.7	27		SSW	15	1027.8
Statistics for July 2024																					
	Mean	3.5	18.8							11.5	80			13	1023.5	17.7	49			21	1020.2
	Lowest	-4.4	11.5							6.2	59			Calm	1014.3	10.5	25		W	6	1010.7
	Highest	13.9	23.7	9.8			#	57		18.7	97		SW	26	1032.0	22.8	93		W	35	1028.6
	Total			21.6																	

Observations were drawn from Dalby Airport {station 041522}

IDCJDW4039.202407 Prepared at 16:01 UTC on 2 Sep 2024